5.6 Plateau Uplift, Regional Warping, and Subsidence

J Babault, Universitat Autònoma de Barcelona, Barcelona, Spain
J Van Den Driessche, Université Rennes 1, Rennes, France

Babault, J., Van Den Driessche, J., 2013. Plateau uplift, regional warping, and subsidence. In: Shroder, J. (Editor in Chief), Owen, L.A. (Ed.), Treatise on Geomorphology. Academic Press, San Diego, CA, vol. 5, Tectonic Geomorphology, pp. 93–128.

Glossary

δ^2H Indicates the hydrogen isotopic composition of a sample. It is the difference between the isotope ratio of ^{2}H to ^{1}H in a sample and that in a standard, divided by the ratio in the standard, and expressed as parts per thousand per million.

δ^{18}O Indicates the oxygen isotopic composition of a sample. It is the difference between the isotope ratio of ^{18}O to ^{16}O in a sample and that in a standard, divided by the ratio in the standard, and expressed as parts per thousand per million.

Convective instability Also potential instability, a condition in which a stable fluid forced to rise or fall becomes unstable thereby triggering its later vertical motion.

Cosmogenic nuclides Rare isotopes within minerals induced by nuclear reactions induced by cosmic rays (mostly neutrons and muons). The length of surface exposure, or alternatively, the rate of surface erosion, is computed from the concentration of cosmogenic nuclides in a landform.

Delamination Separation of the dense lower part of the continental or oceanic lithosphere replaced by warmer, less dense mantle rock.

Endorheic basin Said of a basin characterized by internal drainage, a condition in which no surface drainage reaches the ocean.

Hypsometry The distribution of topographic surface area with respect to altitude.

Knickpoints (Nickpoint) refers to a substantially steepened reach of a stream long profile.

Laramide orogeny Also Columbian orogeny, was an ocean–continent collision orogen like the Andes now. The subducting plate, the Farallon oceanic plate caused thrusting and orogen building from what are now the south-western USA to northern South America.

Local relief Generally calculated in 5 or 10 km, a moving window, depending on the scale at which the topography has to be analyzed. It is the difference between the maximum elevation and the minimum elevation. It can also be calculated along a swath profile.

Magnetotelluric sounding The use of changing components of the geomagnetic field to study the electrical conductivity of the rocks within the Earth. It is generally applied to studies of the lower crust and upper mantle.

Mean elevation The critical variable that measures the force balance in orogens and reflects the isostatic balance of the lithospheric column. It is generally calculated in a 30 km moving window on a digital elevation model (DEM, a raster of altitudes), that is, at the scale of the crust thickness. It can also be calculated along a swath profile of at least 30 km wide.

Paleosurface A relict landscape more or less preserved, often a low-relief landscape deeply incised by the current drainage network. Its local characteristics may vary as a function of bedrock lithology, deformation, elevation, and latitude.

Stable isotope paleoaltimetry Determination of past elevations based on naturally occurring stable isotopes of an element.

Stream power The rate at which a stream can work for erosion and transport of its load, and measured over a specific length.

Abstract

The authors present the physiognomic and deep characteristics of the seven largest plateaus on Earth. In the second part, the evidence used by the Earth science's community to infer rock and/or surface uplifts of plateaus are reviewed. Finally, the authors briefly present the debate between the feedbacks between plateaus uplift and global climate change. Some of the results contained in this chapter are still under debate and ongoing research is still needed to confirm them because different studies invoke for a same object contradictory processes, in that they result in conflicting uplift history.

5.6.1 An Introduction to Surface and Deep Features of High Plateaus

5.6.1.1 Components and Scales of Landscape Dynamics

Earth's surface results from the competition between deep processes induced by the tectonic system that deforms, raises, or lowers the topography, and, from surface processes controlled by the erosion-transport system that destroy the highs and fill the lows. The former deep processes are a combination of the motion of lithospheric plates and/or mantle convection, the vertical component of which moves rocks with respect to the geoid, the sea level, or a reference ellipsoid. This vertical movement is generally referred to as "rock uplift" following England and Molnar's (1990) definition. Surface processes rely on erosion, transport capacity, and sedimentation, processes that are at least dependant on potential energy, hence, on vertical motions.

Taking into account the duration of tectonics and geomorphic events, it is evident that the interactions between deep-Earth and surface-Earth systems depend on the relative rates and response times of one system with respect to the other. For that reason the relative rates and response times act on the resulting topographic evolution. For example, erosion

tends to compensate rock uplift, but by definition a delay exists between both rock uplift and removal of rocks, otherwise no mountains would form.

Large-scale tectonic processes act on the whole thickness of the crust (~30 km) or the entire lithosphere (~100 km thick). Large-scale tectonics breaks, folds, tilts, raises, and lowers the landscape over a very large expanse of land, by more than $10^3 - 10^4$ km^2 (England and Molnar, 1990), defining in this way, the regional-scale of tectonic geomorphology. Consequently, the study of plateau uplift, regional warping and subsidence focus on extensive landmasses. More, in the understanding of plateau generation, rock uplift data only may not be a pertinent measure of plateau uplift since the surface uplift equals the rock uplift minus the erosion (or tectonic denudation) (England and Molnar, 1990; Molnar and England, 1990). Evidence of plateau uplift will be discussed in Section 5.6.2 of this chapter.

Driving mechanisms that produce plateaus uplift have received considerable attention in the literature over the past four decades, since the broad acceptance of plate tectonics are still under debate. Timing and rates of vertical movements are critical to understand which processes are the causes of the vertical forces acting on topography. Low rates of surface uplift (<0.5 mm yr^{-1}) can be explained by crustal shortening, thickening and consequent isostatic compensation, whereas high rates of surface uplift (>0.5 mm yr^{-1}) during one or several millions of years have their origin in mantle dynamics (Garzione et al., 2006). Mantle processes responsible for high rates of surface uplift are (among others): mantle lithosphere delamination following intracontinental subduction (Bird, 1978); convective instability of cold, dense thickened-lithospheric mantle in orogens; and, its replacement by relatively hotter and lighter mantle asthenosphere (England and Houseman, 1989; Houseman et al., 1981). This point will be elaborated in Section 5.6.3 of this chapter. The elevation history of plateaus, and how long high elevations of plateaus last, is also of great interest in order to understand the interaction between asthenospheric, lithospheric and climatic processes. Since paleoelevations can only be obtained using proxies, the way the inferred estimates of vertical motions occur are greatly interpreted and debated (e.g., Molnar, 2005).

Paleoelevation data are, in general, sparse in continental regions; generally they cover only a very small part of a plateau, preventing them being used as representative of the whole plateau (e.g., Molnar et al., 2006). Recently, new tools for paleoelevation's determination based on stable isotope paleoaltimetry (^{13}C-^{18}O bonds) provide new evidence for the dynamics of surface uplift and the nature of its driving mechanism in the Andes (Garzione et al., 2008; Ghosh et al., 2006b; Hoke et al., 2009) and in Tibet (Garzione, 2008). However, doubts have been shed on the reliability of this new method (Poulsen et al., 2010).

5.6.1.2 Definition and Types of Plateaus at Earth's Surface

As defined in the Glossary of Geology (Neuendorf et al., 2005), a plateau is, "broadly, any comparatively flat area of great extent and elevation, specifically an extensive land region considerably elevated (>150 m in altitude) above the adjacent country or above sea level. It is commonly limited on at least one side by an abrupt descent; has a flat or nearly smooth surface but is often dissected by deep valleys and surmounted by high hills or mountains; and has a large part of its total surface at or near the summit level." Although the term tableland also applies to a "broad, elevated region with a nearly level or undulating surface of considerable extent" (Glossary of Geology, Neuendorf et al., 2005), it might be

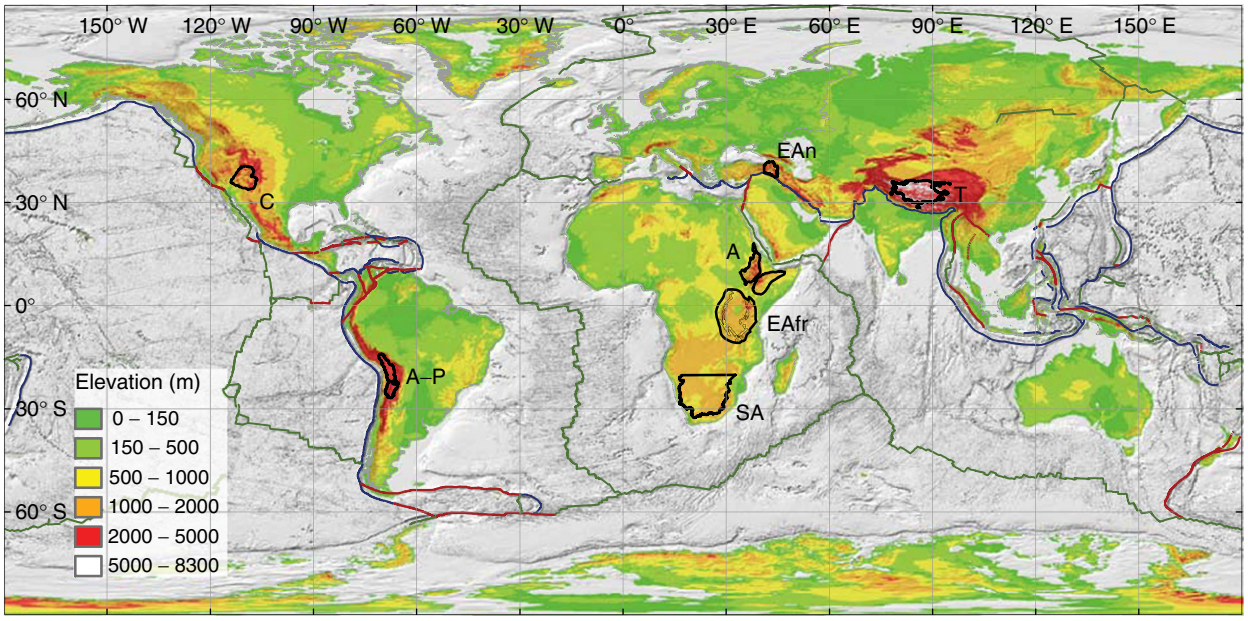

Figure 1 Location of the main studied uplifted-plateaus (black outlined areas) on the ETOPO1 DEM. T: Tibetan Plateau, A-P: Altiplano–Puna plateau, C: Colorado Plateau, EAn: Eastern Anatolian, A: Afar (or Ethiopian) Plateau, SA: southern African plateau, EAfr: East African plateau. Green, Red, and Blue curves correspond to divergent, transform-fault and convergent plate boundaries, respectively.

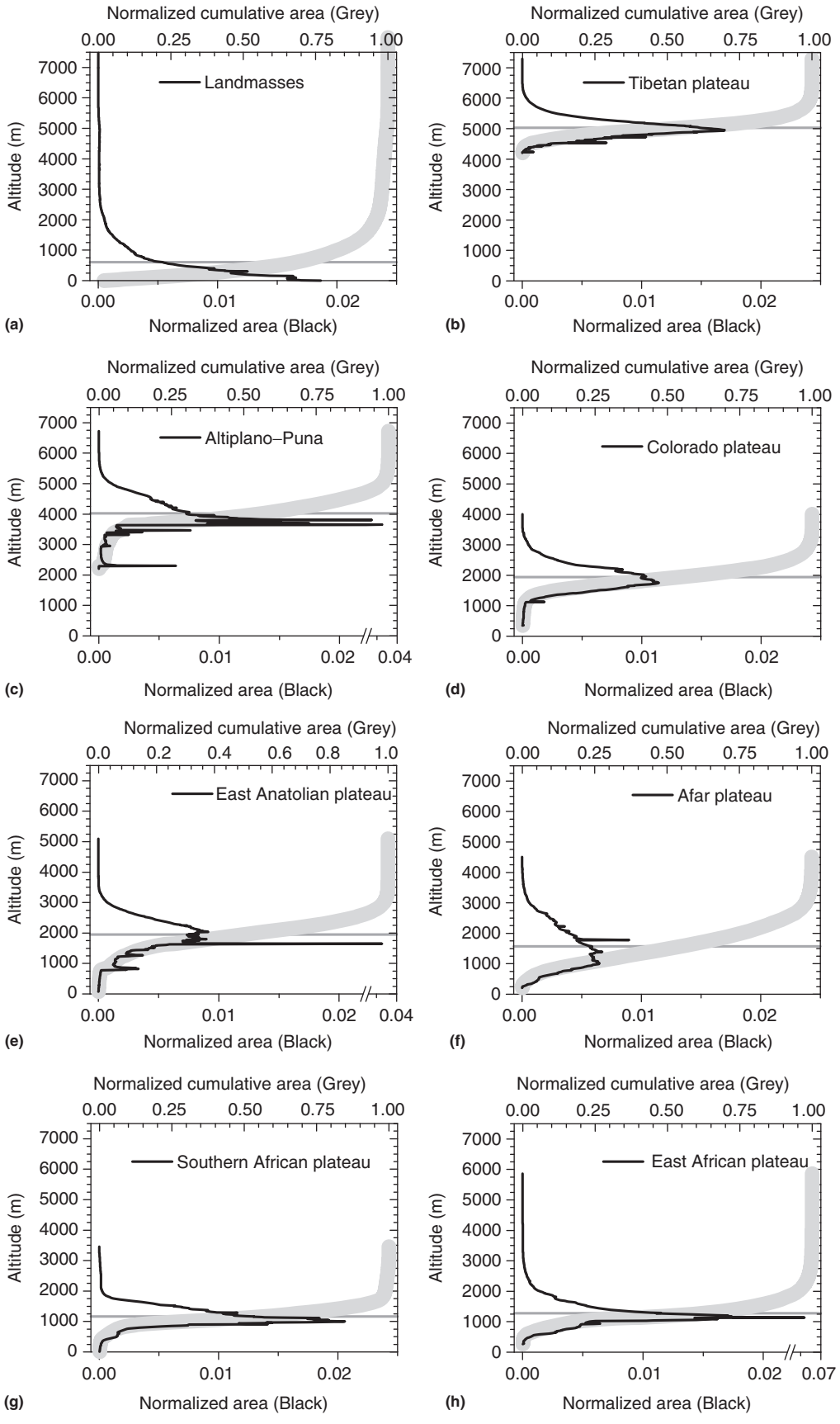
Normalized cumulative area (Grey)
Altitude (m)
Normalized area (Black)
Landmasses
(a)
Tibetan plateau
(b)
Altiplano–Puna
(c)
Colorado plateau
(d)
East Anatolian plateau
(e)
Afar plateau
(f)
Southern African plateau
(g)
East African plateau
(h)

used for smaller plateau-like features (Press et al., 2004) such as the Cheyenne Tablelands, a preserved interfluve between the North and South Platte Rivers located in western Nebraska and southeastern Wyoming, USA (e.g., Leonard, 2002).

From the theory of plate tectonics, the authors know that continental collision produces orogens and, in some cases, high plateaus such as the Tibetan Plateau in central Asia or the Altiplano–Puna plateau in southern America, for the largest and highest plateaus on Earth. However, plateaus can also develop in plate-interior regions, such as the Colorado Plateau in the western US, the Ordos block in China or the southern African plateau. Plateaus also exist in the oceans and they have been extensively studied since the onset of oceanographic campaigns and, sediments and rocks sampling of the seafloor since 1968 when the Deep Sea Drilling Project started, then during the Ocean Drilling Program and now within the Integrated Ocean Drilling Program. The authors center this chapter on landmass plateaus and leave out any synthesis of studies concerned with the oceanic plateaus. Broadly, oceanic plateaus are believed to be formed by extensive basaltic floods induced by rising mantle plumes. The thickening of the oceanic crust and the replacement of cold mantle lithosphere by a hot mantle plume produces significant surface uplift (Olson and Nam, 1986) and generates a plateau that is usually, at least in part, subaerial. After the onset of magmatic activity, the relative plate motion from the plume source forces the plateau to subside below sea level (Coffin, 1992; Detrick et al., 1977). Although the origin of oceanic plateaus is still under debate as it is the case for the Ontong-Java plateau, the largest basaltic plateau on Earth (e.g., Roberge et al., 2005), most studies agree that mantle convection affects subsidence and bathymetry of oceanic sea floor (e.g., Sutherland et al., 2010).

Continental high plateaus stand on almost every continent (**Figure 1**), and if not, they may have formed in the past and they may have then subsided as has occurred in Australia (e.g., Gurnis et al., 1998), or collapsed and eroded as in the Eastern US (Coney and Harms, 1984). The mean elevation of most of the studied high-plateaus lies above 1000 m above sea level (asl) contrasting with the 600 m mean elevation of the continental areas (**Figure 2**). This chapter will summarize the main geomorphologic characteristics of the most carefully studied high plateaus.

5.6.1.3 The Main High Plateaus

To compare the topography of the Tibetan Plateau, the Altiplano–Puna plateau, the Colorado Plateau, the Eastern Anatolian plateau, the East African and Ethiopian plateaus, and the southern African plateau (**Figure 1**) the authors performed a new analysis of elevation and slope frequencies (**Figures 2** and **3**) using the digital elevation model (DEM, SRTM90v4) published by Jarvis et al. (2008).

5.6.1.3.1 The Tibetan plateau

The internally drained area of Tibet (**Figure 1**) is situated on the average at 5023 m ($\pm$200 m) asl, it is characterized by mean slopes of 5° over 250 m windows (Fielding et al., 1994). At longer wavelengths of 100-km-wide swaths crossing Tibet at its greatest width and length, Fielding et al. (1994) obtained relief (maximum minus minimum elevations) estimates of $\sim$1 km or less for most of Tibet. The authors performed an analysis using the SRTM90v4 DEM published by Jarvis et al. (2008) and they obtained a similar mean elevation (5028 m, **Figure 2**) to Fielding et al. (1994) for the internally drained Tibetan Plateau ($\sim$700 000 km^2). Tibet is an almost flat and high area of great extent (**Figure 4**).

Almost 60% of the local slopes are less than 5° (**Figure 3**). Recent and active tectonic structures such as compressional mountain ranges, strike–slip fault-related uplifts and normal fault-related escarpments within the plateau (e.g., Liu-Zeng et al., 2008; Molnar and Tapponnier, 1978) explain the other 40% of slopes that are greater than 5°. The narrow Kunlun Mountains define the northern edge of the Tibetan Plateau, its steepest boundary. To the south it is bounded by the 2500-km-long Himalaya which, mostly in its central part, defines a steep boundary (Duncan et al., 2003). To the east the Tibetan Plateau slopes gently over 1000 km at a mean elevation of 3500 m asl up to the abrupt Longmen Shan topographic front.

Figure 2 Elevation frequencies (black lines) and hypsometries (heavy grey lines) computed at 10 m bins for the main-studied uplifted-plateaus of the world (see **Figure 1** for locations). (a) Histogram of the global landmasses used as a reference plot. Elevation values are derived from the SRTMv4 DEM (Jarvis, A., Reuter, H.I., Nelson, A., Guevara, E., 2008. Hole-filled SRTM for the globe Version 4. Available from the CGIAR-CSI SRTM 90 m: http://srtm.csi.cgiar.org) excepted for the global landmasses analysis (a) for which elevations have been extracted from ETOPO1 bedrock (Amante, C., Eakins, B.W., 2009. ETOPO1 1 Arc-minute global relief model: procedures, data sources and analysis. In: Memorandum, N.T. (Ed.), National Geophysical Data Center, Marine Geology and Geophysics Division, Boulder, CO, p. 19). Hypsometries of Tibet (b) and Altiplano–Puna (c) are computed for the internal drainage areas. The boundaries of the Colorado Plateau (d) used in this study are that used in Roy, M., Jordan, T.H., Pederson, J., 2009. Colorado Plateau magmatism and uplift by warming of heterogeneous lithosphere. Nature (London) 459, 978–982. The boundaries of the Eastern Anatolian Plateau (e) are from that defined by Şengör, A.M.C., Ozeren, M.S., Keskin, M., Sakinc, M., Ozbakir, A.D., Kayan, I., 2008. Eastern Turkish high plateau as a small turkic-type orogen; implications for postcollisional crust-forming processes in turkic-type orogens. Earth-Science Reviews 90, 1–48. The boundaries of the Afar plateau (f) and the East African plateau (h) are from the boundaries published by Ebinger, C.J., Bechtel, T.D., Forsyth, D.W., Bowin, C.O., 1989. Effective elastic plate thickness beneath the East African and Afar plateaus and dynamic compensation of the uplifts. Journal of Geophysical Research 94, 2883–2901; the narrow rift valleys of the Main Ethiopian Rift, the Kenyan and Western rift systems, which correspond to flat and depressed areas superimposed on the plateaus, have been removed for the topographic analysis. Elevations for the southern African plateau (g) correspond to the landmasses south of 20° S and in the hinterland of southern Africa behind the Great Escarpment as defined by Ollier, C.D., Marker, M.E., 1985. The great escarpment of southern Africa. Zeitschrift für Geomorphologie. Supplementband 54, 37–56. Reproduced from Gurnis, M., Mitrovica, J.X., Ritsema, J., van Heijst, H.-J., 2000. Constraining mantle density structure using geological evidence of surface uplift rates; the case of the African Superplume. Geochemistry, Geophysics, Geosystems 1(7), 1020. doi:10.1029/1999GC000035.

To the west, the Tibetan Plateau merges with the jagged relief of the Karakoram and Pamir ranges.

5.6.1.3.2 The Altiplano–Puna plateau

The Altiplano–Puna plateau is the second highest on Earth (~4000 m mean elevation, Isacks, 1988) with much of the plateau (a 250–300 km wide area) being internally drained (Vandervoort et al., 1995) (**Figure 5**). Isacks (1988) defined the plateau as the area of landmasses lying above the 3-km elevation contour which is considerably broader than the internally drained areas of the Altiplano and Puna. The authors analyzed the distribution of elevations and slopes within the internally drained areas, using the SRTM90v4 DEM published by Jarvis et al. (2008), in order to discard the deep incisions of the Andean plateau margins and to get a mean elevation closer to the definition of surface uplift following the definition of England and Molnar (1990). They obtained from the SRTM90v4 (Jarvis et al., 2008) a 4020 m asl mean elevation (**Figure 2(c)**) for the internally drained areas (~330 000 km^2, **Figure 1**), a value a little higher than the 3660 m asl mode value (**Figure 2(c)**) that corresponds to the Salar de Uyuni, in Bolivia. Other spikes in the histogram (**Figure 2(c)**) correspond to other major endorheic basins like the Salar de Atacama basin at 2300 m asl in northern Chile (**Figure 2(c)**). On the Altiplano–Puna plateau, the mean elevation is higher than the mode value and, than all the spikes in the histogram (**Figure 2(c)**) that are due to the mountains that surmount the main sedimentary basins. The mean elevation of the Puna is approximately 1000 m higher than that of the Altiplano (Allmendinger et al., 1997; Isacks, 1988; Wdowinski and Bock, 1994; Whitman et al., 1996). The cumulative hypsometric curve (**Figure 2(c)**) shows that 80% of the internally drained Andes lie between 2270 m and 4400 m asl. The Altiplano–Puna plateau is one of the flattest plateaus on Earth, 84% of local slopes are less than 5° (**Figure 2**) and ~70% are less than 0.6° (1%). The great number and extent of sedimentary basins, combined with the lack of major active tectonics in the Altiplano–Puna plateau, explains the smooth Andean landscape. The Altiplano–Puna plateau is flanked to the West by the Western Cordillera, a smooth edge sloping gently toward the Pacific trench (Farías et al., 2005; Isacks, 1988; Lamb et al., 1997), whereas the Eastern flank, the Eastern Cordillera, consist of a rough topography (Horton, 1999; Isacks, 1988; Lamb and Hoke, 1997; Lamb et al., 1997; Masek et al., 1994) containing smooth, highly elevated, topographic remnants of low-relief paleosurfaces (Kennan, 2000; Kennan et al., 1997; Servant et al., 1989).

5.6.1.3.3 The Colorado Plateau

The Colorado Plateau (**Figure 1**) in the southern United States of America has a mean elevation of 1941 m asl (**Figure 2**). This is the third highest plateau on Earth. The physiographic extent of the Colorado Plateau used here is the same as defined by Hunt (1956) and also used recently by Pederson et al. (2002) and by Roy et al. (2009). The plateau is surrounded to the northwest and to the south by the Basin and Range Province, to the northeast by the Rocky Mountains, to the east by the Rio Grande Rift. Mostly in its southwestern part, the plateau is deeply dissected by the Colorado River and its tributaries (Rigby, 1977). The western and central parts consist of high plateaus separated from each other by faults or more or less incised by canyons (Rigby, 1977). The southeastern part of the plateau is extensively covered by volcanic rocks whereas the northern part consists of the Uinta Basin (Rigby, 1977). Only 63% of the local slopes are less than 5° (**Figure 3**). The relative roughness of the Colorado Plateau is mostly a consequence of its deep dissection by the Colorado River and its tributaries (Pederson et al., 2002).

5.6.1.3.4 The Eastern Anatolian plateau

The East Anatolian plateau in Turkey (**Figure 1**) is bounded to the north by the Caucasus and to the southeast by the Zagros Mountains, and it extends from longitudes 41° E to 45° E (e.g., Şengör et al., 2008) and has a mean elevation of 1947 m asl (**Figure 2**). Two depressions at elevations above 1500 m asl compose the plateau: the Erzurum-Kars plateau in the north (Atalay and Koçman, 1979) and the Murat region in the south. They are separated by the Central Range with crest above 3000 m asl (e.g., Şengör et al., 2008). The Murat region is an internally drained region of 12 000 km^2 restricted to the surrounding of the Saline, 450-m-deep and 4406 km^2 of extent, Lake Van, perched at 1643 m (Spike in **Figure 2**(e)). Elsewhere, the Murat plateaus are dissected by permanent powerful streams including: the Euphrates; the Tigris; the Greater Zap; the Araxes; and their tributaries (e.g., Şengör et al., 2008). Only 38% of the local slopes are less than 5° (**Figure 3**), making the East Anatolian plateau the most rugged of all the plateaus described in this chapter. Recent deformation and deep incisions easily explain such a rough topography.

5.6.1.3.5 The East African and Ethiopian plateaus

A striking feature of the almost 3000 km of the East African Rift System is the presence of high plateaus surrounding the axial rift valley (**Figure 1**). These highly elevated topographies are distributed in two broad domes: the 1500-km-wide East African (or Kenyan) dome, or plateau, and the 1000-km-wide Ethiopian (or Afar) dome, or plateau. Such plateaus are characterized by elevations mainly above 800 m asl (Ebinger et al., 1989). Analysis of the topography of the high plateaus only, using the SRTM90v4 DEM, yields a mean elevation 1572 m asl and 1274 m asl for the Afar and East African plateaus, respectively (**Figure 2**). The frequency of local slopes (**Figure 3**) highlights the highest degree of dissection of the Afar plateau, by the Blue Nile among other streams (Ayalew and Yamagishi, 2004; Gani et al., 2007; Pik et al., 2003), with only 55% of slopes less than 5° compared to 77% for the less incised East African plateau. The spike in the histogram of elevations (**Figure 2**, Afar plateau) is approximately 2000 m asl, corresponding to the Tana basin, which resulted from the junction of three grabens during the late Cenozoic (Chorowicz et al., 1998).

5.6.1.3.6 The southern African plateau

The authors used the SRTM90v4 DEM published by Jarvis et al. (2008) to analyze the region south of latitude 20° S and enclosed by the Great Escarpment that bound the plateau on the coast of South Africa. The South African plateau has a mean elevation of 1166 m asl (**Figure 2**), the lowest value of the seven plateaus we analyzed. Local slope frequency reveals

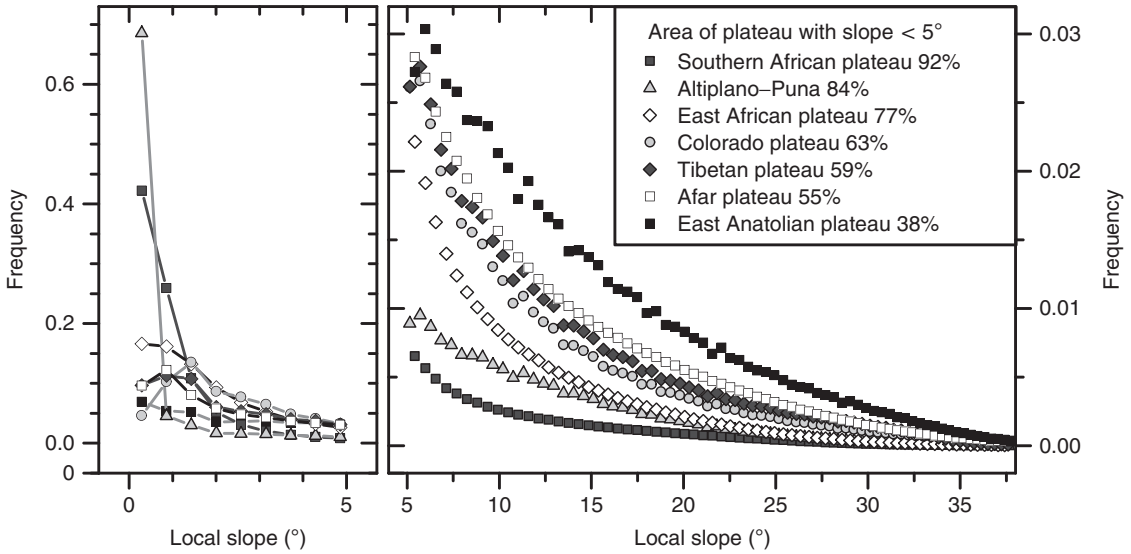

Figure 3 Relative occurrence (frequency) of local slopes binned at 0.01 (m m^{-1}); (left) lower than 5°, and (right) higher than 5°. Data are derived from the SRTMv4 DEM. Reproduced from Jarvis, A., Reuter, H.I., Nelson, A., Guevara, E., 2008. Hole-filled SRTM for the globe Version 4. Available from the CGIAR-CSI SRTM 90m: http://srtm.csi.cgiar.org.

Figure 4 View of the Tibetan Plateau between the Tanggula Shan and the Nyainqentangulha Shan. In the foreground the elevation is ~4500 m asl, and the summits in the background are at 5000–5200 m asl. Photo taken by Lewis Owen on the Golmud and Lhasa highway.

Figure 5 View to the south-east of the Puna plateau. The Salar in the background (white area close to the center of the picture) is at 4200 m asl and the highest summits in the right part of the picture are the Cordón de Puntas Negras, a chain of volcanoes reaching 5850 m asl. Photo taken by Dominique Savanier at 5400 m asl, from the Lascar volcano located on the eastern margin of the Salar de Atacama (Chile) and west of the Aguas Calientes Volcano.

that the southern African plateau is also the flattest with 92% of its area with slopes lower than 5° (**Figure 3**). The southern African plateau, the East African plateau and the southeastern Atlantic Ocean basin to the southwest form together a region of anomalous topography and bathymetry called the African Superswell (Nyblade and Robinson, 1994).

5.6.1.4 Deep Structures of the Main High Plateaus

The crust and upper mantle structures for these high plateaus are important constraints for evaluating possible surface uplift mechanisms. The following is an up-to-date summary of our knowledge of their physical and thermal structures; most of these results and interpretations are still under debate and will probably be improved in the near future.

5.6.1.4.1 Continent–continent collision plateaus (Tibet and Anatolian plateaus)

5.6.1.4.1.1 The Tibetan Plateau

Located within a broad zone of N–S continent–continent collision (**Figure 1**), compression is active on the borders of the Tibetan Plateau, whereas extension is active in its center and orientated E–W (e.g., Armijo et al., 1986; Molnar and Tapponnier, 1978; Chapters 5.3 and 5.15).

The Tibetan Plateau is underlain by 60-up to 80-km-thick crust (**Figure 6**), with the maximum thickness being just beneath the Zangbo (Tsangpo) suture at ~30° N (Hirn et al., 1984a, b; Holt and Wallace, 1990; Li and Mooney, 1998). A widespread low-velocity zone is evidenced from seismic studies in the midcrust and lower crust, and is interpreted as

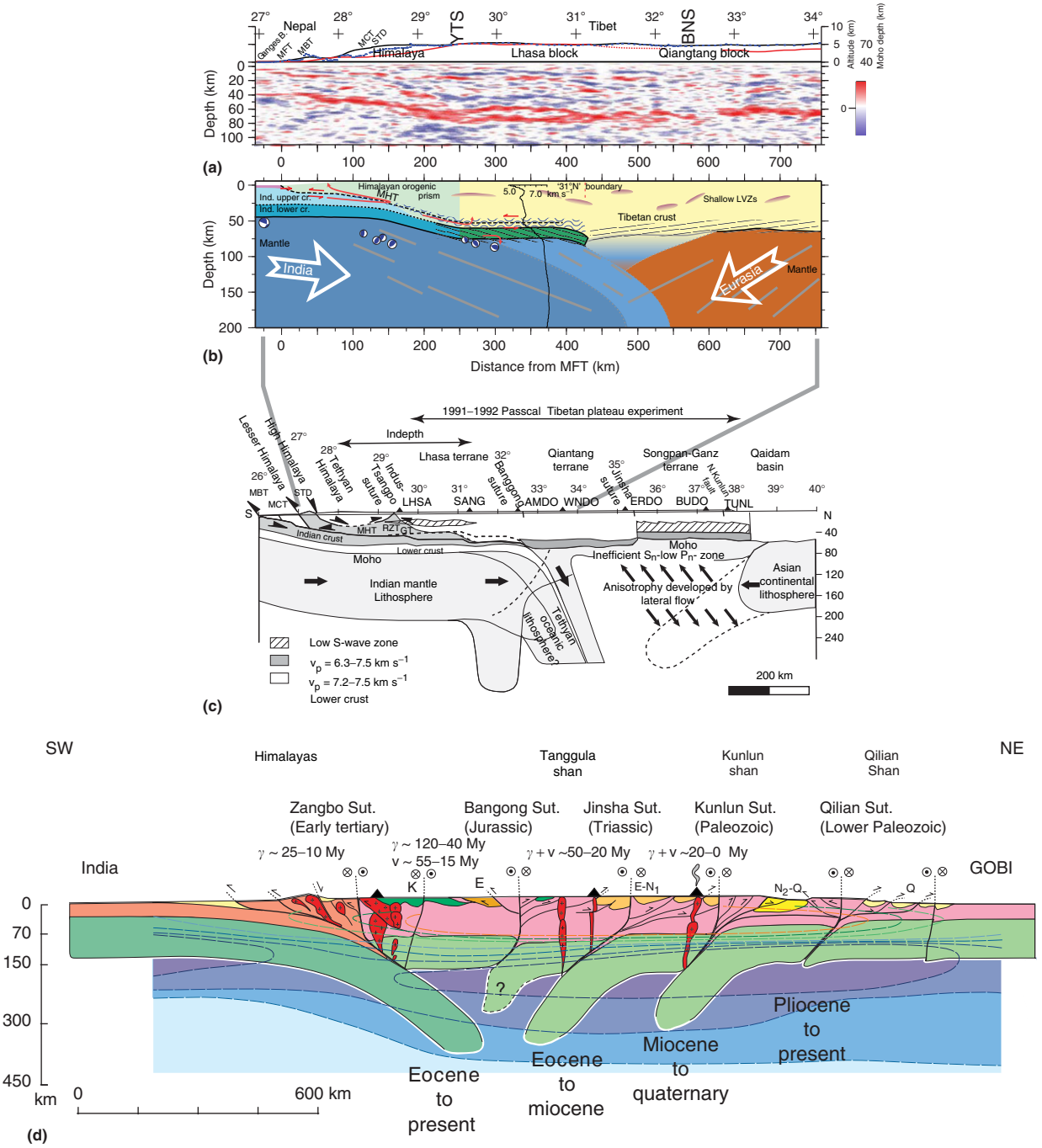

Figure 6 Deep structure of the Himalaya-Tibetan Plateau. (a) Receiver function image along the main profile showing the principal contrasts within the lithosphere (red and blue colors represent interfaces with increasing and decreasing impedance with depth, respectively. Reproduced from Nábělek, J., Hetenyi, G., Vergne, J., et al., 2009. Underplating in the Himalaya-Tibet Collision Zone Revealed by the Hi-CLIMB Experiment. Science 325, 1371–1374. (b) Interpretative cross section of the India–Euria collision zone. Reproduced from Nábělek, J., Hetenyi, G., Vergne, J., et al., 2009. Underplating in the Himalaya-Tibet Collision Zone Revealed by the Hi-CLIMB Experiment. Science 325, 1371–1374. (c) Representative cross-section of the Tibetan Plateau modified from the work of Owens, T.J., Zandt, G., 1997. Implications of crustal property variations for models of Tibetan plateau evolution. Nature 387, 37–43; Beaumont, C., Jamieson, R.A., Nguyen, M.H., Medvedev, S., 2004. Crustal channel flows: 1. Numerical models with applications to the tectonics of the Himalayan-Tibetan orogen. Journal of Geophysical Research 109, B06406; using information compiled by DeCelles, P.G., Robinson, D.M., Zandt, G., 2002. Implications of shortening in the Himalayan fold-thrust belt for uplift of the Tibetan Plateau. Tectonics 21, 1062; Johnson, M.R.W., 2002. Shortening budgets and the role of continental subduction during the India–Asia collision. Earth-Science Reviews 59, 101–123; Tilmann, F., Ni, J., Team, I.I.S., 2003. Seismic imaging of the downwelling Indian lithosphere beneath Central Tibet. Science 300, 1424–1427; Haines, S.S., Klemperer, S.L., Brown, L., et al. , 2003. INDEPTH III seismic data: from surface observations to deep crustal processes in Tibet. Tectonics 22, 1001. (d) Representative cross-section of the Tibetan Plateau by Tapponnier, P., Zhiqin, X., Roger, F., Meyer, B., Arnaud, N., Wittlinger, G., Jingsui, Y., 2001. Oblique stepwise rise and growth of the Tibet Plateau. Science 294, 1671–1677, in which the Asian continental lithospheric manlte is preserved, decoupled from the Asian thickened crust and subducted. Note that cross-sections (a) and (b) correspond only to the left hand half part of the cross-sections (c) and (d) that share the same horizontal scale.

partly molten crust or a layer of aqueous fluids (Xu et al., 2007; Yao et al., 2008). Magnetotelluric data show that this low-velocity zone is consistent with a weak crust at depth of 20–40 km distributed in two main zones that extend from the Tibetan Plateau as far as 800 km into southwest China (Bai et al., 2010).

At lithospheric scale, some seismological studies of the central Tibetan Plateau (at 92° E to 93° E) argue for the Indian plate underthrusting southern Tibet (Figures **6(a)** and **6(b)**) at least up to the south Lhasa block, ~29° N (Hirn et al., 1984b; Li et al., 2008; Nelson et al., 1996; Schulte-Pelkum et al., 2005) but with a northern boundary uncertain. Beneath northern Tibet, north of ~34° N (McNamara et al., 1995, 1997; Ni and Barazangi, 1983), and south of the Kunlun range, south of ~36° N (Wittlinger et al., 1996), studies argue for a low-velocity body in the mantle (**Figure 6(c)**). Together with the mechanical properties of the crust of northern Tibet (Owens and Zandt, 1997) and the volcanic activity of northern Tibet (Turner et al., 1993), such seismic properties have been interpreted as a portion of crust and mantle of higher temperature, that is, a thinned lithosphere and a hot and partially molten crust (Molnar et al., 1993; Owens and Zandt, 1997; Zhu et al., 1995). Such a 250–300 km dome-like structure of hot mantle lies between two cold lithospheres characterized by relatively high seismic velocities (Wittlinger et al., 1996). These deep physical and thermal structures have been interpreted as the evidence for the underthrusting of the cold Indian lithospheric mantle beneath the Asian crust up to the Bangong–Nujiang suture at ~33° N (**Figure 6(c)**) (Owens and Zandt, 1997). Later, Kosarev et al. (1999) reexamined these data and suggested that the Indian lithosphere has underthrust the entire Asian lithosphere (not only the crust) from the base of the Moho (80 km depth), 50 km north of ~29.5° N, where the Indus–Tsangpo suture is located, as far as the Bangong–Nujiang suture at ~33° N, up to a depth of 200 km where it is inferred to be cut by a mostly vertical subducting structure. From 33° N to 36.5° N, Kosarev et al. (1999) also showed a discontinuous Asian lithospheric mantle made of fragments interpreted as a process of destruction and subduction of the sinking Asian lithosphere. Alternatively, Tapponnier et al. (2001) proposed the origin of the low velocity zone between the Tanggula and the Kunlun ranges (between 34° N and 36° N) to lie in the thick crust of the plateau. Their interpretation is based on the seismic work of Griot et al. (1998) and it implies that the Asian lithosphere has not been thinned (**Figure 6(d)**). Recently, Nábělek et al. (2009) have shown with a continuous seismic image that the Indian lithosphere has underthrust the Asian crust only, and that the Indian lower crust extends horizontally beneath the Tibetan Plateau up to approximately 31° N (**Figures 6(a)** and **6(b)**), as it is present in eastern and western Tibet (Kind et al., 2002; Wittlinger et al., 2004). The Asian and Indian crust are shown to be separated by the main Himalayan thrust (MHT) from Nepal (~27.5° N) into a midcrustal low velocity zone observed across the southern Lhasa Block (~29.5° N–31° N). Based on the differences in the seismic characteristics of the lower crust and uppermost mantle, Nábělek et al. (2009) proposed that the zone located around 31° N–32° N, and south of the Bangong–Nujiang suture (~33° N), is a boundary between the Eurasian plate and the Indian plate that is underthrusting the Tibetan upper crust. The Nábělek et al. (2009) interpretation shifts to the south the plate boundary inferred to be at ~33° N by Kosarev et al. (1999). South and north of 31° N–32° N Nábělek et al.'s (2009) boundary, mantle lineations dip north and south, respectively, suggesting a mantle downwelling along this plate boundary (**Figures 6(a)** and **6(b)**), a continental subduction also put in evidence east of Nábělek et al.'s profile (Shi et al., 2004; Tilmann et al., 2003). Such continental subduction of the Indian and Eurasian plates beneath and south of the Bongong–Nujiang suture (southern Tibet) mainly agrees with the lithospheric-scale cross-section proposed by Tapponnier et al. (2001) (**Figure 6(d)**) and based on compiled surface and subsurface data (see references in Tapponnier et al., 2001). One of the main differences between the two models of the deep structure of the Tibetan Plateau is the preservation, or not, of the Asian lithosphere (**Figures 6(c)** and **6(d)**). In Tapponnier et al.'s (2001) model, the crust thickened since the collision of Indian and Asian plates, whereas the mantle did not. Such a model implies that the lithospheric mantle is decoupled from the weak lower crust, and subducted into the hot asthenospheric mantle.

5.6.1.4.1.2 The Eastern Anatolian and Iranian plateaus

Like the Tibetan Plateau, the Eastern Anatolian plateau corresponds to a zone of north–south continental collision (**Figure 1**). Folding is confined to the southwestern part of the plateau (as defined by Şengör et al., 2008) and thrusting is confined to east–west depressions in the southwestern, central, and northeastern parts of the plateau (for a compilation of neotectonic data see Şengör et al., 2008). However, the plateau is dominated by strike–slip faults: a sinistral northeast–southwest orientated set and a dextral northwest–southeast striking set (Şengör et al., 2008 and references herein).

Seismic data show a mean crustal thickness of 45 km beneath the eastern Anatolian plateau (**Figure 7**) with 42 km near the southern part of the Biltis suture zone (the southern edge of the plateau) and 50 km along the northern edge of the Anatolian plateau, whereas in the southeastern part of the plateau the crust is thinner than 40 km (Zor et al., 2003).

Furthermore, seismic data argue for a thinned or totally removed lithospheric mantle beneath the plateau (Al-Lazki et al., 2004; Gök et al., 2003, 2007) which is consistent with the high heat flow and the late Cenozoic volcanic activity (Keskin, 2003; Pearce et al., 1990; Yilmaz et al., 1998). Tomography indicates that it is not only the Turkish plateau but all the Turkish–Iranian plateau, the Middle East region north of the Bitlis–Zagros suture, that is affected by a lithospheric mantle thinning and its replacement by a warm or perhaps partially molten uppermost mantle (Maggi and Priestley, 2005; Tabatabai Mir et al., 2008) to a depth of ~200 km (Zor, 2008). The region also lacks subcrustal earthquakes, which is evidence for the absence of the subducting Arabian Plate beneath the Anatolian plateau (Turkelli et al., 2003).

5.6.1.4.2 Ocean–continent collision plateau (The Andes)

The Andes result from oceanic-continent convergent margin processes. The Nazca oceanic plate is subducted on a 30°-east-dipping direction beneath the Altiplano–Puna plateau,

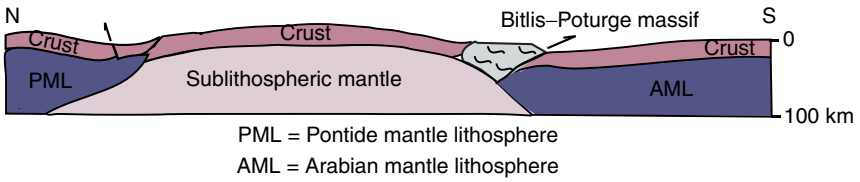

Figure 7 Lithospheric structure beneath eastern Anatolia from Gögüs, O.H., Pysklywec, R.N., 2008. Mantle lithosphere delamination driving plateau uplift and synconvergent extension in eastern Anatolia. Geology 36, 723–726, originally modified from Şengör, A.M.C., Özeren, S., Genç, T., Zor, E., 2003. East Anatolian high plateau as a mantle-supported, north-south shortened domal structure. Geophysical Research Letters 30, 8045; Dhont, D., Chorowicz, J., 2006. Review of the neotectonics of the Eastern Turkish–Armenian Plateau by geomorphic analysis of digital elevation model imagery. International Journal of Earth Sciences 95, 34–49; Gök, R., Michael, E.P., Ekrem, Z., 2007. Lithospheric structure of the continent–continent collision zone: eastern Turkey. Geophysical Journal International 169, 1079–1088, and Keskin, M., 2003. Magma generation by slab steepening and breakoff beneath a subduction-accretion complex: an alternative model for collision-related volcanism in Eastern Anatolia, Turkey. Geophysical Research Letters 30, 8046.

whereas in the narrower northern and southern Andes the plate shallows and becomes nearly flat (Cahill and Isacks, 1992, and references herein). Gephart (1994) showed that the central Andean orogen as well as the underlying Wadati–Benioff zone exhibit a high symmetry with the axis of symmetry for the two surfaces nearly coincident. More, Gephart (1994) showed that these axes were coincident with the Nazca/South America finite relative rotation pole for the period 36–20 Ma, that is, coincident with plate kinematics, which has been stable since the mid-Tertiary. Such geometric and kinematics evidence suggest that the tectonic forces that built the Andean topography are strongly related to the subduction process, or plate tectonics, in this noncollisional orogen (Gephart, 1994) whatever the significant along-strike geological variations.

Crustal thicknesses in the Andes vary strongly on the region considered, and, also depending on the kind of methods used to estimate it (see Allmendinger et al., 1997). From north to south, seismic studies show that they range from 59 to 70 km in southern Peru (**Figure 8**), from 49–60 to 80 km beneath the Central Andes and from 40–50 to 60–70 km above the Pampean flat slab of the Southern Andes (Beck et al., 1996; Fromm et al., 2004; Heit et al., 2008; McGlashan et al., 2008; Yuan et al., 2002). Crust maximum thickness is beneath the Western and Eastern Cordilleras where it reaches ~70 km (Beck and Zandt, 2002; Beck et al., 1996; Swenson et al., 2000). Now considering the Altiplano–Puna plateau alone, depending on different studies, crustal thicknesses vary beneath the Puna–Altiplano from 60 to 65 km (Beck and Zandt, 2002; Beck et al., 1996) or they range between 57 and 82 km beneath the Altiplano, and they thin to 40–45 km beneath the 1000 m higher Puna (McGlashan et al., 2008; Yuan et al., 2002). Alternatively, the crust under the Altiplano and Puna plateau has been deduced to be 60 and 67 km thick, respectively, in correlation with the higher 1000 m asl mean elevation of the Puna (Baumont et al., 2002). Gravity studies also yield the conclusion that the crust beneath the Altiplano and Puna is less than 70-km thick (Fukao et al., 1989; Götze et al., 1994; Kono et al., 1989). Beneath the Altiplano, a low-velocity zone has been inferred for the midcrust to lower crust to be felsic (quartz-rich) composition and it may correspond to a weak layer decoupled from the brittle upper crust (Beck and Zandt, 2002; Koulakov et al., 2006; Yuan et al., 2000). Mafic lower crust is inferred by seismic velocities to be in the eclogite facies or to be absent in the Central Andes (Beck and Zandt, 2002).

Lithospheric thickness has been estimated to reach 150 km beneath the Altiplano, to thin under the Western Cordillera and to thin by 50 km beneath the Puna plateau (Whitman et al., 1992; Whitman et al., 1996). Seismic velocities under the Altiplano–Eastern Cordillera transition also suggest that the asthenosphere reaches near the base of the crust (Dorbath and Granet, 1996; Koulakov et al., 2006; Myers et al., 1998; Wigger et al., 1994). Geochemistry of hydrothermal fluids and gases of the Altiplano and the Eastern Cordillera also supports the views that the lithosphere has been thinned (Hoke et al., 1994). The upper part of the subducted Nazca plate is topped by a low-velocity zone interpretated as magma generation zone induced by dehydratation of subducted material dragged along the slab (Baumont et al., 2002). To the East of the Altiplano, numerous studies suggest that the mechanically strong Brazilian lithosphere has underthrust the Sub Andes and the Eastern Cordillera but not the Altiplano (Beck and Zandt, 2002, and references herein).

5.6.1.4.3 Intraplate plateaus (Colorado and African plateaus)

5.6.1.4.3.1 The Colorado Plateau

A Mesozoic ocean–continent collision started at 150 Ma in the western coast of North America. Consequently, the east dipping Farallon plate subduction, and the associated compression triggered compressional deformation and the formation of the Sevier orogen. During the late Cretaceous and early Tertiary, the shallowing of the Farralon plate subduction (e.g., Dickinson and Snyder, 1978) propagated the deformation into the interior of the North American plate leading to the formation of the Laramide orogen. These orogenies lead to an overthickened crust up to 60 km thick (Coney and Harms, 1984). The Colorado Plateau was located close to the eastern front of the Laramide orogen but it experienced only a very small amount of crustal shortening, less than a few percent (Spencer, 1996). The Colorado Plateau is now bordered by the Basin and Range Province to the west and south and the Rio Grande Rift to the east; both are thinned regions (e.g., Bird, 1988; Sonder and Jones, 1999; Wernicke et al., 1987) where extension is still active. However, no significant extension is reported on the Colorado Plateau.

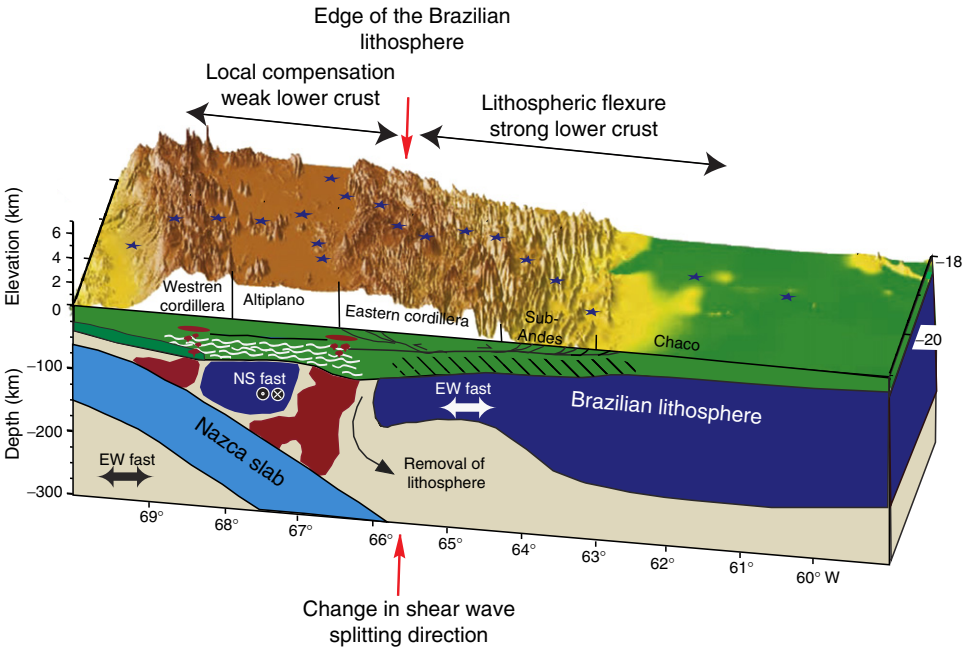

Figure 8 Schematic cross-section from Beck, S.L., Zandt, G., 2002. The nature of orogenic crust in the central Andes. Journal of Geophysical Research 107, 2230 showing their interpretation of the lithospheric structure of the central Andes from geophysical and geological studies. Red and blue indicate upper mantle P wave velocities that are slower and faster, respectively, than the reference IASPEI-91 model. Reproduced from Myers, S.C., Beck, S., Zandt, G., Wallace, T., 1998. Lithospheric-scale structure across the Bolivian Andes from tomographic images of velocity and attenuation for P and S wavesJournal of Geophysical Research 103, 21233–21252.

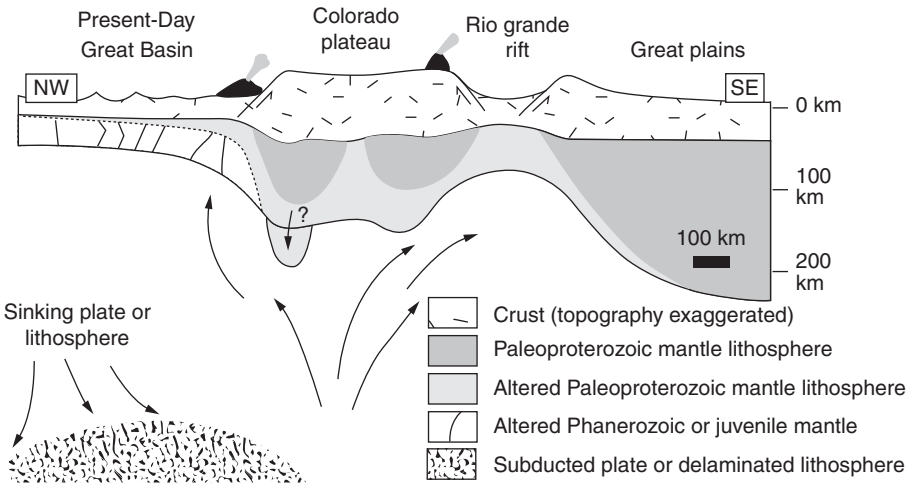

Figure 9 Deep structure beneath the Colorado Plateau and the Basin and Ranges, Rio Grande Rift and Great Plains neighboring regions, from Sine, C.R., Wilson, D., Gao, W., Grand, S.P., Aster, R., Ni, J., Baldridge, W.S., 2008. Mantle structure beneath the western edge of the Colorado Plateau. Geophysical Research Letters 35, L10303.

The crust beneath the Colorado Plateau is inferred by seismic studies to be 44- to 47-km-thick (**Figure 9**) (Das and Nolet, 1998; Wilson et al., 2005). Crustal thickness is almost similar, 42–46 km, in the Great Plains, whereas the crust underwent thinning to 35 km centered on the Rio Grande Rift (Wilson et al., 2005). The Basin and Range Province underwent thinning of the crust up to 20–30 km thick (Coney and Harms, 1984), seismic studies suggest that the crust thins from 30 to 25 km eastward (Das and Nolet, 1998, and references therein). The crust of the Rocky Mountains to the north is inferred to be 50-km-thick (Das and Nolet, 1998, and references therein).

Seismic data argue for a 120- to 150-km-thick lithosphere beneath the Colorado Plateau and ~200 km beneath the Great Plains to the east (West et al., 2004). In between, thinned lithosphere, 45- to 55-km-thick, is inferred to exist

beneath the Rio Grande Rift (West et al., 2004). To the west, the lithosphere is also thin at 60-km-thick beneath the Basin and Range (Zandt et al., 1995).

A thick low-velocity zone is inferred beneath the Colorado Plateau lithosphere (West et al., 2004) from a depth of 150 to 300 km. Based on seismic studies Wang et al. (2008) and Sine et al. (2008) inferred mantle regional flow at the southeastern edge and at the western edge of the Colorado Plateau.

5.6.1.4.3.2 The East African (Kenyan) and Ethiopian plateaus

The East African and Ethiopian plateaus are located in the African plate along the East African Rift System. The Ethiopian plateau is covered by extensive basalts dated at 31–29 Ma (e.g., Hofmann et al., 1997). Sedimentary and volcanic sequences are modeled to reach 2 to 5 km of thickness on the Ethiopian plateau (Mackenzie et al., 2005) with 1 to 2 km of flood basalts and volcanoes on top of the western Ethiopian plateau (Pik et al., 2003). Depending on the studies carried out, the crust is inferred to be 42- to 50-km-thick west of the Ethiopian rift and 37- to 40-km-thick to the east (Mackenzie et al., 2005) or is inferred to be 33- to 44-km-thick on either side of the Main Ethiopian rift (Dugda et al., 2005). Beneath the western Ethiopian plateau, a 15-km-thick layer composing the base of the lower crust is characterized by seismic high-velocities. Crustal thicknesses vary from 37 to 38 km west and from 39 and 42 km east of the Kenyan rift (Dugda et al., 2005). These studies indicate that crust away from the rifts has not been significantly modified by the Cenozoic rifting and magmatism, and the Cenozoic flood basalts on the Ethiopian plateau do not appear to be thick enough to alter the depth of the base of the crust (Dugda et al., 2005). Only a slight thinning of the crust is observed below the Main Ethiopian Rift (Mackenzie et al., 2005) and crustal thickness is inferred to vary from 27 to 38 km (Dugda et al., 2005).

Beneath the Ethiopian plateau, the lithosphere-asthenosphere boundary is imaged at 90 km depth (Ayele et al., 2004). Almost similar values are obtained by Dugda et al. (2007) who inferred the base of the lithosphere at 70–80 km beneath the Ethiopian plateau and at 50 km beneath the Main Ethiopian Rift and the Afar. By contrast, the lithosphere of the Tanzanian craton beneath the East African plateau reaches deeper levels up to approximately 170–200 km (Ritsema and van Heijst, 2000) (**Figure 10(b)**), though 50–80 km shallower than the lithosphere of the thicker Congo craton to the west.

In the Afar and surrounding regions a deep low-velocity anomaly in the upper mantle (Debayle et al., 2001; Ritsema et al., 1999; Ritsema and van Heijst, 2000) is interpreted as hot mantle extending to at least 660-km-depth (e.g., Debayle et al., 2001). Beneath the East African plateau a low-velocity anomaly is present in the upper mantle that is ~500 km wide and extends from the eastern edge of the Main Ethiopian Rift westward (Bastow et al., 2008). A low velocity zone also extends up to a depth of ~400 km and to at least 300 km beneath the eastern branch in Tanzania and in Kenya, respectively (Park and Nyblade, 2006; Ritsema et al., 1998; Weeraratne et al., 2003). The top and bottom of the transition zone (410–660 km) beneath the Eastern Plateau is depressed and it could be related to a thermal anomaly in the lower mantle (**Figure 10(a)**) (Huerta et al., 2009) (see Section 5.6.1.4.3.3).

Following the pioneer work of Dziewonski (1984), Ritsema et al. (1999) presented a global tomographic model inferring (like Dziewonski) a broad low-velocity zone in the lower mantle and initiating at the core mantle boundary beneath southern Africa and propagating up to the upper mantle beneath the Afar Plateau (**Figure 10(a)**). Such anomalous low seismic velocity is interpreted as hot and less dense lower mantle material combined with a chemical anomaly (Ritsema et al., 1999; Simmons et al., 2007) and referred to as the deep-mantle African Superplume.

5.6.1.4.3.3 The Southern African plateau

The southern African plateau is located within a stable continent and bordered by Mesozoic passive margins (**Figure 1**). The southern African plateau is bounded on the coast by rift shoulders, the Great Escarpment and the Drakensburg Mountains, characterized by a warping down of the topography from 1000 m asl toward the margin (Ollier, 1985; Ollier and Marker, 1985; ten Brink and Stern, 1992).

Crustal thickness beneath the southern African plateau varies between 33 and 45 km beneath the Archean cratons and 45 and 50 km beneath the Proterozoic orogenic belts (Nguuri et al., 2001).

A 250 to 300 km thick lithosphere has been inferred by Ritsema and van Heijst (2000) and James and Fouch (2002), respectively. High lithospheric thickness and low heat flow, <45 mW m^{-2} (Nyblade et al., 1990), are considered to mark a strong upper mantle which is corroborated by high estimates of effective lithospheric thicknesses (Stark et al., 2003).

Beneath southern Africa and the southern Atlantic Ocean, global tomography suggests that there is a low-velocity zone in the lower mantle and initiating at the core mantle boundary (Ritsema et al., 1999) (**Figure 10(a)**).

5.6.1.5 High Plateaus: Uplifted Peneplains, Growing Plateau or Applanation at High Elevation?

Davis (1899) interpreted elevated and smooth landscape as a step in a sequence or a cycle in which ongoing erosion of a previous landscape eventually leads to the complete destruction of the relief and the formation of a low-relief erosional surface at almost sea level: the peneplain. Davis's cycle of erosion (1899) was based on the idea that after a rapid surface uplift of the peneplain, the increase in potential energy enhances erosion that in turn increases significantly the local relief and local slopes. A wave of fluvial and hillslope erosion then propagates inside the plateau from the borders. Ongoing erosion eventually leads to the complete destruction of the topography and the formation of another low-relief erosional surface at almost sea level. A new uplift of such peneplain means a wave of erosion starts afresh: a new cycle of erosion began (see Chapter 5.16 for more discussion).

In contrast, several models have been proposed for the non instantaneous development of topography as it has been the case for the Tibetan Plateau. They argue for the progressive surface uplift of the whole plateau (Fielding et al., 1994), or for progressive surface uplift of the whole followed by rapid surface uplift events (England and Houseman, 1989;

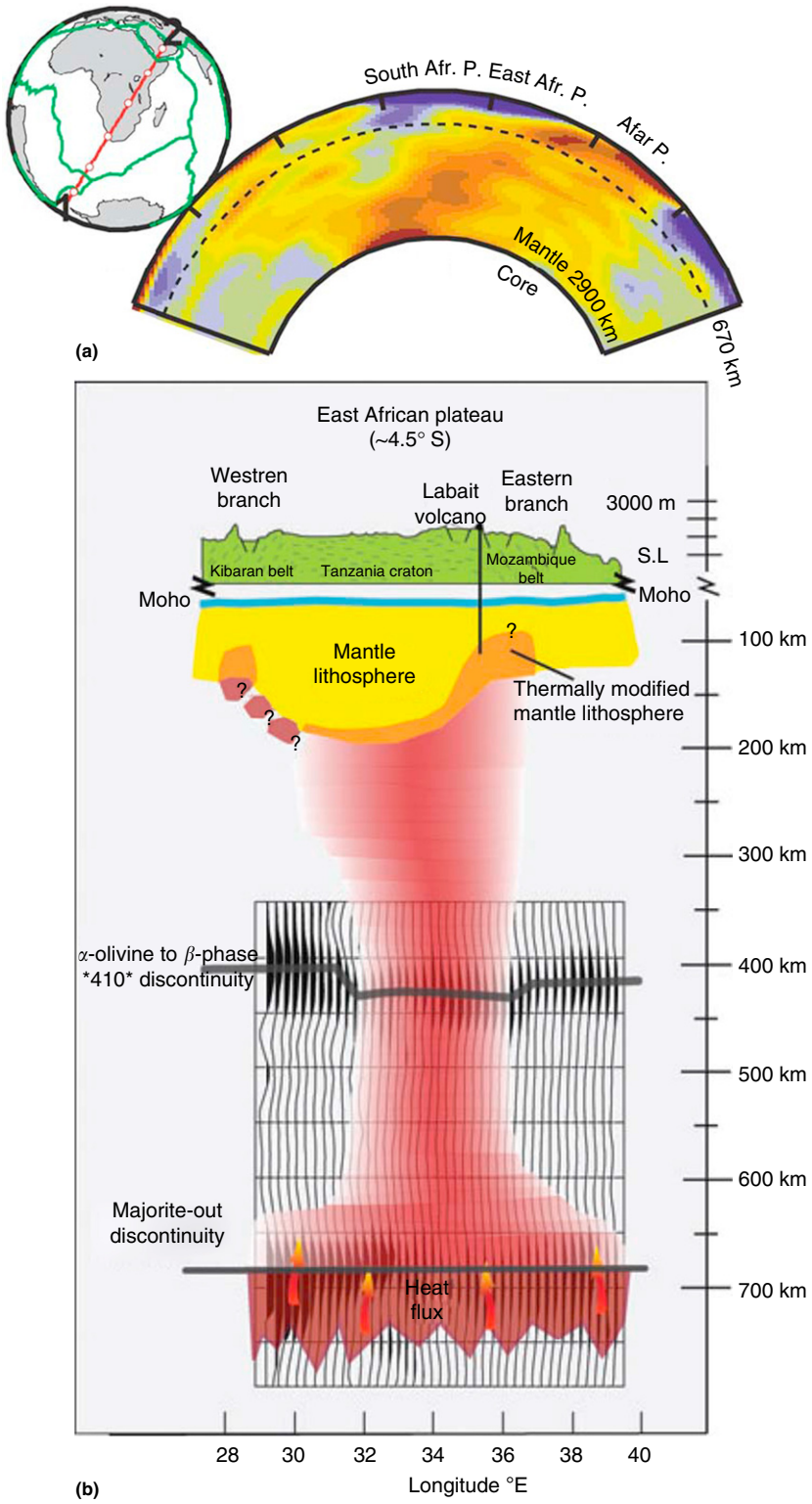

Figure 10 (a) Cross-sections through the South and eastern African plateaus, and across the Afar plateau, obtained from a tomographic model extending up to the core-mantle boundary along a 140° wide great circle arcs (inset). Relatively high velocity and low velocity regions are indicated by blue and red colors, respectively. The dashed line represents the 670-km seismic discontinuity. Reproduced from Ritsema, J., Heijst, H.J.V., Woodhouse, J.H., 1999. Complex shear wave velocity structure imaged beneath Africa and Iceland. Science 286, 1925–1928. (b) Schematic cross-section of the East African plateau at ~4.5° S showing receiver function stacks of mantle transition zone and cartoon of the associated thermal upwelling from Huerta, A.D., Nyblade, A.A., Reusch, A.M., 2009. Mantle transition zone structure beneath Kenya and Tanzania: more evidence for a deep-seated thermal upwelling in the mantle. Geophysical Journal International 177, 1249–1255, which is an updated version from Nyblade, A.A., Owens, T.J., Gurrola, H., Ritsema, J., Langston, C.A., 2000. Seismic evidence for a deep upper mantle thermal anomaly beneath east Africa. Geology 28, 599–602.

Harrison et al., 1992; Molnar et al., 1993) or for the successive surface uplift of external parts of the plateau incorporated into the plateau to produce its present shape (Tapponnier et al., 2001).

Plateaus in compressional settings, such as Tibet and the Andes, are associated with erosion, transport and sedimentation in now highly elevated endorheic sedimentary basins. Forward propagation of the deformation has been proposed as a mechanism for the progressive incorporation of endorheic basins in Tibet (Tapponnier et al., 2001) and in the Altiplano–Puna plateau (Sobel et al., 2003; Strecker et al., 2007). Based on the study of the Pyrenean landscape evolution and experimental modeling of surface processes interaction between rock uplift, erosion, and sedimentation it has been shown that the accumulation of sediments at the foot of mountain ranges produces a rise of the apex of sedimentation, that is, the effective base level for erosion, which in turn inhibits the erosion at high elevation (Babault et al., 2005a, b, 2007). Such processes, combined with the progressive incorporation of internally drained basins, allowed the formation of a low-relief topography in the Tibetan Plateau and in the Altiplano–Puna plateau during and after their rise (Babault et al., 2005a; Liu-Zeng et al., 2008).

5.6.1.6 On the Existence of Past High Plateaus in the Earth History

The demonstration of the existence of past high plateaus requires determining both the paleoelevation and the flatness of large continental areas. This is less easy for past high plateaus that have, by definition, disappeared. Paradoxically, the way they have been destroyed suggests their past existence. Indeed, currently very large areas of continental extension such as the Basin and Range Province are viewed as resulting from the collapse of overthickened crustal welts resembling high plateaus (Coney and Harms, 1984). The intense bimodal magmatism that accompanies extension in such areas is considered as indicative of the partial melting of the thermally relaxed crust and the underlying upper mantle (e.g., Buck, 1991; Dewey and Burke, 1973; Sonder and England, 1989), attesting to crustal thickening and therefore past high elevation of Earth's surface in those areas. But the main reason why this problem is so difficult to resolve relates to the problems of deciphering the paleoelevation of continents.

Paleoelevation is commonly deduced from reconstruction of crustal thickness assuming isostatic compensation, or from paleotemperature estimates through paleoenvironment and stable isotopes studies (see Section 5.6.2). Methods to determine paleoatmospheric pressures allowing the determination of paleoelevation, such as the use of basalt vesicularity are rare (e.g., Sahagian and Proussevitch, 2007; Sahagian et al., 2002a, see Section 5.6.2.5 of this chapter). Whatever the methods used, the results are subjected to debate, mostly because of the great margins of error associated with the methods used in providing paleoelevation estimates.

Coney and Harms (1984) estimated the amount of Tertiary extension in the Basin and Range to be between 40 and 75%. They concluded that the initial crustal thickness could have reached 60 km over a several hundred kilometers width and they suggested that, during the Late Mesozoic–Early Cenozoic times, this area resembled the present-day Tibetan Plateau. However, Coney and Harms (1984) did not provide any information regarding the flatness of this area so that they could not definitively argue the existence of a high plateau. Best et al. (2009) used the compositions of contemporaneous calc-alkaline lava flows as well as the configurations of the ignimbrite sheets to show that the Basin and Range Province during the middle Cenozoic was a relatively smooth plateau underlain by unusually thick crust. In particular, Best et al. (2009) observed that the generally small between-site variations in the palaeomagnetic directions of individual sheets lend further support for a relatively smooth landscape over which the sheets were draped and they conclude that during the middle Cenozoic this area was a relatively flat plateau.

Wolfe et al. (1998) compared the physiognomy of leaves from modern vegetation of known climates with that of Eocene and Oligocene fossil leaf assemblages from middle latitudes of western North America and they concluded that most of the western US and southern Canada was higher in elevation in early Cenozoic time than today. Moreover, where normal faulting has been intense, paleoelevations commonly suggest a subsidence of the region.

Menard and Molnar (1988) have suggested that the Variscan belt of Europe was a 'Hercynian Tibetan plateau' that collapsed into a 'late Paleozoic European Basin and Range Province.' Although most studies on the Variscan belt have concluded that the crust was significantly thickened during the Late Paleozoic, Menard and Molnar (1988) observed that Late Paleozoic sedimentary basins are presently juxtaposed with metamorphic basement rocks. Erosion cannot therefore explain the present-day crust thickness of 30 km. As no pervasive extensional tectonics occurred during the Mesozoic and the Cenozoic, Menard and Molnar (1988) concluded that the thickened crust returned to normal thickness by collapse during the Late Paleozoic, resulting in the exhumation of the deep crust and the concomitant development of sedimentary basins at the surface in a similar way to that of the North American Cordillera, in the western US, during the Cenozoic. Becq-Giraudon and Van Den Driessche (1994) and Becq-Giraudon et al. (1996) have tentatively argued the paleoaltitude of this Variscan belt and its morphology resembled that of a high plateau by looking at the characteristics of the late Carboniferous-early Permian continental sedimentation. In addition, Becq-Giraudon et al. (1996) remarked that the presence of many sedimentary futures such as stratified slope deposits, diamictites, water escape craters and ghosts of ice crystals are related to periglacial effects. The clay mineral assemblage, dominated by the association illite-chlorite-interlayed clays and the absence of significant weathering of feldspathic clasts and granitic pebbles favor the prevalence of a cold to temperate climate during sedimentation. The flora and entomofauna also indicate a seasonally varying climate with cold winters. Furthermore, the extreme homogeneity of the flora composition from one basin to another indicate a lack of appreciable altitude zoning and a plateau-like morphology (Becq-Giraudon et al., 1996). In view of the paleoequatorial position of the Variscan belt during the late Caboniferous-early Permian, Becq-Giraudon et al. (1996) concluded that the

morphology of the chain was that of a near 4500 m asl high plateau.

5.6.2 Evidence for Plateau Uplift, Regional Warping, and Subsidence

5.6.2.1 Geomorphic Markers

5.6.2.1.1 Low-relief, high-elevation erosional surfaces

A striking feature of high plateaus' margins is the occurrence of deeply dissected, almost flat topographic remnants at high elevation. As mentioned above (Section 5.6.1.5) and following Davis's cycle of erosion (1899), a smooth landscape generates from the destruction of a previous smooth landscape uplifted and then progressively more dissected and characterized by steeper slopes. This is followed by successive stages, with a decrease in slope gradients associated with the decrease of the elevations near to sea level. Based on these views, rock uplift is usually deduced from the elevation of more or less localized changes in the local slopes that separate a subdued relief above, also called a relict landscape (for a summary see Widdowson, 1997), from a steeper one below (e.g., Clark et al., 2006; Epis and Chapin, 1975; Gregory and Chase, 1994; Kennan et al., 1997).

Following Powell (1875), a stream cannot erode below its base level, which is the lower limit in the landscape and is ultimately represented by sea level. If the process of formation of low-relief erosional surfaces follows Davis' model, the key point to infer rock uplift from highly elevated remnants of low-relief erosional surfaces lies in the assumption that they formed close to sea level. Such assumption is however almost never demonstrated in orogens and plateaus because of the destructive nature of erosion or the lack of marine sedimentation on the low-relief erosional surfaces. Consequently, where it cannot be demonstrated that low-relief erosional surfaces developed close to sea level, it cannot be ruled out that a smooth landscape may have developed well above sea level. Within continents, if an erosional smooth landscape is 1000 km away from its base level and that the formational regional slope is 0.0057° (10^{-4}) or 0.057° (10^{-3}) then a low-relief erosional surface can develop 100 to 1000 m above its base level.

An alternative model of planation is that of parallel scarp retreat by backwearing of slopes (King, 1953). As that of Davis, in King's model a discontinuous surface uplift is responsible for the high elevation of a smooth landscape that starts to develop near the sea level. The plateau successively expands just above sea level by river incision, scarp retreat, and the formation of pediments at its base. Ongoing erosion creates pediments that coalesce to form a pediplain. A next surface uplift will promote a new planation surface near to sea level. However, ongoing lateral erosion of the first pediplain occurs above sea level and is disconnected from the younger pediplain by an escarpment. Pediments are broad, concave-up and sloping at an angle of 6–7° at the base of the retreating escarpment, whereas pediplains are inclined gently (commonly thought to be less than 1° although never demonstrated) toward the sea level. As a consequence, low-relief erosional surfaces developed in this way form near to sea level only close to the coast line. Such considerations imply that rock uplift cannot be deduced from their elevation alone, a correcting factor must take into account for the regional slope of erosion down to the coast.

Drainages of mountains and plateaus are not always open to the sea. Where streams flow into closed basins (endorheic basins), their base level is considered to be the basin floor or the terminal lake. In the Andes or in Tibet, for example, highly elevated endorheic basins cover extensive areas setting the base level for their streams at high elevation. But long-term landscape evolution of mountain belts argues for the apex of sedimentation in foreland basins to be the effective base level for erosion below which no erosion occurs on the long-term (Babault et al., 2005a, b; Carretier and Lucazeau, 2005), instead of a coastline or a lake's shoreline where drainages are opened or closed, respectively. Babault et al. (2005a, b) and Carretier and Lucazeau (2005) considered that it is not so much the ultimate base level of stream waters but the transport capacity of rivers, in controlling the long-term limit between the erosion and deposition, that sets the effective base level for erosion. In such a case, slopes and concavity of the rivers, of the alluvial and of the fluvial fans, control how high the elevation of the apex of sedimentation stands above the coastline or the terminal lake. Gradually over time, the aggradation of the products of erosion raises the base level when a sedimentary basin is overfilled, whether its nature is endorheic or not (Babault et al., 2005a). However, the apex of sedimentation, the effective base level in an endorheic basin can be expected to be always higher than that of a basin opened to the sea.

Davis' cycle of erosion in which a landscape is smoothed close to sea level can therefore be valid at high elevation whether drainage is endorheic or not, at least but not necessarily provided that tectonic uplift has ended (Babault et al., 2007). The same is true for the formation of stepped pediments in continental and internally drained areas like those of the Iberian range in Spain (e.g., Casas-Sainz and Cortes-Gracia, 2002). The corollary of this conclusion is that where remnants of low-relief erosional surfaces are bounded by overfilled sedimentary basins, smoothing might have occurred well above sea level. In such geological settings, rock uplift cannot be inferred from the elevation of remnants of low-relief erosional surfaces alone (Babault et al., 2005b, 2007). The paleoelevation of the apex of sedimentation as well as the distance from it and the fluvial paleogradient must be taken into account to infer rock uplift from smooth relict landscapes. Another requisite to infer rock uplift from relict landscapes is the slow long-term erosion rates of the remnant surfaces (e.g., Clark et al., 2006). High erosion rates of the remnant surfaces would lead to an underestimation of the rock uplift.

It is important to note that the above considerations of landscape evolution allow the inferring of rock uplift, but in most cases not surface uplift. When a high-elevation, low-relief landscape is incised by the modern fluvial system, surface uplift is always lower than rock uplift (Molnar and England, 1990). Another important point to underline is that the erosionally driven unloading of the crust induces a flexural isostatic rebound at the regional scale. Consequently, a fraction of the measured rock uplift has to be attributed to the isostatic response of the missing masses, whereas the

remaining fraction has to be linked to one or more deep processes in the crust or in the mantle (e.g., Abbott et al., 1997; Leonard, 2002; Roy et al., 2009).

In the Andes, ~2000 m of rock uplift have been deduced from the study of channel longitudinal profiles and in particular the reconstruction of past longitudinal profiles in the eastern Cordillera of Bolivia based on low-relief paleosurface remnants (Kennan et al., 1997). As defined above, uplift of low-relief paleosurface remnants, now incised by the current drainage network, is rock uplift and not surface uplift. In their topographic reconstruction at ~10 Ma, Kennan et al. (1997) obtained a downstream profile ranging from 500 to mostly 1500 m in elevation. Such results argue for the low-relief erosional surfaces of Bolivia to have developed above 500 to 1500 m depending on their distance from the coastline, ~25 to 325 km, respectively. Barke and Lamb (2006) reconstructed the paleoprofiles of the Eastern Cordillera using values of concavity and steepness (see Section 5.6.2.1.4) and they obtained a more accurate estimate of rock uplift at 1705 ± 695 m.

In the eastern Tibetan Plateau, Clark et al. (2006) deduced a minimum of 3000 to 4000 m surface uplift of the highest parts of the southeastern Plateau from the elevation of remnants of a high elevation, low-relief surface. Clark et al. (2006) based their reasoning on the low values of erosion (0.01–0.02 mm yr^{-1}) of remnant surfaces to argue that rock uplift can be deduced from relict landscape elevations, assuming a paleoslope to the east ranging between 0.0057° (10^{-4}) and 0.057° (10^{-3}).

5.6.2.1.2 Drainage network development and reorganization on a plateau

Although drainage development and reorganization might be complex in some cases it can be used to unravel the tectonic evolution of a region. Uplift influences drainages via baselevel changes, drainage reversals, and capture processes. The dictum 'Drainage systems have a heritage rather than an origin' (in Summerfield, 1991, Chapter 16) summarizes well the constant interaction between tectonics, erosion, and deposition. This view is opposed to an old and unrealistic one that considers that a drainage network originally grows on an initial slope before channels adapt their course to structure. Although drainage does not generally start to develop on a flat, gently sloping topography, overfilling of landscapes by lava flows or sediments can lead to a smoothing of the local relief and to the resetting of a previous channel network. The incorporation in an orogen of a drainage network newly formed in an overfilled foreland basin could, however, explain the similarity of network geometry in orogens (Castelltort and Simpson, 2006).

Where the local relief is low, a trunk of a gently sloping river can be reversed by only a slight regional tilt of the topography. This occurs only if the rate of incision downstream of that trunk cannot balance the rate of rock uplift. Plumes generate dome-like plateaus and consequently they can trigger a modification of the drainage network associated with drainage reversals and captures that eventually lead to a radial drainage (Cox, 1989). Later, such drainage can be more or less captured by a structurally controlled drainage that develops in a rift valley superimposed on the domal plateau like that of the East African plateau (Cox, 1989; Moore and Blenkinsop, 2002). The result of the channel network reorganization is a barbed drainage pattern with junction angles greater than 90°, see Figures 12.7 and 16.9 in Ollier (1981) and in Summerfield (1991), respectively.

Rock uplifts of plateaus induce a gain in potential energy that enhances the stream power (e.g., Whipple and Tucker, 1999) of the surrounding channels. Consequently, internally drained areas with higher local base level are expected to be captured by external transverse drainages with lower base level and located on rims of plateaus. If so, stream piracies can provide evidence of plateau uplift. Captures can be identified by a series of drainage patterns and deposits that indicate poorly–integrated drainage. These include the occurrence of hanging valleys with wind gaps in the drainage divide, and wind gap sediments (if preserved) in the headwaters of a beheaded river, elbows of capture, and a river paleoflow direction different than present flow direction (see Douglass et al., 2009, for a compilation of the various criteria). Drainage reorganization by captures have been used to indicate surface uplift in the southeastern Tibetan Plateau margin (Clark et al., 2004) and in the Anatolian plateau (Nicoll, 2010).

5.6.2.1.3 River longitudinal profiles: Steepness indices

Rock uplift increases the potential energy and triggers an increase in the stream power (e.g., Whipple and Tucker, 1999). Consequently, the increase in incision modifies the streams' morphologies, first at the rims of a plateau and eventually inside the plateau. The downstream slopes of rivers increase and in most cases knickpoints develop (Whipple and Tucker, 1999). Local slopes are not the only variable in bed morphology that rock uplift can potentially modify; channel width, (e.g., Whittaker et al., 2007) and sinuosity (among others) can also be affected and in turn they can change the relationship between local slopes and rock uplift (See Wobus et al., 2006, for a review). However, a relation between rock uplift and downstream slopes has been highlighted in many different natural landscapes. In the following the authors summarize the methodology developed to derive rock uplift from digital elevation models, which is based on the empirical power-law that relates the downstream slope in a river bed to the contributing drainage area (Flint, 1974; Howard and Kerby, 1983):

$$S = k_s A^{-\theta}$$

where S is the local downstream slope, A is the upstream drainage area, θ is the concavity index and k_s is the steepness index. Studies in California (Snyder et al., 2000) and in the Siwalik Hills in front of the Himalaya (Wobus et al., 2006) demonstrated a positive correlation between the steepness indices of a set of channels with comparable morphologies (normalized to a common concavity index), and spatially uniform rock uplift rates encompassing each drainage basin. In these studies, steady-state conditions are assumed, that is, rock uplift is everywhere balanced by erosion. Inference of rock uplift rates using steepness indices derived from digital elevation data requires first a calibration area with known uplift rates and similar channel morphologies. If not, the spatial variability of steepness indices provides at least a high spatial resolution estimate of the rock uplift pattern

(Hodges et al., 2004; Wobus et al., 2003). Special care must be taken in the interpretation of steepness indices as a proxy for rock uplift rates. Rock uplift rates not only modify the local slopes leading to a simple relation between steepness indices and uplift rates. Steepness index depends also on other factors (e.g., Whipple, 2004; Whipple and Tucker, 1999) including rock strength (erosivity), sediment flux (tools for erosion or cover of the bedrock that inhibits erosion), channel width, drainage basin hydrology, river incision process(es) (plucking, abrasion, and weathering) and critical shear stress for incision. For example, where the pattern of the channel width, W, with respect to the cumulative drainage area, A, varies downstream in a different fashion from that commonly assumed, $W = 0.35A^{0.5}$ (Montgomery and Gran, 2001), steepness indices may not reflect rock uplift rates. Fluvial erosion is commonly understood to scale with bed shear stress and water flow velocity. Both variables depend on the local slope and on the channel cross-sectional geometry. Consequently, local channel width and water depth modifications can strongly alter the relationship between steepness indices and rock uplift rates (e.g., Whittaker et al., 2007). That some of the parameters listed above might be expected to vary with tectonic rates and consequently alter the significance of the steepness index, it is not the only limitation to use it as a proxy for rock uplift rates. It is important to note that some of the parameters listed above vary with lithology and climate. However, local significant variations of steepness indices values are thought to reflect changes in rock uplift rates, where the spatial variations of the factors listed above are negligible (Wobus et al., 2003).

In the eastern Tibetan Plateau, this method has been used to infer the distribution of active rock uplift (Kirby et al., 2003). However, since the obtained steepness indices are assumed to relate to the rates of rock uplift, no total amount of rock uplift can be derived from this method alone until the duration of the considered tectonic event is known.

5.6.2.1.4 Longitudinal paleoprofile reconstruction of rivers

The total amount of rock uplift can be deduced from the reconstruction of a river's paleoprofile. Two methods can be used based on the longitudinal profile equation and paleomarkers of the river longitudinal profile such as river terraces.

The first method relies on the study of a series of rivers characterized by segments bounded by a knickpoint. First, it is assumed that an increase in fluvial incision in response with a sudden base level fall, or an increase in the rate of a base level fall (conceptually equivalent to an increase in rock uplift), propagates upward along a channel and is associated with a knickpoint that separates an unmodified upstream part from a downstream segment that adapts its slopes to the new boundary conditions imposed by the new rock uplift rate (e.g., Whipple and Tucker, 1999). Second, it is assumed that the upstream part corresponds to a river profile that is adjusting or adjusted to a prior state of base level fall. Third, incision rates in the upstream part above the knickpoint must be slow, a condition matched under dominated semiarid to hyperarid climate conditions as indicated by the preservation of transient landscape, such that profile lowering is negligible and the inferred rock uplift is not underestimated. Under those assumptions an empirical power-law gradient–area relationship can be used (Flint, 1974; Howard and Kerby, 1983) along with the well-known relationship between downstream distance, x, and cumulative drainage area (Hack, 1957) to reconstruct a river paleoprofile from the equation of a longitudinal river profile elevation, $z(x)$, in two dimensions (Whipple, 2001; Whipple and Tucker, 1999):

$$z(x) = k_s k_a^{-\theta}(1 - h\theta)^{-1}(L^{1-h\theta} - x^{1-h\theta}) + z(L); \quad h\theta \neq 1; \quad x_c \leq x \leq L$$

where z is the elevation, x_c is the distance from the division to the channel head, L is the distance of outlet from source, k_s is the steepness index, θ concavity index, k_a is Hack's coefficient, and h Hack's exponent. The river paleoprofile is obtained from a fit of the longitudinal river profile elevation equation, $z(x)$, to the preserved paleoprofile in the upstream parts. The difference in elevation between the reconstructed profile set high up and the modern downstream segment at the outlet elevation provides an estimate of the rock uplift even if it is not spatially uniform (e.g., Hoke et al., 2007).

In the Andes, at least 1000 m of relative rock uplift of the Western Cordillera and adjacent central Andean plateau with respect to the Central Depression, located between the Pacific coast and the Western Cordillera, has been deduced using this method (Hoke et al., 2007). Based on perched paleoprofiles near to the Pacific Coast, Hoke et al. (2007) also proposed that the Central Depression could have undergone a rock uplift of 1000 m. If this interpretation can be confirmed by another proxy, and if the Central Depression is not tectonically decoupled from the Altiplano, then ~2000 m of rock uplift of the Western Cordillera and adjacent central Andean plateau can be deduced from the paleoprofiles reconstruction. Using a similar approach, 2000–2700 m of rock uplift have been estimated for the Eastern Cordillera at the eastern edge of the paleodrainage systems that drained the Eastern Cordillera as indicated by the paleosurface remnants and the associated fluvial deposits (Barke and Lamb, 2006). Barke and Lamb (2006) also inferred rock uplift from upstream propagation of the modern river profile and its difference in elevation with respect to the paleosurface remnants, and the heights above the foreland basin of the knickpoints that separate the paleodrainage system from the modern downstream profiles. From the combination of all these measures they obtained a value of 1705 ± 695 m for rock uplift for the eastern edge of the Eastern Cordillera.

In the eastern margin of the Tibetan Plateau, Schoenbohm et al. (2004) calculated the Red River incised ~1400 m in the regional low-relief landscape from the paleoprofiles of a series of perched tributaries above the Red River. Since the paleoprofile of the Red River is estimated at 1500 m and considering that it has risen from 0–100 m, sea level and present day elevation respectively, they deduced a value of 1400–1500 m for surface uplift in the Red River region (Yunnan Province of China).

The second method to derive an amount of rock uplift is based on paleomarkers of the river profile such as river terraces. The strong assumption is that rock uplift is balanced by river incision (e.g., Burbank et al., 1996). However, such assumption is difficult to demonstrate in most cases, and because river incision is not only a response to rock uplift, then

this method has to be validated by other data. For example, climate can be responsible for incision in the piedmont leading to a fall of the base level, which results in an upstream propagation of incision in the mountainous area without any change in rock uplift (e.g., Carretier and Lucazeau, 2005). Upstream integration of drainage areas by river network growth also leads to deep incisions in the downstream parts of a longitudinal profile (e.g., Carretier et al., 2009; Vassallo et al., 2007). In both cases paleoriver profiles will overestimate rock uplift.

5.6.2.2 Paleoaltimetry from Sedimentology

To understand the continental tectonic processes responsible for surface uplift, and to understand how the feedbacks between such tectonic processes and climate and erosion processes modify the surface uplift, the appropriate paleoaltimetric methods need to be used. As pointed out by Clark (2007), a need exists to assess the paleo-mean elevation of region, not only the local paleoelevation. This comes from the fact that, although an increase in local elevations, local relief or drainage basin relief can be associated to some rock uplift, it does not necessarily indicate a surface uplift (an increase of the mean elevation) (Molnar and England, 1990).

5.6.2.2.1 Paleoaltimetry from marine sediments

The easiest way to infer rock uplift is from the elevation of the youngest shallow marine sediments preserved in the studied region (including eustasy). The choice of mapping the youngest strata instead of an older strata preserved everywhere has the advantage to minimize the underestimation of rock uplift when the upper limit of the marine unit is partially eroded (e.g., Pederson et al., 2002). Any localized incision or spatially homogenous erosion into these marine sediments implies that a fraction of the rock uplift is to be attributed to the erosionally driven isostatic rebound. As a consequence the deduced rock uplift does not match the necessarily lower surface uplift. An important constraint for any tectonic model of plateau uplift can be deduced from the surface uplift rate. However, the ratio between the elevation and the age of the youngest shallow marine sediments only gives a minimum estimate of the mean rock uplift rate since a time-lag can exist between the depositional age and the subsequent rock uplift. In the following the authors show two examples of surface uplift deduced from marine strata.

In the Colorado Plateau, the Late Cretaceous landscape reconstruction represents the last known time surface elevation. Based on the widespread distribution of the Late Cretaceous shallow-marine and coastal sediments, Roy et al. (2009) estimated the Colorado Plateau underwent $\sim$1.9 km of rock uplift using data from the previous work of Pederson et al. (2002) and taking into account that the Late Cretaceous sea level was 200 to 250 m higher than today. Roy et al. (2009) estimated $\sim$0.5 km of net erosion (erosion minus sedimentation) during the Cenozoic, taking into account the amount of erosion of the Late Cretaceous marine sediments and the amount of preserved younger continental deposits and volcanic rocks. To the rock uplift associated with erosional-unloading, Roy et al. (2009) added the flexural response of the plateau to the tectonic unloading at the plateau margins where extension took place during the Cenozoic (Basin and Range and Rio Grande Rift). They obtained $\sim$0.5–0.6 km and $\sim$1 km of rock uplift associated with crustal unloading (erosion and extension) at the center of the plateau and at the edges, respectively. They deduced that $>$1.6 km of the remaining mean rock/surface uplift must be explained by tectonic processes that occurred during the Cenozoic. In summary, widespread evidence of sea level or slightly below sea level paleoelevations are very useful where preserved to deduce rock and surface uplift.

The Andes were also at sea level during the Cretaceous such that the surface uplift of the Altiplano must have been later (e.g., Hoke and Garzione, 2008). In contrast, on the southern Tibetan Plateau, Fielding (1996) deduced 5 km of surface uplift from Cretaceous marine limestone deposited in the Lhasa block (Hennig, 1915; Norin, 1946). As Fielding (1996) noticed, it is difficult to generalize the paleoelevation of an extensive region like the Tibetan Plateau from just a small part of it, given that Tibet results from the accretion of several crustal blocks and volcanic arcs associated with oceanic subduction under the southern margin of Asia before the collision. If the Andes are a contemporary analog of what Tibet was like before the collision between India and Asia, then mean elevations were probably well above the sea level, at least in some part of it (Fielding, 1996). Consequently, the 5 km surface uplift since the Cretaceous (Fielding, 1996) might be an overestimation when applied to the whole of Tibet.

5.6.2.2.2 Paleoaltimetry from paleohorizontality of lacustrine sediments

Some shallow lake deposits form in flat regions where they can be used to deduce differential rock uplift. Changes in elevation between deposits of the same age and of the same facies that cannot be accounted for by any variation in depositional depth indicate relative rock uplift. South of the Eastern Moroccan Atlas belts and plateau, the remnants of the lower Pliocene shallow lacustrine sedimentation closer to the Atlas lie at $\sim$1200 m asl and the more distant at $\sim$600 m asl. The $\sim$600 m difference of elevation have been inferred by Babault et al. (2008) as a postdepositional tilting to the south indicating up to $\sim$600 m of relative rock uplift of the southern margin of the Atlas since the early Pliocene. If the lake deposits are assumed to have not undergone subsidence and the elevation of the lower deposits is considered to have remained the same, such estimate corresponds to minimum rock uplift.

5.6.2.2.3 Paleoaltimetry from paleoslopes: Large-scale patterns of deposition

Postdepositional changes in slope can also be determined from fluvial sediments or erosional landforms.

Since slopes in braided rivers are generally less than 1.14° (Paola and Mohrig, 1996) then greater slopes can be used to deduce a tilt of such depositional surfaces. Moreover, paleoslopes can be back calculated in order to quantify more accurately the amount of tilting. The method is based on the assumption that the basal shear stress at bankfull stage has to be higher than the critical shear stress required to transport the coarsest clast (Paola and Mohrig, 1996). The paleoslope is

then derived from measuring the median clast size in channel scours and the depth of such ancient channels of preserved coarse-grained braided rivers. Errors from this method come from the underestimation of the paleodepth resulting in an overestimation of the paleoslope by $30-40\%$, and from the underestimation of the surface grain size leading to an underestimation of the paleoslope by $30-40\%$. Paola and Mohrig (1996) compared estimated values of slopes from their formula to the actual slopes of modern braided rivers and they show that the error in the estimated slopes is about a factor of 2.

McMillan et al. (2002) have shown that the paleoslopes to the east of the Rocky Mountains piedmont, estimated using the method of Paola and Mohrig (1996), ranged between $\sim 0.006^\circ$ to $\sim 0.06^\circ$ during the Miocene–Pliocene and that they have been subsequently increased up to $\sim 0.6^\circ$. The Great Plains are connected to the Rocky Mountains that are themselves connected to the south to the Colorado Plateau and defined the Rocky Mountain orogenic plateau (McMillan et al., 2006). As a consequence, the regional rock uplift associated with the tilt to the east observed in the Great Plains over 250 km has then been used to infer 680 m (410–815 m) of regional rock uplift that affected the whole Rocky Mountain orogenic plateau (McMillan et al., 2002).

The same concept has been roughly applied to the western flank of the Western Cordillera in the Andes of Chile. Based on the models of Stanistreet and McCarthy (1993), the depositional slope of the Oligocene–Miocene braided fluvial fan that mantle the Paleozoic basement of the Precordillera of northern Chile, in the western flank of the Altiplano have been assumed to be less than 1°. Today these piedmont sediment dips varies between 2° and 4° to the West and such westward tilts have been used to infer a post-10 Ma rock uplift of the Western Cordillera (Mortimer, 1973; Riquelme et al., 2003) ranging between 500 and 1400 m (Farías et al., 2005).

5.6.2.2.4 Grain size distribution in piedmont sedimentation

If it is assumed that an increase in rock uplift of the upstream mountainous areas induce both a change in the sedimentary flux that enters the basins from the rivers draining the rim of a plateau and the slope of the streams, then a change in facies can be expected from fined-grained sediments to clasts and boulders as well as higher sedimentation rates. However, erosion and transport also depend on water discharge, which is subject to changes throughout the history of plateau building in response to regional or global climate changes (e.g., Blackstone, 1975; Frostick and Reid, 1989). Consequently the relation between grain size and rock uplift is not straightforward (e.g., Molnar and England, 1990) and overall, the method does not allow any quantification of either rock uplift or surface uplift.

A change in depositional facies in the northwestern Tibetan Plateau and southern margin of the Tarim basin is interpreted as a response to a main rock and surface uplift of the Kunlun Mountains with respect to the Tarim basin (Zheng et al., 2000). The shift from distal alluvial fan or flood-plain environments to proximal debris-flow accumulation is associated with an increase in sedimentation rate from an average $\sim 0.15\ \mathrm{mm\ yr^{-1}}$ to $1.4\ \mathrm{mm\ yr^{-1}}$, as well as growth strata (Zheng et al., 2000). Such association of increase in grain size, as well as sedimentation rate can be interpreted as the evidence for the main rock/surface uplift of the northwestern Tibetan Plateau (Zheng et al., 2000).

5.6.2.3 Paleoaltimetry Data Based on Paleobotany

Three methods that analyze plant physiognomy have been proposed to infer paleoaltimetry. Two of them use floras (1) to estimate temperature then divided by lapse rate (the rate of temperature change with elevation) to give an elevation, and (2) to estimate enthalpy that is combined with gravitational acceleration to deduce an elevation. The third method uses stomatal frequency in leaves to deduce changes in CO_2 partial pressure, which is a function of elevation.

Within the first method, paleotemperatures from fossil floras, three fundamentally different approaches are used (see Meyer, 2007, for a review). The first two are based on the climatic distribution of nearest living relatives (or the floristic method), and on the correlation of plant physiognomic characters with climate. The third differs by the way the lapse rates can be utilized to derive a paleoelevation. Most of the current methods use the plant physiognomic method rather than the nearest living relatives, which is believed to be less accurate. Following the work of Bailey and Sinnott (1916) that demonstrate that leaf margins correlate with climate in modern floras, the plant morphological characters used in the physiognomic method include leaf size and the presence or absence of teeth. An extensive database called the Climate-Leaf Analysis Multivariate Program (Wolfe, 1993, 1995; Wolfe and Spicer, 1999) relates many physiognomic characters of leaves from modern forests to climate variables (e.g., untoothed leaf margins correlate to warm mean annual temperature and large leaf size correlates to high levels of moisture). The main results of the Climate-Leaf Analysis Multivariate Program is that the mean annual temperature is the most accurate climatic parameter estimated (1σ error $\leq 1\ ^\circ\mathrm{C}$). Giving that temperature change varies with elevation, continentality, and the effect of broad uplifted land surfaces, three different lapse rates exist depending on the spatial scale considered with values ranging between $3\ ^\circ\mathrm{C\ km^{-1}}$ in the regional (between the coast and the continental interior of a continent) lapse rate method (Wolfe, 1992a), $5.5\ ^\circ\mathrm{C\ km^{-1}}$ in the global mean terrestrial lapse rate (e.g., Axelrod, 1966), and 3.64 to $8.11\ ^\circ\mathrm{C\ km^{-1}}$ in the local lapse rate method (e.g., Meyer, 1992). Almost the double of palaeoelevation estimate can be derived from the regional instead of the global lapse rate, highlighting the major impact lapse rate has on the paleoelevation calculations.

Global climate changes through time imply that the mean temperature at a given altitude does not remain constant. As a consequence, paleotemperature estimates at a given locality must be compared to paleotemperature estimates at sea level for isochronous floras. The late Eocene Florissant flora of central Colorado is a good candidate to estimate the error of the different methodologies employed to deduce paleotemperature from fossil floras and paleoatlimetry from lapse rates methods since it has been studied by many workers using one or more of these methods (Meyer, 2007). Excluding low elevation estimates (455 m) derived from the global

lapse rate method (Axelrod, 1998) the estimates of paleoelevation range between 1900–3200 m (Meyer, 1992) and 1900–2300 m (Gregory, 1994; Gregory and Chase, 1992; Gregory and McIntosh, 1996) for the local lapse rate method and values of 2900 m asl (Wolfe, 1992b) and 4133 m asl (Wolfe, 1994) are obtained using the regional lapse rate method. All these studies lead to a high to very high paleoelevation range of 3000 ± 1100 m asl. In the second method, paleoelevation from fossil leaves is obtained from the moist static energy, h ($J\,Kg^{-1}$) (Forest, 2007; Forest et al., 1995, 1999). In the mean annual temperature method, present lapse rates are transferred to past climate with no meteorologically sound physical basis and such empirical lapse-rates with large spatial variations (Meyer, 1992; Wolfe, 1992a) are used to infer paleoelevation leading to estimates that can vary by a factor of two. Unlike the mean annual temperature method, the aim of the moist static energy method is to quantify a variable with a theoretically and by observation, well-constrained behavior with altitude and longitude. At mid-latitudes the mean flow of the atmosphere is from west to east. Since moist static energy is conserved along air masses it is also generally constant across a region with longitude. Finally, moist static energy is constrained by thermodynamics such that

$$h = c_p' T + L_v q + gZ,$$

where c_p' is the specific heat capacity at constant pressure of moist air, T is the temperature (in K), L_v is the latent heat of vaporization for water, q is the specific humidity, g is the gravitational acceleration, Z is altitude, and

$$H = c_p' T + L_v q,$$

where H is moist enthalpy.

Assuming that h is invariant within the same latitudinal band, if we can estimate the enthalpy at sea level and at a site of unknown elevation Z for a particular latitude, then such elevation is given by (Forest, 2007; Forest et al., 1995, 1999)

$$Z = \frac{H_{\text{sealevel}} - H_z}{g}.$$

Both enthalpy estimates are derived from fossil leaf assemblage with the Climate-Leaf Analysis Multivariate Program. The total expected error in this method comes from two sources of error (Forest, 2007; Forest et al., 1999): (1) from the standard deviation from zonal invariance (the longitudinal variability) of h (yielding a minimum estimate of the error in altitude of 460 m); and (2) from the uncertainty in predicting mean annual enthalpy from fossil leaf physiognomy (yielding 560 m of uncertainty in altitude). Forest et al. (2007, 1999) estimated the paleoelevation difference between two isochronous fossil assemblage sites is ± 910 m assuming that the expected errors apply to past.

Recently, Peppe et al. (2010) argued that many sources of large potential error are related to this method. Specifically, they demonstrated a significant bias toward underestimation of leaf area in the Climate-Leaf Analysis Multivariate Program data set affecting all predicted climatic variables such as enthalpy, leading to an uncertainty in mean annual enthalpy higher than that predicted by Forest et al. (1999). Errors in paleoelevation estimates when the leaf size bias is included are ± 2000 m or more. Peppe et al. (2010) concluded that among others, this bias affects previously published paleoelevations inferred by this method and that such paleoelevations are unlikely to be accurate either in magnitude or estimated error (e.g., Forest et al., 1995; Gregory-Wodzicki, 1997; Spicer et al., 2003; Wolfe et al., 1997, 1998).

The third method is based on the stomatal frequency change over altitudinal gradients (Kouwenberg et al., 2007; McElwain, 2004). Atmospheric pressure decreases with altitude and is shown to depend on the molecular weight of air, elevation, acceleration due to gravity, the gas constant and mean July temperature (Jones, 1992). CO_2 partial pressure is a fraction of the atmospheric pressure that does not vary with altitude (Gale, 1972). The globally averaged atmospheric pressure at sea level has not changed significantly over the Cenozoic and the available estimates of molar volume of CO_2 at sea level are sufficiently accurate for the Cenozoic. Consequently, the CO_2 partial pressure at any elevation is a function of the CO_2 partial pressure at sea-level and the atmospheric pressure divided by a constant (Beerling and Royer, 2002; McElwain, 2004; McElwain et al., 2002). McElwain (2004) shows an inverse relationships between stomatal density of plant leaves and the CO_2 partial pressure, converting the stomatal density into a potential tool to infer paleoaltimetry, independent of ecological or local climatic variability. This is true for many species but not all. Therefore the sensitivity of the selected fossil leaves needs to be tested as well as the response limit to high or low CO_2 partial pressure due to morphological and physiological constraints (Kouwenberg et al., 2007). This method applies to extant floras since stomatal density of modern leaves of same or close to the fossil species need to be calibrated to CO_2 partial pressure or elevation (Kouwenberg et al., 2007). McElwain (2004) obtained a ± 300 m of average error. However, Kouwenberg et al. (2007) highlighted other types of errors such as the light intensity-related uncertainties due to mixture of sun and shade leaves and varying for different species, and from uncertainties in exact sea-level CO_2 concentrations. For the species studied by McElwain (2004) and Kouwenberg et al. (2007) estimated errors related to the light intensity give error ranges of 162 and 558 m whereas errors introduced in estimating sea-level CO_2 from proxy data when sea-level CO_2 estimates on the same species are not available, hypothetically range between ± 450 m and ± 1200 m and could increase to ± 1400 m (Kouwenberg et al., 2007). When the uncertainty in sea-level CO_2 estimates is high, such method is not better than the others based on paleobotany, whereas it is the best one when sea-level CO_2 estimates from proxies are accurate or modern low-elevation leaf of extant species available (Kouwenberg et al., 2007).

In summary, the paleoelevations inferred in the Rocky Mountain orogenic plateau from paleobotanic methods indicate the plateau was already high in the late Eocene but the accuracy of such estimates are low, more than ± 1100 m, and the many factors that influence the character of the flora prevent a reliable estimation of the accuracy of the paleoelevation. The new paleoaltimetric method based on stomatal frequency and stomatal index may be a good alternative in the

particular cases where the uncertainty in sea-level CO_2 estimates is low.

In the case of the Altiplano–Puna plateau of the Andes, paleoelevation estimates from fossil floras (nearest-living-relative and foliar-physiognomy methods) now lying at 4000 to 4300 m asl argue for low elevations at 1000 m asl in the early Miocene (25 to 19 Ma) and ranging from 0 m to 2800 m asl in the mid Miocene ($\sim$20 to $\sim$10 Ma) but with large uncertainties ranging from $\pm$1200 to $\pm$2000 m (see Gregory-Wodzicki, 2000 for a review).

5.6.2.4 Paleoaltimetry Data Based on Stable Isotopes

5.6.2.4.1 Paleoaltimetry data based on the stable isotopic records ($\delta^{18}O$ and $\delta^{2}H$) of carbonates derived from meteoric and surface waters

Empirical and theoretical approaches have used the $\delta^{18}O$ and the $\delta^{2}H$ to deduce paleoelevation estimates. The condensation of water vapor driven by the ascension of regional winds along orographic obstacles creates a fractionation of H and O in atmospheric water vapor, rainfall, and snowfall. At the equilibrium water-vapor transformation, heavy isotopes (^{18}O and ^{2}H (D)) are removed from water vapor because they form stronger bonds than those formed by lighter isotopes (^{16}O and ^{1}H) which are more likely to break and to remain in the gas phase. Consequently, rainfall is enriched in heavy isotopes, whereas continuing rising air is depleted in heavy isotopes and the observation of decreasing in $\delta^{18}O$ and $\delta^{2}H$ values in rainfall as elevation increases has been used as a proxy for paleoelevations.

Rowley et al. (2001) and Rowley and Garzione (2007) have presented a theory that tracks the change in oxygen isotopic composition of precipitation based on the equilibrium fractionation during Rayleigh distillation coupled with the thermodynamics of atmospheric ascent and water vapor condensation. In their model, however, the complex processes involved in the conversion from condensate to precipitation and its influence on isotopic compositions is based on an empirical relationship (based on data from the Alps). They show that low-elevation temperature primarily controls the vertical distribution of condensation whereas low-elevation relative humidity only results in a small contribution. The low-elevation temperature, especially, and to a lesser degree the relative humidity, consequently control the vertical distribution of the difference in isotopic composition ($\Delta(\delta^{18}O)$) between a low, preferably near sea level, composition of meteoric water and a potentially elevated sample of meteoric water. Their model fits well with the modern vertical profiles of $\delta^{18}O$ in precipitation (Rowley and Garzione, 2007). Hence, they theoretically demonstrate that $\Delta(\delta^{18}O)$ can be used as a measure of elevation with a greater accuracy of the modeled elevations at higher elevations, and a general tendency of the modeled elevations to be underestimated. Where the low-elevation temperature and the relative humidity of local climate is used, instead of global means, the model is also more accurate (Rowley and Garzione, 2007).

Studies that track paleoelevation changes through geological times generally use carbonates derived from surface of ground waters that integrate precipitation waters. The quantity of precipitation varies along months and seasons with precipitations of different isotopic compositions. It explains why the mean isotopic composition at any given station is precipitation amount-weighted. Streams also spatially integrate precipitation above the sample site with isotopic compositions that vary with elevation. But the frequency of elevations within a catchment (the hypsometry) is not a linear function and must be computed individually. Furthermore, the amount of precipitation also varies as a function of elevation (Anders et al., 2006; Rowley and Garzione, 2007). Consequently, the isotopic compositions of surface water reflect the amount of precipitation falling as a function of elevation on that hypsometry: the precipitation amount-weighted hypsometric mean elevation of Rowley and Garzione (2007). An important conclusion is that the isotopic lapse rate of precipitation and that determined by surface waters are expected to be different (Rowley and Garzione, 2007).

In the following, important advantages, restrictions and uncertainties inherent of the methods, and highlighted by Rowley and Garzione (2007), are briefly summarized.

First, since the resulting paleoelevation corresponds to the precipitation amount-weighted hypsometric mean elevation, it does not give any information on the distribution of drainage basin elevations and particularly on the maximum elevations. For that reason estimates of paleoelevations from low-elevation samples of fluvial origin taken in foreland basins cannot discriminate between plateau-like topographies and rugged mountains, both implying different tectonic implications. Intermontane basins at higher elevations are then considered to be better targets to reduce the effects of the hypsometric and elevation dependence (e.g., Garzione et al., 2006; Ghosh et al., 2006b).

Second, past climates were globally warmer than today leading to a shallower isotopic lapse rate, which means that the use of modern isotopic lapse rate underestimates paleoelevations in the cases past-climates were really warmer.

Third, evaporation of precipitation in the atmosphere before reaching the ground or in stream waters results in ^{18}O enrichment relative to ^{2}H when plotted against the Global Meteoritic Water Line. Data from regions where evaporation occurs do not fit the model of Rowley et al. (2001), or Rowley and Garzione (2007). Although sedimentary carbonates reflect as well as stream waters various sources with hypsometric and elevation-dependent precipitation amount effects as potentially evaporation effects, paleosol carbonates have the advantage to reflect rainfall that directly infiltrates through the soil making them potentially better proxies for local rainfall composition estimates.

Fourth, although isotopic compositions of precipitation may be highly variable at short time scales, the low values of carbonate sedimentation rates imply that samples integrate isotopic compositions at least over thousands of years and maybe tens of thousands of years. This is an advantage to deduce the long-term variation of Δ ($\delta^{18}O$) and the associated changes of elevations.

Fifth, the isotopic composition of carbonates is different, however, from that of surface waters from which they precipitate, with an additional fractionation of oxygen isotopes that depend on the temperature ($\sim -1\%$ each $5\,^{\circ}C$).

Consequently, the assumption of a given paleotemperature when the carbonate formed adds a significant uncertainty for calculations of paleoelevations. Mean annual temperature can, for example, be deduced from the Climate-Leaf Analysis Multivariate Program (Wolfe, 1993, 1995; Wolfe and Spicer, 1999). However, it may neither correspond to the temperature of formation of paleosol carbonates since they are associated with evaporation events that only occur during the dry season, or during the growing season when evapotranspiration rates are highest (Cerling and Quade, 1993; Liu et al., 1996), nor the temperature of formation of lacustrine carbonates since they form during the summer when the evaporation rates are highest and the carbonate solubility is lowest (e.g., Duston et al., 1986; Effler and Johnson, 1987). The recently published carbonate thermometer based on ^{13}C-^{18}O bonds is however a good alternative to deduce the mean temperature of carbonate formation and finally, knowing $\delta^{18}O$ of carbonates, to calculate the $\delta^{18}O$ of meteoric water from which they form. Rowley and Garzione (2007) also pointed out that diagenesis can also alter $\delta^{18}O$ of carbonates where temperature of recrystallization exceeds 40 °C, leading to useless carbonates for paleoelevation estimates. In summary, the uncertainties in this method come from various sources like the low-elevation temperature used in modeled $\delta^{18}O$ of meteoric waters, the dispersion of the data used to deduce empirical isotopic lapse rates, and the temperature of carbonate precipitation (see Rowley and Garzione, 2007 for more details), and are estimated to range between ± 400 to ± 500 m (1σ errors) at paleoelevations higher than 4000 m asl to ± 1000 m at paleoelevations lower than 500 m asl (errors are deduced from bootstrap simulations in both the Andes and the Himalaya/Tibet). However, other errors come from global or local climate changes, as well as from the evaporation of surface waters, but their impact on the accuracy of paleoelevation estimates is not easy to quantify (Rowley and Garzione, 2007).

5.6.2.4.2 Paleoaltimetry data based on the abundance of $^{18}O^{13}C^{16}O$ (Δ_{47}): The 'carbonate clumped' isotope paleothermometer

Recently a new technique has been developed to estimate paleoelevations using a new paleothermometer: the 'clumped-isotope' Δ_{47} (Ghosh et al., 2006a). The ionic group $^{13}C^{18}O^{16}O_2^{-2}$ is a multiply substituted isotopolog in carbonate minerals. The two heavy isotopes make it to have lower zero-point energies than its isotopically 'normal' and singly substituted relatives ($^{12}C^{16}O_3$, CO_3, COO_2, and COO_2). A direct consequence is that rare isotopes are clumped by a thermodynamic driving force creating bonds with each other instead of being randomly dispersed throughout the mineral lattice. The abundance of multiply substituted molecules increases with decreasing temperature (Wang et al., 2004). The abundance of $^{13}C^{18}O^{16}O$ (mass 47) in CO_2 produced by digesting a carbonate mineral in phosphoric acid has been shown to be proportional to the abundance of $^{13}C^{18}O^{16}O^{-2}$ in carbonates (Ghosh et al., 2006a). It is hence possible to measure the $\delta^{18}O$, $\delta^{13}C$, and abundance of Δ_{47} isotopologs (mostly $^{13}C^{18}O^{16}O$) in the product CO_2 (e.g., Ghosh et al., 2006b). The abundance of $^{13}C^{18}O^{16}O$ (mass 47) is measured relative to $^{16}O^{12}C\ ^{16}O$ (mass 44) and called R^{47}. R^{47} is normalized by the R^{47}_{random} and called:

$$\Delta_{47} = (R^{47}_{measured}/R^{47}_{random} - 1) \times 1000),$$

with R^{47}_{random} calculated from the random distribution of heavy isotopes in the sample based on the measured $\delta^{18}O$, $\delta^{13}C$ values (Eiler and Schauble, 2004). The temperature-dependant enrichment in $^{13}C^{18}O^{16}O$ has been calibrated using synthetic calcites precipitated under a temperature range of 1 °C to 50 °C, representative of surface conditions (Ghosh et al., 2006a) leading to a relation between the new paleothermometer Δ_{47} and the temperature (T in °K) of carbonate precipitation in nature:

$$\Delta_{47} = 0.0592 \times 10^6 \times T^{-2} - 0.02.$$

This new paleothermometer is particularly useful since it allows paleoelevations to be obtained in three ways (Ghosh et al., 2006b; Quade et al., 2007; Rowley, 2007). Firstly obtained paleotemperature can be compared to the measured temperature lapse rate to deduce paeloelevations, especially in arid regions where $\delta^{18}O$ and $\delta^{2}H$ techniques cannot be applied due to evaporation of precipitation before reaching the ground. The second way to use the Δ_{47} and the associated paleotemperature is to deduce the isotopic composition of meteoric water from which carbonate precipitates, since the $\delta^{18}O$ of carbonate is known and can be used to compare such values to the altitude dependence of $\delta^{18}O$ (Garzione et al., 2006). The third way to obtain paleoelevations is to sample a vertical transect to obtain the modern mean annual and mean summer surface temperature as a function of the modern annual weighted mean $\delta^{18}O$. The same two variables are obtained from the Δ_{47} and can be compared to the expected values estimated from the modern vertical transect (Ghosh et al., 2006b). The similarity in slope in these two dimensions between sampled data and the modern mean annual trend is shown to reflect primarily the change in elevation (which is the strength of this method) and not a change in the global climate or latitude or changes in the season of formation of soil carbonates (although these second-order effects must be corrected) (Ghosh et al., 2006b). The modern meteoric water $\delta^{18}O$ values and surface temperatures vary with season during the year and soil carbonates may grow during different seasons leading to an offset from the modern mean annual trend (meteoric waters $\delta^{18}O$ vs. temperatures). At each elevation, the seasonal variation of meteoric waters $\delta^{18}O$ versus temperatures is shown to be a series of lines almost perpendicular to the modern mean annual trend in the graph of meteoric waters $\delta^{18}O$ versus temperatures (cf. **Figure 1** of Ghosh et al., 2006b). Linking seasonal extreme values with the mean annual trend for corresponding altitudes allows the generation of lines of constant altitude (isohypse) from which paleoelevations can be derived.

The uncertainties linked to the Δ_{47} method are significantly lower than most of any other method. Ghosh et al. (2006b) presented values of paleoelevations for the Bolivian Altiplano from the Late Miocene to Pliocene of -200 ± 200 m between

11.4 and 10.3 Ma, 2500 ± 500 m between 7.6 and 7.3 Ma, and 3500 ± 400 m between 6.7 and 5.8 Ma.

This method is based on the assumption that atmospheric circulation patterns have not changed significantly in the past 10 to 15 Ma at the latitude of the Andes (Ghosh et al., 2006b). Any change in climate and atmospheric circulations would however modify the moisture supply, the amount of rain that falls before the clouds reach the studied orogen and consequently the $\delta^{18}O$ values (Ghosh et al., 2006b; Poulsen et al., 2010). Poulsen et al. (2010) used a global circulation model that tracked the water vapor and rainfall isotopic composition in space and time. Poulsen et al. (2010) also showed that surface uplift of the Atliplano results in spatially heterogeneous variations in the amounts of precipitations over the Andes, with positive or negative variations. They showed that the decrease in rainfall $\delta^{18}O$ is not systematic with surface uplift.

Here the authors present only two examples from the paper of Poulsen et al. (2010) to illustrate their results. First, as surface uplift increases, precipitation $\delta^{18}O$ also increases in the eastern flanks of the central Andes where moisture supply coming from the enriched $\delta^{18}O$ of the Amazon Basin is enhanced as a consequence of intensification and a shift to the west toward the Andes of the South American low-level jetstream. Second, modifications of the South American low-level jet also lead to large increases in precipitation in the northern central Andes and consequently to a substantial decrease in meteoric water $\delta^{18}O$ due to amount effects (the $\delta^{18}O$ of airmasses is correlated to rainfall rates). Poulsen et al.'s (2010) model shows that isotopic lapse rates can change through time from low to high isotopic lapse rates, leading to an underestimation of paleoelevations and consequently an overestimation of a recent surface uplift if modern isotopic lapse rates are applied to past $\delta^{18}O$ values to estimate paleoelevations. Poulsen et al. (2010) concluded that the depletion in meteoric water $\delta^{18}O$ preserved in Miocene soil carbonates of the central Andes (Ghosh et al., 2006b) partially explains an increase in mean elevations. The remaining part reflects the initiation and the intensification of convective rainfall induced by orographic lifting of water vapor, which is in turn enhanced by climate change (atmospheric circulation changes in wind directions and speeds) and obviously by surface uplift (Poulsen et al., 2010).

5.6.2.5 Paleoaltimetry Data Based on Paleoatmospheric Pressure from Basalt Vesicularity

Atmospheric pressure is simply the mass of air above a given level, and the mass of air above a given level decreases with elevation as well as the density of molecules that constitute our atmosphere. Consequently air pressure decreases with elevation and it does so at a standard atmospheric lapse rate of ~ 100 mb km^{-1} in the lower atmosphere. During the Cenozoic atmospheric pressure at sea level probably did not change significantly. Since the atmosphere composition did not evolve significantly, the standard atmospheric lapse rate can be considered constant. Everyone knows from weather forecast maps that surface atmospheric pressures vary spatially, with anticyclonic centers of high pressure and cyclonic centers of low pressure. Such meteorologic features move horizontally at daily to season timescales as a function of insolation, a spatial distribution also influenced by the landmass distribution and the oceanic circulations. Since landmass distribution varies at the geological timescale one can also expect variations in the spatial distribution of highs and lows at the geological time scale. However, modern surface atmospheric pressure changes range between ~ 970 mb in deep lows (hurricane) to ~ 1040 mb in strong highs at sea level, leading to maximum modern climate-driven variations on the order of ~ 70 mb between highs and lows, a value reduced to a most likely 30 mb by Sahagian et al. (2002b). As a consequence, a change in topographic elevation of 3 km will result in a mean surface air pressure decrease of 300 mb leading to a signal 10-fold higher than that of a likely climate-driven maximum change in air pressure. Since the standard atmospheric lapse rate is constant through time (during at least the Cenozoic) and known, a measure of a past surface air pressure is a direct measure of paleoelevation independent of long term climate changes.

The pressure near the surface of a lava flow is mostly the atmospheric pressure whereas at the bottom of a lava flow the pressure is the sum of the hydrostatic pressure that the column of lava exerts, plus the atmospheric pressure. Hence, the difference in internal pressure in bubbles at the base and top of a lava flow depends on atmospheric pressure and lava flow thickness (Sahagian et al., 1989, 2002a; Sahagian and Maus, 1994; Sahagian et al., 2002b). Because lava flow thickness is easy to measure in the field, the size of bubbles in vesicular basalts records the paleoatmospheric pressure, the variation of which can be interpreted in terms of elevation changes, assuming a known air pressure lapse rate (Sahagian and Proussevitch, 2007; Sahagian et al., 2002a, and references herein). The measurement of vesicle size in 2.5 cm core samples is realized using numerical analysis techniques (Proussevitch and Sahagian, 2001; Proussevitch et al., 2007) of slice images obtained by X-ray computed tomography (Ketcham and Carlson, 2001).

The uncertainties associated with the method are ± 400 m (σ) based on elevation of modern Hawaiian lavas used to validate the method with more accurate results with multiple sampling. The accuracy of the technique asserted by another approach, including errors from the measurements of vesicle size and lava flow thickness, and the use of average sea-level barometric pressure is ± 410 m agreeing with the standard deviation approach (Sahagian et al., 2002a).

This method has been applied to unravel the uplift history of the Colorado Plateau (Sahagian et al., 2002a). Studied lavas were emplaced between 800 and 2000 m regardless of the age suggesting that basalts were erupted in all parts of the Colorado Plateau since 25 Ma (Sahagian et al., 2002a). This means the plateau was not flat during the past 25 Ma with a relief of at least 1200 m and a mean elevation higher than 800 m. Sahagian et al. (2002a) obtained a rock uplift rate of 40 m Ma^{-1} between 25 and 5 Ma (800 m of rock uplift), and an acceleration to 220 m Ma^{-1} since 5 Ma (1100 m of rock uplift).

5.6.2.6 Paleoaltimetry Data Based on Cosmogenic Nuclides

Cosmogenic nuclide production rates increase with elevation above sea level (e.g., Lal and Peters, 1967). As such, this might

be used to determine a paleoaltimetry (e.g., Blard et al., 1995, 2005; Dunai, 2010; Gosse and Phillips, 2001; Libarkin et al., 2002; Riihimaki and Libarkin, 2007; Schäfer et al., 1999; Van der Wateren and Dunai, 2001). First, the exposure history of a sample must be well constrained to derive a paleoelevation or an average uplift rate from its cosmogenic nuclide concentration. Two methods have been used and summarized by Riihimaki and Libarkin (2007) and Dunai (2010).

The simplest one consists of determining the paleoelevation of a dated volcanic flow. The lava flow sampled must have been preserved from erosion and unshielded by sediments during the time of exposure, which must be known accurately. Duration of exposure can be deduced where the sampled lava flow has been buried under a more recent, sufficiently thick and also dated lava flow that prevents further cosmogenic nuclides from being produced (Blard et al., 2005). Dividing the paleoelevation estimate by the age of the overlying lava gives a mean rock uplift rate since the end of exposure. True rock uplift rate may be higher if the uplift event lasted less than the time passed since the emplacement of the overlying lava flow. Uncertainties come from the analytical methods of both cosmogenic nuclide concentration and dating method used to constrain the lava ages, and from the uncertainties in the depth-history of a sample and duration of exposure (Riihimaki and Libarkin, 2007). In order to be able to measure a paleoelevation, the duration of exposure must exceed tens of thousands years and in some cases up to several hundred thousand years (Dunai, 2010). The depth history of a sample is the primary source of uncertainties. Riihimaki and Libarkin (2007) illustrated clearly that the high density contrast between atmosphere and rocks makes a 0.5 m uncertainty in depth equivalent to more than 1000 m of error in altitude.

The only way to deduce complex exposure history where a sedimentary layer may have once capped the sample site is to perform depth profiles and to analyze the exposure history by multiple nuclides (Riihimaki et al., 2006). At best paleoelevation will not be more accurate than $\sim$200 m at a low paleoelevation to $\sim$500 m at a high paleoelevation (Riihimaki and Libarkin, 2007). This is a minimum range of error because this estimate does not include any uncertainty in the depth of the sample due to erosion or burying (Riihimaki and Libarkin, 2007), but Blard et al. (2005) argued that the cosmogenic ^{3}He paleoaltimeter can potentially reach resolutions better than $\sim$1000 m. However, this method has been seldom used for dating probably due to the usually poorly constrained depth history of potential targets. The second method is a test for recent rapid uplift (Brook et al., 1995; Brown et al., 1991). Brook et al. (1995) have shown that high concentration of ^{10}Be in poorly dated glacial deposits of the Dry Valleys in Antarctica suggest that they were deposited at their current high elevation, which deny any recent high (0.43–1 mm yr^{-1}) rock uplift rate as previously proposed. However, the method did not allow the discarding of an alternative explanation in which the glacial sediments are older and that they have been raised, with a moderate uplift rate of 0.2 mm yr^{-1}, for example, allowing enough exposure time to produce the high concentration of cosmogenic nuclides.

5.6.2.7 Cooling-History and Erosion Rates as a Proxy for Rock or Surface Uplift

Cooling-ages can be deduced from thermochronologic data (e.g., Reiners, 2007, and references herein). A cooling-age defines a specific temperature (or range of temperatures) during cooling history of a sample. Cooling-history $T(t)$ can also be tracked by thermochronological data. Moreover, a thermal model of the crust allows converting temperatures into depth and cooling histories that can be transformed into exhumation histories (erosional denudation or tectonic exhumation in normal fault footwalls). Thermochronologic techniques and interpretations relevant to uplifts and topographic changes can be found in Reviews in Mineralogy and Geochemistry (Reiners and Ehlers, 2005).

First, thermochronology describes the cooling of rocks (exhumation when temperatures are converted into depth): the movement of rocks relative to Earth's free cooling surface, which may raise or decrease in elevation through time. Consequently, thermochronology alone neither provides estimates of paleoelevation, nor of rock and surface uplift. Second, the cooling-ages do not directly relate to changes in mean elevation or mean local relief and changes in erosion rates (e.g., Reiners, 2007, and references herein). For that reason, in most cases, it is the spatial changes in cooling-ages or cooling-histories that are used to unravel the topographic evolution, that is, the changes in local relief. Third, thermochronologic data allow amounts of mean elevation change or rock uplift to be estimated only when combined with geologic data. Fourth, channel incision and erosion on coupled hillslopes can reflect transient response to tectonically driven rock uplift (e.g., Whipple and Tucker, 1999). But it can also reflect transient response to climatically driven changes in sediment supply and fluvial discharge (Molnar and England, 1990). Provided prior sufficient thickening of the crust, moderate to high mean elevations are supported by a crustal root. Rock uplift in thickened settings is then the sum of the tectonic rock uplift and the erosionally driven rock uplift (e.g., Whipple, 2009).

5.6.2.7.1 *Vertical profiles of thermochronological data combined with other lines of evidence as a proxy for rock and surface uplift*

Age-elevation relationships in a vertical profile show a normal correlation where erosion rates and rock uplift rates are uniform and the slope of this relation is the erosion rate. Provided additional geologic information on paleoelevation is available (e.g., stratigraphic) and assuming a geothermal gradient, vertical profiles of thermochronologic cooling-dates can be used to deduce rock-uplift and surface-uplift rates even if direct paleoelevation markers like marine sediments are missing (e.g., Ducea et al., 2003). In the Santa Lucia Mountains of California (US), the last major transition from submarine to subaerial sedimentation occurred at approximately 4 Ma. Ducea et al. (2003) deduced the topography was at sea level at 4 Ma. Assuming a geothermal gradient of 25 °C km^{-1}, a mean surface temperature of 10 °C and the (U-Th)/He closure isotherm for apatite at 76 °C, they deduced the closure depth in the Santa Lucia Mountains of California (US) at 2640 m below the sea level at 4 Ma. The current elevation (800 m) of the 4 Ma closure depth (deduced from the vertical

profile) plus the paleoelevation of the closure depth at 4 Ma (-2640 m) led to $\sim$3440 m of rock uplift since then (0.86 mm yr^{-1}). The next step consisted of using the acquired estimates of erosion rates (0.66 mm yr^{-1}) from the vertical profile (0.35 mm yr^{-1} for the period 4–2.3 Ma and $\sim$0.9 mm yr^{-1} since 2.3 Ma) to calculate the corresponding surface uplift (rock uplift minus erosion rates) (Molnar and England, 1990). Ducea et al. (2003) deduced both the rock uplift (0.86 mm yr^{-1}) and the surface uplift (0.2 mm yr^{-1}) from denudation rates and stratigraphic data. Such an approach however makes the assumption that erosion rates are uniform in space, at least at the scale of mean elevation, that is, 1000 km^2 (at the same spatial scale than that of the crust, see Section 5.6.1.1).

5.6.2.7.2 Horizontal profiles of thermochronological data combined with other lines of evidence as a proxy for rock/surface uplift

Spatially extensive sampling over horizontal distances is more useful to constrain the local relief evolution rather than rock/surface uplift evolution (e.g., Reiners, 2007, and references herein). A paleorelief (paleo local-relief) for a specific location gives a minimum estimate of paleoelevation above sea level. But both the distribution of the paleorelief within the landscape and the history of change in base level must be known to convert a local relief change in a mean elevation change (Clark, 2007), a geodynamically more grounded measure of elevations. As long as there is no direct relationship between mean elevation or local relief and erosion rates there is no direct relation between mean elevation and local relief. In settings like high plateaus (e.g., Tibet, Altiplano), low-relief in the internally drained regions dominates whereas mean elevations are the highest in the world. Clark (2007) stressed that local relief is expected to increase during a fall in base level without an increase in mean elevation. The low local-relief of the high plateaus will undoubtedly increase when it is integrated into the drainage network draining the edges of the plateaus down to the sea without a need for the mean elevation to increase if any geodynamic process that could account for it occurs in the meantime.

The crustal thermal field is composed of deep isotherms ($T > 100$ °C) parallel to the long topographic wavelengths (or mean elevations). Lower isotherms progressively fold toward the shallow depths where isotherms closely fit to the short-wavelength topography (local relief). The perturbation depth of the disturbance is shown numerically to be a strong function of the short wavelength of the topography, but it is weakly dependent on its amplitude (Braun, 2002a, b, 2003; Braun et al., 2006; Reiners et al., 2003). However, additional geologic information is here also needed since any thermal perturbation can also result from thrust kinematics and from changes in erosion rates and rock uplift rates (e.g., Braun, 2005; Brewer and Burbank, 2006; Ehlers et al., 2005; Huntington et al., 2007). Many studies used the influence of topography on cooling-ages or cooling-histories to demonstrate local relief changes through time in orogens (Braun, 2002a; Clark et al., 2005a, b; Densmore et al., 2007; Ehlers et al., 2006; House et al., 2001; Mancktelow and Grasemann, 1997; Reiners et al., 2006; Stock et al., 2006; Stockli, 2006; Stüwe et al., 1994). Because warping of isotherms is higher for the lowest temperature thermochronometers, local relief changes will be best evidenced by the lowest thermochronometers (see Valla et al., 2010).

In the Sierra Nevada of California, House et al. (1998, 2001) have shown using a constant-elevation sample transect parallel to the orogen that the apatite helium cooling-ages for the closure temperature of 68–75 °C are roughly anticorrelated with modern valleys and ridges transverse to the range. They interpret this spatial correlation as the evidence for a long-wavelength ($\lambda = 70$ km) relief of 1500 ± 500 m higher in the Late Cretaceous–early Tertiary than today. They also correlated the local relief to a mean elevation higher than 3000 m asl by analogy with the modern Andes. Clark et al. (2005b) showed that such an analogy is misleading and they combined the results on local relief obtained from thermochronologic data with geomorphic data allowing them to argue for a range elevation of only 1500 m asl during the same time. This highlights the constant need from other lines of evidence to better interpret thermochronologic data in terms of paleotopography.

Braun (2002a) showed that decreasing or increasing local relief can modify the age-elevation relation in vertical profiles leading to, respectively, steeper or shallower slopes of the linear regressions than the actual erosion rate. Braun (2002a, b, 2005) defined a method of unraveling the transient state of landscape evolution, that is, whether local relief increases or decreases through time. It is based on an analysis of the age-elevation relationship over a continuous three dimensional spectrum of topographic wavelengths. The main assumptions are constant geothermal gradient, steady landforms, and no horizontal advection of rock (Braun, 2002b). When applied to the Sierra Nevada of California, Braun's (2002a) approach leads to the same conclusion of House et al.'s (1998, 2001), that is, a local relief decrease since the Late Cretaceous. However, it does not define the mean elevation change, which is critical in the understanding of high plateaus.

The lithosphere flexural strength controls the isostatic-flexural rebound to erosion and consequently potentially controls the spatial distribution of thermochronologic data. In the postorogenic evolution of an orogen, a greater reduction in topographic relief (at shorter and longer wavelengths, 12 and 150 km, respectively, for the case of the Dabie Shan, China) has a similar effect on the spatial distribution of the thermochronologic ages as does a thinner lithosphere (Braun and Robert, 2005). In their study of the postorogenic decay of the Dabie Shan and following the spectral method of Braun (2002a, b, 2005), Braun and Robert (2005) confirmed that a low elastic thickness and flexural isostatic rebound can explain the recent ages in the center of the orogen without any need for a recent (Cenozoic) tectonic event and associated surface uplift.

5.6.2.7.3 Incision rates obtained from thermochronological data combined with other lines of evidence as a proxy for uplift

Local relief history can also be unraveled by measuring depth in incision evolution of a canyon where it is incised within a smooth and mainly uneroded paleolandscape. Under particular conditions local relief (canyon depth) can be used as a proxy for rock uplift and surface uplift. First, depth in incision is limited by rock uplift. The incision response time to rock uplift is controlled by a geomorphic response time that can

reach several million years (e.g., Hoke et al., 2007; Schildgen et al., 2010; Schlunegger et al., 2006). Second, the thermal response to changes in the shape of Earth free cooling surface is likely to lag ~1 Ma (e.g., Schildgen et al., 2007). As a consequence the incision amounts and rates inferred from cooling-histories give a minimum rock uplift amount and rate (Schildgen et al., 2007). Only if climate is steady or becomes drier during the period of incision, rock uplift and the resulting incision can be interpreted as tectonics in origin, and they are accompanied with surface uplift (e.g., Schildgen et al., 2007).

Incision history can be deduced from dating methods such as low-temperature thermochronology of samples collected in vertical profiles or collected along valley at river level. K/Ar or Ar/Ar dates of tuffs or lava flows preserved above the current river level are also used to deduce mean incision rates since their formation (e.g., Thouret et al., 2007). But thermochronology is not a unique technique. Cosmogenic nuclide dates of terraces also give values of mean incision since the abandonment of a terrace. Cosmogenic nuclide techniques, however, generally allow dating of surfaces for the last tens of thousands to hundreds of thousands years, rarely up to a few million or tens million years (e.g., Dunai et al., 2005).

In the western slopes of the Peruvian Altiplano, Schildgen et al. (2007) have deduced from samples collected along a valley at river level and their He ages, a minimum of 2.4 km of erosion between 9 and 2.3 Ma in the Cotahuasi-Ocoña Canyon, a canyon of up to 3 km depth. They interpret it as the evidence for rock uplift of tectonic origin since climate shifted to drier conditions in the meantime (e.g., Ehlers and Poulsen, 2009; Gaupp et al., 1999; Hartley, 2003; Rech et al., 2006). Rock uplift can then be converted to surface uplift since erosion is restricted to canyon incision into a well preserved paleosurface older than 14–16 Ma.

At the eastern margin of the Tibetan Plateau, Kirby et al. (2002) and Clark et al. (2005a) showed in age-elevation relations a break in slope at ~5–12 Ma and 9–13 Ma, respectively. They interpreted the recent (late Miocene or early Pliocene) rapid incision of rivers within a widespread relict landscape, with mean elevations now above 1000 m asl and up to 3000 m asl, slowly eroding since the Jurassic as evidence for eastward plateau growth, that is, surface uplift.

On the Colorado Plateau, in the upper reaches of the Grand Canyon, Flowers et al. (2008) determined cooling-histories similar during the Early- to mid-Tertiary in samples now separated by 1500 m in both elevation and stratigraphic position. They interpret it as evidence for a proto-Grand Canyon that was ~1 km deep, implying a minimum rock uplift of 1 km before mid-Tertiary and that the watershed of the Grand Canyon already lay at high elevation by that time.

5.6.3 Tectonic Mechanisms and Associated Surface Uplift Rates for Plateau Uplift, Regional Warping, and Subsidence

Uplift of Earth's surface expresses the isostatic response to the thickness variation of the lithosphere resting on the asthenosphere (e.g., Fleitout and Froidevaux, 1982), as well as the differential buoyancy of the convective mantle resulting in 'dynamic topography' (e.g., Hager et al., 1985). So, whatever the tectonic model envisioned to explain uplift, including the case of dynamic topography, it implies a change of density at depth. Density changes in the lithosphere may be achieved in two ways: (1) changing rock densities; and (2) changing the respective thickness of the crust and the mantle, more precisely thickening the crust and thinning the lithosphere mantle. Changing rock densities requires changing temperature such as increasing temperature induces decreasing density, increasing buoyancy forces and eventually surface uplift. Rocks of the mantle lithosphere are much denser than the rocks of the crust and the mantle lithosphere is much thicker than the crust. Therefore, temperature increase in the lithospheric mantle will be much more efficient to Earth's surface uplift than it does in the crust. The boundary between lithosphere and asthenosphere is of thermal nature, so thinning of the mantle lithosphere can be achieved either by mechanical processes or a temperature increase. Crustal thickening requires mechanical processes, even if magma underplating from underlying mantle can be considered as 'thermal' thickening regarding the role of temperature in magma production. For a normal geothermal gradient, the shear strength of the crust is much lower than that of the lithospheric upper mantle, and crustal thickening is easier than lithosphere mantle thinning, considering mechanical processes. Finally, there are multiple ways to change density at depth in the lithosphere, which results in numerous models for plateau surface uplift. The line of argument for plateau uplift has its symmetrical thinking for subsidence: decreasing temperature will induce increasing rocks density, decreasing buoyancy and plateau subsidence, and thickening of the mantle lithosphere as well, and so on.

Discussing exhaustively the numerous tectonic models that have been proposed to explain the uplift of large areas at Earth surface is beyond the scope of this chapter. First, we must remember that we are dealing with plateaus as we recall the definition in the first section, that is, large areas with flat topography. We must also remember that two types of hypotheses sustain the interpretation of such features at Earth's surface: the acquirement of the flat topography precedes uplift; and smoothing of topography results from the interaction of surface processes (erosion/sedimentation) with tectonics during uplift.

The question arises as to what kind of data allow us to discern between the effective mechanisms that are proposed to explain plateau uplift. We can group together these increasingly numerous models into three types: (1) crustal thickening as the driving mechanism; (2) uplift due to the thinning of the mantle lithosphere; and (3) the role of the deep convective mantle as the cause of uplift and referring to 'dynamic' uplift.

Crustal thickening and thinning of the mantle lithosphere may be achieved either by homogeneous or heterogeneous deformation. Of course, end-member models imply hybrid models. Symmetrical end-members models, that is, crustal thinning and mantle lithosphere thickening, either by homogeneous or heterogeneous deformation, exist to explain subsidence.

Crustal thickening can be induced either by: (1) crustal shortening beneath the uplifting plateau (e.g., Argand, 1924; Bird, 1978; Dewey and Burke, 1973; Froidevaux and Ricard, 1987); (2) by lateral flow of ductile crust from immediately adjacent thickened area (e.g., Bird, 1991; Zhao and Morgan, 1987); (3) by crustal underplating of material coming from the continental margin and tectonically eroded by the subducting plate (e.g., Baby et al., 1997; Schmitz, 1994); and (4) by magmatic addition (Gotberg et al., 2010; Kono et al., 1988; Thorpe et al., 1981) but to a much smaller contribution than shortening and, mid and lower crustal flow (e.g., Baby et al., 1997; Francis and Hawkesworth, 1994; Giese et al., 1999; Sheffels, 1990). Crustal thickening by thrust faults, that is, involving strain localization, corresponds to a heterogeneous deformation mode. Crustal shortening by homogeneous deformation will require homogeneous ductile rheology, which implies a high geothermal gradient. As heterogeneous deformation is likely to produce strong topographic gradients and relief roughness at Earth's surface, mass redistribution by erosion/sedimentation process is needed to maintain a flat topography. Lateral flow of ductile crust may be assimilated to a homogeneous deformation mode. In this case, flat topography may exist long before uplift, unlike the previous case where syn- or late uplift sedimentation will be inevitably observed at the plateau surface.

Thinning of the mantle lithosphere may develop in two ways. First as mentioned above, the thermal boundary between lithosphere and asthenosphere migrates upward as the geothermal gradient increases. Mantle plumes may generate such processes resulting in surface uplift (e.g., Eaton, 2008; Teixell et al., 2005). Second, the lithosphere mantle, which is colder and denser than the underlying asthenosphere mantle, may be removed from the buoyant crust and sink into the asthenosphere. Whether such lithospheric mantle removal is considered to result from progressive peeling away during continental collision, or more or less sudden foundering by convective removal after lithosphere thickening, it is named lithosphere delamination (Bird, 1978) or detachment (e.g., Houseman et al., 1981).

The term 'dynamic uplift' is often used when Earth's mantle, including the lithospheric mantle, is suspected of being involved in surface uplift processes, but strictly speaking it does not imply a thinning of the mantle lithosphere. Dynamic topography refers to vertical stress generated by the deep convective mantle that results in subsidence or uplift of Earth's surface (e.g., Gurnis, 1993; Hager et al., 1985; Lithgow-Bertelloni and Silver, 1998).

Most interpretations of uplifted plateaus appeal to hybrid models, that is, a more or less complex combination of the different processes discussed above. For the same object, different contradictory processes, in that they result in a conflicting uplift history, are invoked. For example, as crustal thickening is related to plate convergence, the rate of surface uplift controlled by this process must match the rate of plate convergence and it implies a gradual growth of the plateau (e.g., Liu-Zeng et al., 2008; Tapponnier et al., 2001). Sudden detachment of a lithospheric root should generate faster uplift and plateau uplift as a whole (e.g., Garzione et al., 2006; Molnar et al., 1993).

To illustrate the complexity of this problem, the authors provide the following, but not exhaustive, interpretations

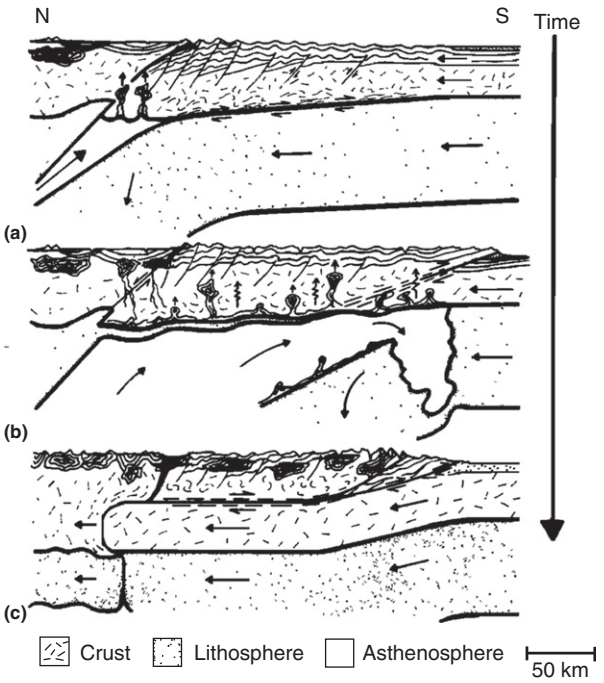

Figure 11 Himalaya-Tibet tectonic history involving crustal thickening and delamination of the mantle lithosphere first proposed by Bird, P., 1978. Initiation of intracontinental subduction in the Himalaya. Journal of Geophysical Research 83, 4975–4987.

that have been proposed for the surface uplift of the Tibetan, Altiplano, and Colorado plateaus:

1. For the Tibetan Plateau (**Figure 11**): crustal thickening by localized deformation (Dewey and Burke, 1973; Tapponnier et al., 2001) or by lateral flow of ductile crust (Clark and Royden, 2000), crustal thickening and lithosphere delamination (Bird, 1978), homogeneous deformation of the whole lithosphere and consecutive detachment of the mantle lithospheric root (England and Houseman, 1988; Houseman et al., 1981; Molnar et al., 1993).
2. For the Altiplano (for an exhaustive review of mechanisms see Barnes and Ehlers, 2009): crustal thickening by lateral flow of ductile crust (Husson and Sempere, 2003), crustal thickening and detachment of the mantle lithosphere (Garzione et al., 2006), crustal thickening, magma underplating, and thinning of the mantle lithosphere (Allmendinger et al., 1997).
3. For the Colorado Plateau: crustal thickening (McQuarrie and Chase, 2000), delamination of the lithospheric mantle (Bird, 1979), lateral flow of ductile crust (Bird, 1991), thinning of the lithosphere mantle due to mantle plume (Eaton, 1987) or Laramide subduction (Spencer, 1996), or by warming the lithosphere (Roy et al., 2004), dynamic uplift (Liu and Gurnis, 2010; Moucha et al., 2009).

5.6.4 Plateau Uplift and Global Climate Change

Uplift of Earth's surface as a cause of climate change goes back at least to Dana (1856) who argued, through geomorphologic

and tectonic analysis, that the Paleozoic Appalachians had been rejuvenated during the Late Cenozoic. A few decades later, Chamberlin (1899) postulated that the simultaneous occurrence of orogens and ice ages in Earth's history was not a coincidence but a causal relation: enhanced chemical weathering of aluminosilicate minerals, consecutive to intense erosion of rocks in mountain belts, subtracts CO_2 from the atmosphere resulting in decreasing atmospheric greenhouse effect and global cooling (e.g., Raymo, 1991; Raymo and Ruddiman, 1992). As the authors are concerned with high continental plateaus, erosion in such areas is weak by definition, and this process will be limited. The primary physical effects of plateau surface uplift are changes in the atmospheric circulations that are induced by the presence of an elevated surface at cooler upper levels in the atmosphere. This may result in increasing erosion and chemical weathering and eventually in climate change. The authors will not discuss here this indirect consequence of plateau surface uplift that is largely debated elsewhere (e.g., Ruddiman, 1997).

Plateau uplift has three main effects on climate (Ruddiman and Prell, 1997): (1) lapse-rate cooling of high-elevation surfaces; (2) perturbation of jet stream meanders; and (3) creation and intensification of monsoon circulations.

The main present-day high plateaus arose during the Late Cenozoic, a period of progressive cooling of Earth's climate that culminates in the Late Neogene. So, it is difficult, indeed even impossible, to determine the influence of a distinctive plateau on global climate change during this period. Most of works recognize the primary influence of the Tibetan plateau because of its extent and elevation, which are far greater than the other plateaus, and because of its particular latitudinal position as well (Raymo and Ruddiman, 1992).

Lapse-rate cooling, that is, the atmospheric cooling with increasing elevation ($6.5\ ^{\circ}C\ km^{-1}$), refers to the fact that it causes the high plateaus to be much colder than the nearby plains. This is especially the case in winter because temperatures are further lowered by snow cover, through albedo-temperature feedback. Depending on the extent and the height of the plateau, and its latitudinal position, this effect may result in nucleating continental ice sheets and global cooling (Birchfield and Wertman, 1983).

The second effect concerns the increase in amplitude of the meanders of the subtropical jet stream, as most high plateaus are lying in lower middle latitudes. Uplifting plateaus create obstacles to the west-to-east flow that results in the diversion into a broad poleward meander around the obstacles, and eventually large meanders develop upstream and downstream from the high plateaus (e.g., Kutzbach et al., 1989; Rind and Chandler, 1991; Ruddiman and Kutzbach, 1991; Ruddiman et al., 1989).

The third direct effect of plateau uplift is the intensification, and even the creation, of seasonal monsoon circulation (Molnar et al., 1993; Ruddiman and Prell, 1997). The symmetrical Hadley cells describe the atmospheric circulation in a general west-to-east flow between equatorial and mid-latitudes. Warm moist air rises in the intertropical convergence zone. Condensation and precipitation release latent heat that causes this now drier air to rise in the troposphere, then to flow poleward. At approximately 30° N and S latitudes, it flows east and sinks causing a high pressure area at the surface. Because of adiabatic heating, this air dries further as evidenced by the pervasive occurrence of deserts at this latitude. The uplift of a high plateau such as the Tibetan Plateau at this latitude has two effects. First, the general west-to-east flow is altered, so that the high pressure zone at latitude 30° is displaced northward and a low pressure zone develops aloft in northern India in the summer monsoon. Consequently, the summer winds originate in the Arabian Sea moving to India, and the eastern Himalaya receive increasing moisture owing to the barrier erected by the plateau (orographic effect). Second, the presence of the 'hot' Tibet in summer causes air to rise near and above the plateau and to flow toward the equator. This creates a cell with a reverse sense of rotation compared to the Hadley cell, that is, air is drawn from equatorial areas and ascent above the plateau, producing the Indian summer monsoon, characterized by moisture-bearing winds at surface blowing from the southwest (from the sea) to the northeast (to the continent).

In the case of southeast Asia, this perturbation of the general circulation of the atmosphere due to the Tibet uplift, which originates from lithosphere dynamics, is considered to have a strong impact on Earth's climate, although timing of uplift and of related climate change are still strongly debated (e.g., Dupont-Nivet et al., 2007; Molnar et al., 2006; Rowley and Currie, 2006). The question remains open and is best summarized by Molnar et al. (1993) who finally asked the question: "Did convective removal of the lower lithosphere beneath the Tibetan Plateau force a rapid uplift at approximately 8 Ma that created a heat source sufficient to strengthen the monsoon, which in turn increased precipitation and weathering in the Himalaya, causing sufficient extraction of CO_2 from the atmosphere to induce global cooling?"

5.6.5 Conclusion

Most of interpretations of uplifted plateaus appeal to models with a more or less complex combination of the different tectonic processes discussed above. Such a situation underscores the urgent need to obtain more pertinent and clear records of the surface uplift and subsidence history of present-day and past plateaus, respectively, and to come back to the difficulty of determining paleoaltitudes and structures at depth.

Acknowledgments

This review was conducted with support from the MINISTERIO DE CIENCIA E INNOVACIÓN (CGL2006-07226 y CGL2010-15416). An anonymous reviewer helped clarify aspects of the manuscript. The authors also thank Lewis Owen for comments and corrections that improved the manuscript.

References

Abbott, L.D., Silver, E.A., Anderson, R.S., et al., 1997. Measurement of tectonic surface uplift rate in a young collisional mountain belt. Nature 385, 501–507.

Al-Lazki, A., Eric, I., Dogan, S., Muawia, S., Niyazi, B., Randa, M., T., 2004. Pn tomographic imaging of mantle lid velocity and anisotropy at the junction of the Arabian, Eurasian, and African plates. Geophysical Journal International 158, 1024–1040.

Allmendinger, R.W., Jordan, T.E., Kay, S.M., Isacks, B.L., 1997. The evolution of the Altiplano–Puna Plateau of the Central Andes. Annual Review of Earth and Planetary Sciences 25, 139–174.

Amante, C., Eakins, B.W., 2009. ETOPO1 1 Arc-minute global relief model: procedures, data sources and analysis. In: Memorandum, N.T. (Ed.), National Geophysical Data Center, Marine Geology and Geophysics Division, Boulder, CO, 19 pp.

Anders, A.M., Roe, G.H., Hallet, B., Montgomery, D.R., Finnegan, N.J., Putkonen, J., 2006. Spatial patterns of precipitation and topography in the Himalaya. Geological Society of America Special Papers 398, 39–53.

Argand, E., 1924. La Tectonique de l'Asie. Compte-rendu du 13e Congrès Géologique International, Bruxelles, pp. 171–372.

Armijo, R., Tapponnier, P., Mercier, J.L., Han, T.-L., 1986. Quaternary extension in southern Tiber; field observations and tectonic implications. Journal of Geophysical Research 91, 13,803–13,872.

Atalay, I., Koçman, A., 1979. Kuzeydoğu Anadolu'nun jeotektonik ve morfotektonik evriminin ana çizgileri. Jeomorfoloji Dergisi 8, 41–75.

Axelrod, D.I., 1966. A method for determining the altitudes of Tertiary floras. The Palaeobotanist 14, 144–171.

Axelrod, D.I., 1998. The Oligocene Haynes Creek flora of eastern Idaho. University of California Publications in Geological Sciences 143, 99.

Ayalew, L., Yamagishi, H., 2004. Slope failures in the Blue Nile basin, as seen from landscape evolution perspective. Cosmogenic isotopes in geomorphology 57, 95–116.

Ayele, A., Stuart, G., Kendall, J.-M., 2004. Insights into rifting from shear wave splitting and receiver functions: an example from Ethiopia. Geophysical Journal International 157, 354–362.

Babault, J., Bonnet, S., Crave, A., Van Den Driessche, J., 2005a. Influence of piedmont sedimentation on erosion dynamics of an uplifting landscape: an experimental approach. Geology 33, 301–304. http://dx.doi.org/10.1130/G21095.1.

Babault, J., Bonnet, S., Van Den Driessche, J., Crave, A., 2007. High elevation of low-relief surfaces in mountain belts: does it equate to postorogenic surface uplift? Terra Nova 19, 272–277.

Babault, J., Teixell, A., Arboleya, M.L., Charroud, M., 2008. A Late Cenozoic age for long–wavelength surface uplift of the Atlas Mountains of Morocco. Terra Nova 20, 102–107. http://dx.doi.org/10.1111/j.1365-3121.2008.00794.x.

Babault, J., Van Den Driessche, J., Bonnet, S., Castelltort, S., Crave, A., 2005b. Origin of the highly elevated Pyrenean peneplain. Tectonics 24, TC2010. http://dx.doi.org/10.1029/2004TC001697.

Baby, P., Rochat, P., Mascle, G., Herail, G., 1997. Neogene shortening contribution to crustal thickening in the back arc of the Central Andes. Geology 25, 883–886.

Bai, D., Unsworth, M.J., Meju, M.A., et al., 2010. Crustal deformation of the eastern Tibetan plateau revealed by magnetotelluric imaging. Nature Geosci. 3, 358–362.

Bailey, I.W., Sinnott, E.W., 1916. The climatic distribution of certain types of Angiosperm leaves. American Journal of Botany 3, 24–39.

Barke, R., Lamb, S., 2006. Late Cenozoic uplift of the Eastern Cordillera, Bolivian Andes. Earth and Planetary Science Letters 249, 350–367.

Barnes, J.B., Ehlers, T.A., 2009. End member models for Andean Plateau uplift. Earth–Science Reviews 97, 105–132.

Bastow, I.D., Nyblade, A.A., Stuart, G.W., Rooney, T.O., Benoit, M.H., 2008. Upper mantle seismic structure beneath the Ethiopian hot spot: rifting at the edge of the African low-velocity anomaly. Geochemistry Geophysics Geosystems 9, Q12022.

Beaumont, C., Jamieson, R.A., Nguyen, M.H., Medvedev, S., 2004. Crustal channel flows: 1. Numerical models with applications to the tectonics of the Himalayan–Tibetan orogen. Journal of Geophysical Research 109, B06406.

Baumont, D., Paul, A., Zandt, G., Beck, S.L., Pedersen, H., 2002. Lithospheric structure of the central Andes based on surface wave dispersion. Journal of Geophysical Research–Solid Earth, 107.

Beck, S.L., Zandt, G., 2002. The nature of orogenic crust in the central Andes. Journal of Geophysical Research 107, 2230.

Beck, S.L., Zandt, G., Myers, S.C., Wallace, T.C., Silver, P.G., Drake, L., 1996. Crustal-thickness variations in the central Andes. Geology 24, 407–410.

Becq-Giraudon, J.F., Montenat, C., Van Den Driessche, J., 1996. Hercynian high-altitude phenomena in the French Massif Central: tectonic implications. Palaeogeography, Palaeoclimatology, Palaeoecology 122, 227–241.

Becq-Giraudon, J.F., Van Den Driessche, J., 1994. Depots periglaciaires dans le Stephano-Autunien du Massif Central; temoin de l'effondrement gravitaire d'un haut plateau hercynien. Comptes Rendus de l'Academie des Sciences, Serie II. Sciences de la Terre et des Planetes 318, 675–682.

Beerling, D.J., Royer, D.L., 2002. Fossil plants as indicators of the phanerozoic global carbon cycle. Annual Review of Earth and Planetary Sciences 30, 527–556.

Best, M.G., Barr, D.L., Christiansen, E.H., Gromme, S., Deino, A.L., Tingey, D.G., 2009. The Great Basin Altiplano during the middle Cenozoic ignimbrite flareup: insights from volcanic rocks. International Geology Review 51, 589–633.

Birchfield, G.E., Wertman, J., 1983. Topography, albedo-temperature feedback, and climate sensitivity. Science 219, 284–285.

Bird, P., 1978. Initiation of intracontinental subduction in the Himalaya. Journal of Geophysical Research 83, 4975–4987.

Bird, P., 1979. Continental delamination and the Colorado Plateau. Journal of Geophysical Research 84, 7561–7571.

Bird, P., 1988. Formation of the Rocky Mountains, Western United States: a continuum computer model. Science 239, 1501–1507.

Bird, P., 1991. Lateral extrusion of lower crust from under high topography, in the isostatic limit. Journal of Geophysical Research 96, 10,275–10,286.

Blackstone, D.L., 1975. Late cretaceous and cenozoic history of laramie basin region, Southeast Wyoming. Geological Society of America Memoirs 144, 249–279.

Blard, P.-H., Lavé, J., Pik, R., Quidelleur, X., Bourlès, D., Kieffer, G., 2005. Fossil cosmogenic ^{3}He record from K-Ar dated basaltic flows of Mount Etna volcano (Sicily, 38°N): evaluation of a new paleoaltimeter. Earth and Planetary Science Letters 236, 613–631.

Braun, J., 2002a. Estimating exhumation rate and relief evolution by spectral analysis of age– elevation datasets. Terra Nova 14, 210–214.

Braun, J., 2002b. Quantifying the effect of recent relief changes on age-elevation relationships. Earth and Planetary Science Letters 200, 331–343.

Braun, J., 2003. Pecube: a new finite-element code to solve the 3D heat transport equation including the effects of a time-varying, finite amplitude surface topography. Computers & Geosciences 29, 787–794.

Braun, J., 2005. Quantitative constraints on the rate of landform evolution derived from low-temperature thermochronology. Reviews in Mineralogy and Geochemistry 58, 351–374.

Braun, J., Robert, X., 2005. Constraints on the rate of post-orogenic erosional decay from low-temperature thermochronological data: application to the Dabie Shan, China. Earth Surface Processes and Landforms 30, 1203–1225.

Braun, J., van der Beek, P., Batt, G., 2006. Quantitative Thermochronology: Numerical Methods for the Interpretation of Thermochronological Data. Cambridge University Press, Cambridge.

Brewer, I.D., Burbank, D.W., 2006. Thermal and kinematic modeling of bedrock and detrital cooling ages in the central Himalaya. Journal of Geophysical Research 111, B09409.

Brook, E.J., Brown, E.T., Kurz, M.D., Ackert, R.P., Raisbeck, G.M., and Yiou, F., 1995.Constraints on age, erosion, and uplift of Neogene glacial deposits in the Transantarctic Mountains determined from in situ cosmogenic 10Be and 26Al. Geology 23, 1063-1066.

Brown, E.T., Edmond, J.M., Raisbeck, G.M., Yiou, F., Kurz, M.D., Brook, E.J., 1991. Examination of surface exposure ages of Antarctic moraines using in situ produced 10Be and 26Al. Geochimica et Cosmochimica Acta 55, 2269–2283.

Buck, W.R., 1991. Modes of continental lithospheric extension. Journal of Geophysical Research 96, 20161–20178.

Burbank, D.W., Leland, J., Fielding, E., Anderson, R.S., Brozovic, N., Reid, M.R., Duncan, C., 1996. Bedrock incision, rock uplift, and threshold hillslopes in the northwestern Himalayas. Nature 379, 505–510.

Cahill, T., Isacks, B.L., 1992. Seismicity and shape of the subducted Nazca Plate. Journal of Geophysical Research 97, 17503–17529.

Carretier, S., Lucazeau, F., 2005. How does alluvial sedimentation at range fronts modify the erosional dynamics of mountain catchments? Basin Research 17, 361–381.

Carretier, S., Poisson, B., Vassallo, R., Pepin, E., Farias, M., 2009. Tectonic interpretation of transient stage erosion rates at different spatial scales in an uplifting block. Journal of Geophysical Research 114, F02003.

Casas-Sainz, A.M., Cortes-Gracia, A.L., 2002. Cenozoic landscape development within the central Iberian Chain, Spain. Cosmogenic Isotopes in Geomorphology 44, 19–46.

Castelltort, S., Simpson, G., 2006. River spacing and drainage network growth in widening mountain ranges. Basin Research 18, 267–276.

Cerling, T.E., Quade, J., 1993. Stable carbon and oxygen isotopes in soil carbonates. In: Swart, P., Lohmann, K.C., McKenzie, J.A., Savin, S. (Eds.),

Continental Indicators of Climate. American Geophysical Union, Jackson Hole, WY, pp. 217–231.
Chamberlin, T.C., 1899. An attempt to frame a working hypothesis of the cause of glacial periods on an atmospheric basis. Journal of Geology, 545–584.
Chorowicz, J., Collet, B., Bonavia, F.F., Mohr, P., Parrot, J.F., Korme, T., 1998. The Tana Basin, Ethiopia; intra-plateau uplift, rifting and subsidence. Tectonophysics 295, 351–367.
Clark, M.K., 2007. The significance of paleotopography. Reviews in Mineralogy and Geochemistry 66, 1–21.
Clark, M.K., House, M.A., Royden, L.H., Whipple, K.X., Burchfiel, B.C., Zhang, X., Tang, W., 2005a. Late Cenozoic uplift of southeastern Tibet. Geology 33, 525–528.
Clark, M.K., Maheo, G., Saleeby, J., Farley, K.A., 2005b. The nonequilibrium landscape of the southern Sierra Nevada, California. GSA Today 15, 4–10.
Clark, M.K., Royden, L.H., 2000. Topographic ooze: building the eastern margin of Tibet by lower crustal flow. Geology 28, 703–706.
Clark, M.K., Royden, L.H., Whipple, K.X., Burchfiel, B.C., Zhang, X., Tang, W., 2006. Use of a regional, relict landscape to measure vertical deformation of the eastern Tibetan Plateau. Journal of Geophysical Research 111, F03002.
Clark, M.K., Schoenbohm, L.M., Royden, L.H., et al., 2004. Surface uplift, tectonics, and erosion of eastern Tibet from large-scale drainage patterns. Tectonics 23, TC1006. doi:10.1029/2002TC001402.
Coffin, M.F., 1992. Emplacement and subsidence of Indian Ocean plateaus and submarine ridges. Geophysical Monograph 70, 115–125.
Coney, P.J., Harms, T.A., 1984. Cordilleran metamorphic core complexes: Cenozoic extensional relics of Mesozoic compression. Geology 12, 550–554.
Cox, K.G., 1989. The role of mantle plumes in the development of continental drainage patterns. Nature (London) 342, 873–877.
Dana, J.D., 1856. On American geological history; address before the American Association for the Advancement of Science, August, 1855. American Journal of Science and Arts 22, 305–334.
Das, T., Nolet, G., 1998. Crustal thickness map of the western United States by partitioned waveform inversion. Journal of Geophysical Research 103, 30021–30038.
Davis, W.M., 1899. The geographical cycle. Geographical Journal 14, 481–504.
Debayle, E., Lévêque, J.-J., Cara, M., 2001. Seismic evidence for a deeply rooted low-velocity anomaly in the upper mantle beneath the northeastern Afro/Arabian continent. Earth and Planetary Science Letters 193, 423–436.
DeCelles, P.G., Robinson, D.M., Zandt, G., 2002. Implications of shortening in the Himalayan fold-thrust belt for uplift of the Tibetan Plateau. Tectonics 21, 1062.
Densmore, M.S., Ehlers, T.A., Woodsworth, G.J., 2007. Effect of Alpine glaciation on thermochronometer age-elevation profiles. Geophysical Research Letters 34, L02502.
Detrick, R.S., Sclater, J.G., Thiede, J., 1977. The subsidence of aseismic ridges. Earth and Planetary Science Letters 34, 185–196.
Dewey, J.F., Burke, K.C.A., 1973. Tibetan, Variscan, and Precambrian basement reactivation: products of continental collision. The Journal of Geology 81, 683–692.
Dickinson, W.R., Snyder, W.S., 1978. Plate tectonics of the Laramide Orogeny. Memoir – Geological Society of America, 355–366.
Dorbath, C., Granet, M., 1996. Local earthquake tomography of the Altiplano and the Eastern Cordillera of northern Bolivia. Tectonophysics 259, 117–136.
Douglass, J., Meek, N., Dorn, R.I., Schmeeckle, M.W., 2009. A criteria-based methodology for determining the mechanism of transverse drainage development, with application to the southwestern US. Geological Society of America Bulletin 121, 586–598.
Ducea, M., House, M.A., Kidder, S., 2003. Late Cenozoic denudation and uplift rates in the Santa Lucia Mountains, California. Geology 31, 139–142.
Dugda, M.T., Nyblade, A.A., Julia, J., 2007. Thin lithosphere beneath the Ethiopian plateau revealed by a joint inversion of rayleigh wave group velocities and receiver functions. Journal of Geophysical Research 112, B08305.
Dugda, M.T., Nyblade, A.A., Julia, J., Langston, C.A., Ammon, C.J., Simiyu, S., 2005. Crustal structure in Ethiopia and Kenya from receiver function analysis: implications for rift development in eastern Africa. Journal of Geophysical Research 110, B01303.
Dunai, T.J., 2010. Cosmogenic Nuclides Principles, Concepts and Applications in the Earth Surface Sciences. Cambridge University Press, New York.
Dunai, T.J., Lopez, G.A.G., Juez-Larre, J., 2005. Oligocene-Miocene age of aridity in the Atacama Desert revealed by exposure dating of erosion-sensitive landforms. Geology 33, 321–324.
Duncan, C., Masek, J., Fielding, E., 2003. How steep are the Himalaya? Characteristics and implications of along-strike topographic variations. Geology 31, 75–78.
Dupont-Nivet, G., Krijgsman, W., Langereis, C.G., Abels, H.A., Dai, S., Fang, X., 2007. Tibetan plateau aridification linked to global cooling at the Eocene–Oligocene transition. Nature 445, 635–638.
Duston, N., Owen, R., Wilkinson, B., 1986. Water chemistry and sedimentological observations in Littlefield Lake, Michigan: implications for lacustrine marl deposition. Environmental Geology 8, 229–236.
Dziewonski, A.M., 1984. Mapping the Lower Mantle: determination of lateral heterogeneity in P velocity up to degree and order 6. Journal of Geophysical Research 89, 5929–5952.
Eaton, G.P., 1987. Topography and Origin of the Southern Rocky Mountains and Alvarado Ridge. Geological Society, London, Special Publications 28, 355–369.
Eaton, G.P., 2008. Epeirogeny in the southern Rocky Mountains region: evidence and origin. Geosphere 4, 764–784.
Ebinger, C.J., Bechtel, T.D., Forsyth, D.W., Bowin, C.O., 1989. Effective elastic plate thickness beneath the East African and Afar plateaus and dynamic compensation of the uplifts. Journal of Geophysical Research 94, 2883–2901.
Effler, S.W., Johnson, D.L., 1987. Calcium carbonate precipitation and turbidity measurements in Otisco Lake, New York. Journal of the American Water Resources Association 23, 73–79.
Ehlers, T.A., Chaudhri, T., Kumar, S., et al., 2005. Computational tools for low-temperature thermochronometer interpretation. Reviews in Mineralogy and Geochemistry 58, 589–622.
Ehlers, T.A., Farley, K.A., Rusmore, M.E., Woodsworth, G.J., 2006. Apatite (U-Th)/He signal of large-magnitude accelerated glacial erosion, southwest British Columbia. Geology 34, 765–768.
Ehlers, T.A., Poulsen, C.J., 2009. Influence of Andean uplift on climate and paleoaltimetry estimates. Earth and Planetary Science Letters 281, 238–248.
Eiler, J.M., Schauble, E., 2004. $^{8}O^{13}C^{16}O$ in Earth's atmosphere. Geochimica et Cosmochimica Acta 68, 4767–4777.
England, P., Houseman, G.A., 1989. Extension during continental convergence, with application to the Tibetan Plateau. Journal of Geophysical Research 94, 17,561–17,579.
England, P., Molnar, P., 1990. Surface uplift, uplift of rocks, and exhumation of rocks. Geology 18, 1173–1177.
England, P.C., Houseman, G.A., 1988. The mechanics of the Tibetan Plateau. The Evolution of Passive Continental Margins in the Light of Recent Deep Drilling Results 326, 301–320.
Epis, R.C., Chapin, C.E., 1975. Geomorphic and tectonic implications of the post-Laramide Late Eocene erosion surface in the Southern Rocky Mountains. Geological Society of America Memoirs 144, 45–74.
Farías, M., Charrier, R., Comte, D., Martinod, J., Herail, G., 2005. Late Cenozoic deformation and uplift of the western flank of the Altiplano; evidence from the depositional, tectonic, and geomorphologic evolution and shallow seismic activity (northern Chile at 19 degrees 30′S). Tectonics 24, TC4001. http://dx.doi.org/10.1029/2004TC001667.
Fielding, E., Isacks, B., Barazangi, M., Duncan, C., 1994. How flat is Tibet? Geology 22, 163–167.
Fielding, E.J., 1996. Tibet uplift and erosion. Tectonphysics 260, 55–84.
Fleitout, L., Froidevaux, C., 1982. Tectonics and topography for a lithosphere containing density heterogeneities. Tectonics 1, 21–56.
Flint, J.J., 1974. Stream gradient as a function of order, magnitude, and discharge. Water Resource Research 10, 969–973.
Flowers, R.M., Wernicke, B.P., Farley, K.A., 2008. Unroofing, incision, and uplift history of the southwestern Colorado Plateau from apatite (U-Th)/He thermochronometry. Geological Society of America Bulletin 120, 571–587.
Forest, C.E., 2007. Paleoaltimetry: a review of thermodynamic methods. Reviews in Mineralogy and Geochemistry 66, 173–193.
Forest, C.E., Molnar, P., Emanuel, K.A., 1995. Palaeoaltimetry from energy conservation principles. Nature 374, 347–350.
Forest, C.E., Wolfe, J.A., Molnar, P., Emanuel, K.A., 1999. Paleoaltimetry incorporating atmospheric physics and botanical estimates of paleoclimate. Geological Society of America Bulletin 111, 497–511.
Francis, P.W., Hawkesworth, C.J., 1994. Late Cenozoic rates of magmatic activity in the Central Andes and their relationships to continental crust formation and thickening. Journal of the Geological Society 151, 845–854.
Froidevaux, C., Ricard, Y., 1987. Tectonic evolution of high plateaus. Tectonophysics 134, 227–238.
Fromm, R., Zandt, G., Beck, S.L., 2004. Crustal thickness beneath the Andes and Sierras Pampeanas at 30° S inferred from Pn apparent phase velocities. Geophysical Research Letters 31, L06625.
Frostick, L.E., Reid, I.A.N., 1989. Climatic versus tectonic controls of fan sequences: lessons from the Dead Sea, Israel. Journal of the Geological Society 146, 527–538.

Fukao, Y., Yamamoto, A., Kono, M., 1989. Gravity anomaly across the Peruvian Andes. Journal of Geophysical Research 94, 3867–3890.
Gale, J., 1972. Availability of carbon dioxide for photosynthesis at high altitudes: theoretical considerations. Ecology 53, 494–497.
Gani, N., Gani, M., Abdelsalam, M., 2007. Blue Nile incision on the Ethiopian Plateau: pulsed plateau growth, Pliocene uplift, and hominin evolution. GSA Today 17, 4–11.
Garzione, C.N., 2008. Surface uplift of Tibet and Cenozoic global cooling. Geology 36, 1003–1004.
Garzione, C.N., Hoke, G.D., Libarkin, J.C., et al., 2008. Rise of the Andes. Science 320, 1304–1307.
Garzione, C.N., Molnar, P., Libarkin, J.C., MacFadden, B.J., 2006. Rapid late Miocene rise of the Bolivian Altiplano: evidence for removal of mantle lithosphere. Earth and Planetary Science Letters 241, 543–556.
Gaupp, R., Kött, A., Wörner, G., 1999. Palaeoclimatic implications of Mio-Pliocene sedimentation in the high-altitude intra-arc Lauca Basin of northern Chile. Palaeogeography, Palaeoclimatology, Palaeoecology 151, 79–100.
Gephart, J.W., 1994. Topography and subduction geometry in the central Andes: clues to the mechanics of a noncollisional orogen. Journal of Geophysical Research 99, 12279–12288.
Ghosh, P., Adkins, J., Affek, H., et al., 2006a. ^{13}C-^{18}O bonds in carbonate minerals: a new kind of paleothermometer. Geochimica et Cosmochimica Acta 70, 1439–1456.
Ghosh, P., Garzione, C.N., Eiler, J.M., 2006b. Rapid uplift of the Altiplano revealed through ^{13}C-^{18}O bonds in paleosol carbonates. Science 311, 511–515.
Giese, P., Scheuber, E., Schilling, F., Schmitz, M., Wigger, P., 1999. Crustal thickening processes in the Central Andes and the different natures of the Moho-discontinuity. Journal of South American Earth Sciences 12, 201–220.
Gök, R., Michael, E.P., Ekrem, Z., 2007. Lithospheric structure of the continent–continent collision zone: eastern Turkey. Geophysical Journal International 169, 1079–1088.
Gök, R., Sandvol, E., Türkelli, N., Seber, D., Barazangi, M., 2003. Sn attenuation in the Anatolian and Iranian plateau and surrounding regions. Geophysical Research Letters 30, 8042.
Gosse, J.C., Phillips, F.M., 2001. Terrestrial in situ cosmogenic nuclides: theory and application. Quaternary Science Reviews 20, 1475–1560.
Gotberg, N., McQuarrie, N., Caillaux, V.C., 2010. Comparison of crustal thickening budget and shortening estimates in southern Peru (12–14° S): implications for mass balance and rotations in the "Bolivian orocline". Geological Society of America Bulletin 122, 727–742.
Götze, H.J., Lahmeyer, B., Schmidt, S., Strunk, S., 1994. The lithospheric structure of the Central Andes (20–25S) as inferred from quantitative interpretation of regional gravity. In: Reutter, K., Scheuber, E., Wigger, P. (Eds.), Tectonics of the Southern Central Andes: Structure and Evolution of an Active Continental Margin. Springer-Verlag, Berlin, pp. 23–48.
Gregory, K.M., 1994. Paleoclimate and paleoelevation of the 35 Ma Florissant flora, Front Range, Colorado. Palaeoclimates 1, 23–57.
Gregory, K.M., Chase, C.G., 1992. Tectonic significance of paleobotanically estimated climate and altitude of the late Eocene erosion surface, Colorado. Geology 20, 581–585.
Gregory, K.M., Chase, C.G., 1994. Tectonic and climatic significance of a late Eocene low-relief, high-level geomorphic surface, Colorado. Journal of Geophysical Research 99, 20,141–20,160.
Gregory, K.M., McIntosh, W.C., 1996. Paleoclimate and paleoelevation of the Oligocene Pitch-Pinnacle flora, Sawatch Range, Colorado. Geological Society of America Bulletin 108, 545–561.
Gregory-Wodzicki, K.M., 1997. The late Eocene House Range flora, Sevier Desert, Utah; paleoclimate and paleoelevation. Palaios 12, 552–567.
Gregory-Wodzicki, K.M., 2000. Uplift history of the Central and Northern Andes: a review. Geological Society of America Bulletin 112, 1091–1105.
Griot, D.-A., Montagner, J.-P., Tapponnier, P., 1998. Phase velocity structure from Rayleigh and Love waves in Tibet and its neighboring regions. Journal of Geophysical Research 103, 21215–21232.
Gurnis, M., 1993. Phanerozoic marine inundation of continents driven by dynamic topography above subducting slabs. Nature 364, 589–593.
Gurnis, M., Mitrovica, J.X., Ritsema, J., van Heijst, H.-J., 2000. Constraining mantle density structure using geological evidence of surface uplift rates; the case of the African Superplume. Geochemistry, Geophysics, Geosystems 1(7), 1020. http://dx.doi.org/10.1029/1999GC000035.
Gurnis, M., Mueller, R.D., Moresi, L., 1998. Cretaceous vertical motion of Australia and the Australian-Antarctic discordance. Science 279, 1499–1504.
Hack, J.T., 1957. Studies of longitudinal stream profiles in Virginia and Maryland. United States Geological Survey Professional Paper 294, 45–94.
Hager, B.H., Clayton, R.W., Richards, M.A., Comer, R.P., Dziewonski, A.M., 1985. Lower mantle heterogeneity, dynamic topography and the geoid. Nature 313, 541–545.
Haines, S.S., Klemperer, S.L., Brown, L., et al., 2003. INDEPTH III seismic data: from surface observations to deep crustal processes in Tibet. Tectonics 22, 1001.
Harrison, T.M., Copeland, P., Kidd, W.S.F., Yin, A., 1992. Raising Tibet. Science 255, 1663–1670.
Hartley, A., 2003. Andean uplift and climate change. Journal of the Geological Society 160, 7–10.
Heit, B., Yuan, X.H., Bianchi, M., Sodoudi, F., Kind, R., 2008. Crustal thickness estimation beneath the southern central Andes at 30° S and 36° S from S wave receiver function analysis. Geophysical Journal International 174, 249–254.
Hennig, A., 1915. Zur Petrographie und geologie von Sudwest Tibet. In: Hedin, S. (Ed.), Southern Tibet. Norstedt, Stockholm, 220 pp.
Hirn, A., Lepine, J.-C., Jobert, G., et al., 1984a. Crustal structure and variability of the Himalayan border of Tibet. Nature (London) 307, 23–25.
Hirn, A., Nercessian, A., Sapin, M., et al., 1984b. Lhasa Block and bordering sutures; a continuation of a 500-km Moho traverse through Tibet. Nature (London) 307, 25–27.
Hodges, K.V., Wobus, C., Ruhl, K., Schildgen, T., Whipple, K., 2004. Quaternary deformation, river steepening, and heavy precipitation at the front of the Higher Himalayan ranges. Earth and Planetary Science Letters 220, 379–389.
Hofmann, C., Courtillot, V., Feraud, G., Rochette, P., Yirgu, G., Ketefo, E., Pik, R., 1997. Timing of the Ethiopian flood basalt event and implications for plume birth and global change. Nature 389, 838–841.
Hoke, G.D., Garzione, C.N., 2008. Paleosurfaces, paleoelevation, and the mechanisms for the late Miocene topographic development of the Altiplano plateau. Earth and Planetary Science Letters 271, 192–201.
Hoke, G.D., Garzione, C.N., Araneo, D.C., Latorre, C., Strecker, M.R., Williams, K.J., 2009. The stable isotope altimeter: do Quaternary pedogenic carbonates predict modern elevations? Geology 37, 1015–1018.
Hoke, G.D., Isacks, B.L., Jordan, T.E., Blanco, N., Tomlinson, A.J., Ramezani, J., 2007. Geomorphic evidence for post-10 Ma uplift of the western flank of the central Andes 8°30′-22° S. Tectonics 26, TC5021.
Hoke, L., Hilton, D.R., Lamb, S.H., Hammerschmidt, K., Friedrichsen, H., 1994. 3He evidence for a wide zone of active mantle melting beneath the Central Andes. Earth and Planetary Science Letters 128, 341–355.
Holt, W.E., Wallace, T.C., 1990. Crustal thickness and upper mantle velocities in the Tibetan plateau region from the inversion of regional Pnl waveforms: evidence for a thick upper mantle lid beneath Southern Tibet. Journal of Geophysical Research 95, 12499–12525.
Horton, B.K., 1999. Erosional control on the geometry and kinematics of thrust belt development in the Central Andes. Tectonics 18, 1292–1304.
House, M.A., Wernicke, B.P., Farley, K.A., 1998. Dating topography of the Sierra Nevada, California, using apatite (U-Th)/He ages. Nature 396, 66–69.
House, M.A., Wernicke, B.P., Farley, K.A., 2001. Paleo-Geomorphology of the Sierra Nevada, California, from (U-TH) /He Ages in Apatite. American Journal of Science 301, 77–102.
Houseman, G.A., McKenzie, D.P., Molnar, P., 1981. Convective instability of a thickened boundary layer and its relevance for the thermal evolution of continental convergent belts. Journal of Geophysical Research 86, 6115–6132.
Howard, A.D., Kerby, G., 1983. Channel changes in badlands. GSA Bulletin 94, 739–752.
Huerta, A.D., Nyblade, A.A., Reusch, A.M., 2009. Mantle transition zone structure beneath Kenya and Tanzania: more evidence for a deep-seated thermal upwelling in the mantle. Geophysical Journal International 177, 1249–1255.
Hunt, C.B., 1956. Cenozoic geology of the Colorado Plateau. U.S. Geological Survey Professional Paper 279, 99.
Huntington, K.W., Ehlers, T.A., Hodges, K.V., Whipp, Jr. D.M., 2007. Topography, exhumation pathway, age uncertainties, and the interpretation of thermochronometer data. Tectonics 26, TC4012.
Husson, L., Sempere, T., 2003. Thickening the Altiplano crust by gravity-driven crustal channel flow. Geophysical Research Letters 30, 1243.
Isacks, B.L., 1988. Uplift of the Central Andean plateau and bending of the Bolivian Orocline. Journal of Geophysical Research 93, 3211–3231.
James, D.E., Fouch, M.J., 2002. Formation and evolution of Archaean cratons; insights from Southern Africa. Coastal tectonics 199, 1–26.
Jarvis, A., Reuter, H.I., Nelson, A., Guevara, E., 2008. Hole-filled SRTM for the globe Version 4. Available from the CGIAR-CSI SRTM 90 m: http://srtm.csi.cgiar.org.

Johnson, M.R.W., 2002. Shortening budgets and the role of continental subduction during the India–Asia collision. Earth-Science Reviews 59, 101–123.
Jones, H., 1992. Plants and Microclimate: A Quantitative Approach to Environmental Plant Physiology. Cambridge University Press, New York, 456 pp.
Kennan, L., 2000. Large-scale geomorphology of the Andes; interrelationships of tectonics, magmatism and climate. In: Summerfield, M.A. (Ed.), Geomorphology and Global Tectonics. Wiley, Chichester, pp. 167–199.
Kennan, L., Lamb, S.H., Hoke, L., 1997. High altitude palaeosurfaces in the Bolivian Andes: evidence for late Cenozoic surface uplift. In: Widdowson, M. (Ed.), Palaeosurfaces: Recognition, Reconstruction, and Interpretation. Geological Society of London Special Publications, Bath, UK, pp. 307–324.
Keskin, M., 2003. Magma generation by slab steepening and breakoff beneath a subduction-accretion complex: an alternative model for collision-related volcanism in Eastern Anatolia. Turkey. Geophysical Research Letters 30, 8046.
Ketcham, R.A., Carlson, W.D., 2001. Acquisition, optimization, and interpretation of X-ray computed tomographic imagery: applications to the geosciences. Computers & Geosciences 27, 381–400.
Kind, R., Yuan, X., Saul, J., et al., 2002. Seismic images of Crust and Upper Mantle beneath Tibet: evidence for Eurasian Plate subduction. Science 298, 1219–1221.
King, L.C., 1953. Canons of landscape evolution. Geological Society of America Bulletin 64, 721–752.
Kirby, E., Reiners, P.W., Krol, M.A., et al., 2002. Late Cenozoic evolution of the eastern margin of the Tibetan Plateau: inferences from 40Ar/39Ar and (U-Th)/He thermochronology. Tectonics 21, 1001.
Kirby, E., Whipple, K.X., Tang, W., Chen, Z., 2003. Distribution of active rock uplift along the eastern margin of the Tibetan Plateau: inferences from bedrock channel longitudinal profiles. Journal of Geophysical Research 108, 2217.
Kono, M., Fukao, Y., Yamamoto, A., 1988. Mountain building in the Central Andes. Rock Magnetism and Paleogeophysics 15, 73–80.
Kono, M., Fukao, Y., Yamamoto, A., 1989. Mountain Building in the Central Andes. Journal of Geophysical Research 94, 3891–3905.
Kosarev, G., Kind, R., Sobolev, S.V., Yuan, X., Hanka, W., Oreshin, S., 1999. Seismic evidence for a detached Indian lithospheric Mantle beneath Tibet. Science 283, 1306–1309.
Koulakov, I., Sobolev, S.V., Asch, G., 2006. P- and S-velocity images of the lithosphere–asthenosphere system in the Central Andes from local-source tomographic inversion. Geophysical Journal International 167, 106–126.
Kouwenberg, L.L.R., Kurschner, W.M., McElwain, J.C., 2007. Stomatal frequency change over altitudinal gradients: prospects for paleoaltimetry. Reviews in Mineralogy and Geochemistry 66, 215–241.
Kutzbach, J.E., Guetter, P.J., Ruddiman, W.F., Prell, W.L., 1989. Sensitivity of climate to Late Cenozoic uplift in southern Asia and the American West: numerical experiments. Journal of Geophysical Research 94, 18393–18407.
Lal, D., Peters, B., 1967. Cosmic-Ray Produced Radioactivity on the Earth, Handbook of Physics 46. Springer-Verlag, Berlin, pp. 551–662.
Lamb, S., Hoke, L., 1997. Origin of the high plateau in the Central Andes, Bolivia, South America. Tectonics 16, 623–649.
Lamb, S., Hoke, L., Kennan, L., Dewey, J., 1997. Cenozoic evolution of the Central Andes in Bolivia and northern Chile. Coastal Tectonics 121, 237–264.
Leonard, E.M., 2002. Geomorphic and tectonic forcing of late Cenozoic warping of the Colorado piedmont. Geology 30, 595–598.
Li, C., van der Hilst, R.D., Meltzer, A.S., Engdahl, E.R., 2008. Subduction of the Indian lithosphere beneath the Tibetan Plateau and Burma. Earth and Planetary Science Letters 274, 157–168.
Li, S., Mooney, W.D., 1998. Crustal structure of China from deep seismic sounding profiles. Tectonophysics 288, 105–113.
Libarkin, J.C., Quade, J., Chase, C.G., Poths, J., McIntosh, W., 2002. Measurement of ancient cosmogenic 21Ne in quartz from the 28 Ma Fish Canyon Tuff, Colorado. Chemical Geology 186, 199–213.
Lithgow-Bertelloni, C., Silver, P.G., 1998. Dynamic topography, plate driving forces and the African superswell. Nature (London) 395, 269–272.
Liu, B., Phillips, F.M., Campbell, A.R., 1996. Stable carbon and oxygen isotopes of pedogenic carbonates, Ajo Mountains, southern Arizona: implications for paleoenvironmental change. Palaeogeography, Palaeoclimatology, Palaeoecology 124, 233–246.
Liu, L., Gurnis, M., 2010. Dynamic subsidence and uplift of the Colorado Plateau. Geology 38, 663–666.
Liu-Zeng, J., Tapponnier, P., Gaudemer, Y., Ding, L., 2008. Quantifying landscape differences across the Tibetan plateau: implications for topographic relief evolution. Journal of Geophysical Research 113, F04018.
Mackenzie, G.D., Thybo, H., Maguire, P.K.H., 2005. Crustal velocity structure across the Main Ethiopian Rift: results from two-dimensional wide-angle seismic modeling. Geophysical Journal International 162, 994–1006.
Maggi, A., Priestley, K., 2005. Surface waveform tomography of the Turkish-Iranian plateau. Geophysical Journal International 160, 1068–1080.
Mancktelow, N.S., Grasemann, B., 1997. Time-dependent effects of heat advection and topography on cooling histories during erosion. Tectonophysics 270, 167–195.
Masek, J.G., Isacks, B.L., Gubbels, T.L., Fielding, E.J., 1994. Erosion and tectonics at the margins of continental plateaus. Journal of Geophysical Research 99, 13,941–13,956.
McElwain, J.C., 2004. Climate-independent paleoaltimetry using stomatal density in fossil leaves as a proxy for CO_2 partial pressure. Geology 32, 1017–1020.
McElwain, J.C., Mayle, F.E., Beerling, D.J., 2002. Stomatal evidence for a decline in atmospheric CO_2 concentration during the Younger Dryas stadial: a comparison with Antarctic ice core records. Journal of Quaternary Science 17, 21–29.
McGlashan, N., Brown, L., Kay, S., 2008. Crustal thickness in the central Andes from teleseismically recorded depth phase precursors. Geophysical Journal International 175, 1013–1022.
McMillan, M.E., Angevine, C.L., Heller, P.L., 2002. Postdepositional tilt of the Miocene–Pliocene Ogallala Group on the western Great Plains: evidence of late Cenozoic uplift of the Rocky Mountains. Geology 30, 63–66.
McMillan, M.E., Heller, P.L., Wing, S.L., 2006. History and causes of post-Laramide relief in the Rocky Mountain orogenic plateau. Geological Society of America Bulletin 118, 393–405.
McNamara, D.E., Owens, T.J., Walter, W.R., 1995. Observations of regional phase propagation across the Tibetan Plateau. Journal of Geophysical Research 100, 22,215–22,229.
McNamara, D.E., Walter, W.R., Owens, T.J., Ammon, C.J., 1997. Upper mantle velocity structure beneath the Tibetan Plateau from Pn travel time tomography. Journal of Geophysical Research 102, 493–505.
McQuarrie, N., Chase, C.G., 2000. Raising the Colorado Plateau. Geology 28, 91–94.
Menard, G., Molnar, P., 1988. Collapse of a Hercynian Tibetan Plateau into a late Palaeozoic European Basin and Range province. Nature 334, 235–237.
Meyer, H.W., 1992. Lapse rates and other variables applied to estimating paleoaltitudes from fossil floras. Palaeogeography, Palaeoclimatology, Palaeoecology 99, 71–99.
Meyer, H.W., 2007. A Review of paleotemperature lapse rate methods for estimating paleoelevation from fossil floras. Reviews in Mineralogy and Geochemistry 66, 155–171.
Molnar, P., 2005. Mio-pliocene growth of the Tibetan Plateau and evolution of East Asian climate. Palaeontologia Electronica 8(1), 2A:23 pp.
Molnar, P., England, P., 1990. Late Cenozoic uplift of mountain ranges and global climate change: chicken or egg? Nature 346, 29–34.
Molnar, P., England, P., Martinod, J., 1993. Mantle dynamics, uplift of the Tibetan Plateau, and the Indian monsoon. Reviews of Geophysics 31, 357–396.
Molnar, P., Houseman, G.A., England, P.C., 2006. Palaeo-altimetry of Tibet. Nature 444, E4.
Molnar, P., Tapponnier, P., 1978. Active tectonics of Tibet. Journal of Geophysical Research 83, 5361–5375.
Montgomery, D.R., Gran, K.B., 2001. Downstream variations in the width of bedrock channels. Water Resource Research 37, 1841–1846.
Moore, A., Blenkinsop, T., 2002. The role of mantle plumes in the development of continental-scale drainage patterns: the southern African example revisited. South African Journal of Geology 105, 353–360.
Mortimer, C., 1973. The Cenozoic history of the southern Atacama Desert, Chile. Journal of the Geological Society 129, 505–526.
Moucha, R., Forte, A.M., Rowley, D.B., Mitrovica, J.X., Simmons, N.A., Grand, S.P., 2009. Deep mantle forces and the uplift of the Colorado Plateau. Geophysical Research Letters 36, L19310.
Myers, S.C., Beck, S., Zandt, G., Wallace, T., 1998. Lithospheric-scale structure across the Bolivian Andes from tomographic images of velocity and attenuation for P and S waves. Journal of Geophysical Research 103, 21233–21252.
Nábělek, J., Hetenyi, G., Vergne, J., et al., 2009. Underplating in the Himalaya-Tibet Collision Zone Revealed by the Hi-CLIMB Experiment. Science 325, 1371–1374.
Nelson, K.D., Zhao, W., Brown, L.D., et al., 1996. Partially molten middle crust beneath southern Tibet; synthesis of Project INDEPTH results. Science 274, 1684–1688.
Neuendorf, K.K.E., Mehl, Jr. J.P., Jackson, J.A., 2005. Glossary of Geology. Alexandria, Virginia, 779 pp.

Nguuri, T.K., Gore, J., James, D.E., et al., 2001. Crustal structure beneath southern Africa and its implications for the formation and evolution of the Kaapvaal and Zimbabwe cratons. Geophysical Research Letters 28, 2501–2504.
Ni, J., Barazangi, M., 1983. High-frequency seismic wave propagation beneath the Indian Shield, Himalayan Arc, Tibetan Plateau and surrounding regions; high uppermost mantle velocities and efficient Sn propagation beneath Tibet. Geophysical Journal of the Royal Astronomical Society 72, 665–689.
Nicoll, K., 2010. Landscape development within a young collision zone; implications for post-Tethyan evolution of the upper Tigris River system in southeastern Turkey. International Geology Review 52, 404–422.
Norin, E., 1946. Geological explorations in western Tibet. In: Hedin, S. (Ed.), Reports from the Scientific Expedition to the Northwestern Provinces of China Under the Leadership of Dr. Sven Hedin. Tryckeri Aktiebolaget, Thule, Stockholm, 214.
Nyblade, A.A., Owens, T.J., Gurrola, H., Ritsema, J., Langston, C.A., 2000. Seismic evidence for a deep upper mantle thermal anomaly beneath east Africa. Geology 28, 599–602.
Nyblade, A.A., Pollack, H.N., Jones, D.L., Podmore, F., Mushayandebvu, M., 1990. Terrestrial heat flow in East and southern Africa. Journal of Geophysical Research 95, 17371–17384.
Nyblade, A.A., Robinson, S.W., 1994. The African superswell. Geophysical Research Letters 21, 765–768.
Ollier, C.D., 1981. Tectonics and Landforms. Longman, London and New York, 324 pp.
Ollier, C.D., 1985. Morphotectonics of passive continental margins: introduction. Zeitschrift für Geomorphologie, Supplementbände 54, 1–9.
Ollier, C.D., Marker, M.E., 1985. The great escarpment of southern Africa. Zeitschrift fuer Geomorphologie Supplementband 54, 37–56.
Olson, P., Nam, I.S., 1986. Formation of seafloor swells by mantle plumes. Journal of Geophysical Research 91, 7181–7191.
Owens, T.J., Zandt, G., 1997. Implications of crustal property variations for models of Tibetan plateau evolution. Nature 387, 37–43.
Paola, C., Mohrig, D., 1996. Palaeohydraulics revisited: palaeoslope estimation in coarse-grained braided rivers. Basin Research 8, 243–254.
Park, Y., Nyblade, A.A., 2006. P-wave tomography reveals a westward dipping low velocity zone beneath the Kenya Rift. Geophysical Research Letters 33, L07311.
Pearce, J.A., Bender, J.F., De Long, S.E., et al., 1990. Genesis of collision volcanism in Eastern Anatolia, Turkey. Journal of Volcanology and Geothermal Research 44, 189–229.
Pederson, J.L., Mackley, R.D., Eddleman, J.L., 2002. Colorado Plateau uplift and erosion evaluated using GIS. GSA Today 12, 4–10.
Peppe, D.J., Royer, D.L., Wilf, P., Kowalski, E.A., 2010. Quantification of large uncertainties in fossil leaf paleoaltimetry. Tectonics 29, TC3015.
Pik, R., Marty, B., Carignan, J., Lave, J., 2003. Stability of the upper Nile drainage network (Ethiopia) deduced from (U-Th)/He thermochronometry; implications for uplift and erosion of the Afar Plume dome. Earth and Planetary Science Letters 215, 73–88.
Poulsen, C.J., Ehlers, T.A., Insel, N., 2010. Onset of convective rainfall during gradual late Miocene rise of the Central Andes. Science 328, 490–493.
Powell, J.W., 1875. Exploration of the Colorado River of the West and its Tributaries. Publisher unknown, Washington, DC.
Press, F., Siever, R., Grotzinger, J., Jordan, T.H., 2004. Understanding Earth. W. H. Freeman and Company, New York, NY.
Proussevitch, A.A., Sahagian, D.L., 2001. Recognition and separation of discrete objects within complex 3D voxelized structures. Computers & Geosciences 27, 441–454.
Proussevitch, A.A., Sahagian, D.L., Carlson, W.D., 2007. Statistical analysis of bubble and crystal size distributions: Application to Colorado Plateau basalts. Journal of Volcanology and Geothermal Research 164, 112–126.
Quade, J., Garzione, C., Eiler, J., 2007. Paleoelevation Reconstruction using Pedogenic Carbonates. Reviews in Mineralogy and Geochemistry 66, 53–87.
Raymo, M.E., 1991. Geochemical evidence supporting chamberlin,T.,C. theory of glaciation. Geology 19, 344–347.
Raymo, M.E., Ruddiman, W.F., 1992. Tectonic forcing of late Cenozoic climate. Nature (London) 359, 117–122.
Rech, J.A., Currie, B.S., Michalski, G., Cowan, A.M., 2006. Neogene climate change and uplift in the Atacama Desert, Chile. Geology 34, 761–764.
Reiners, P.W., 2007. Thermochronologic approaches to paleotopography. Reviews in Mineralogy and Geochemistry 66, 243–267.
Reiners, P.W., Ehlers, T.A., 2005. Low-Temperature Thermochronology; Techniques, Interpretations, and Applications. Mineralogical Society of America, Alexandria Virginia, 622 pp.
Reiners, P.W., McPhillips, D., Brandon, M.T., Mulch, A., Chamberlain, C.P., 2006. Thermochronologic approaches to paleotopography. Geochimica et Cosmochimica Acta 70, A525.
Reiners, P.W., Zhou, Z., Ehlers, T.A., Xu, C., Brandon, M.T., Donelick, R.A., Nicolescu, S., 2003. Postorogenic evolution of the Dabie Shan, eastern China, from (U-Th)/He and fission-track thermochronology. American Journal of Science 303, 489–518.
Rigby, J.K., 1977. Southern Colorado Plateau, K/H Geology Field Guide Studies. Kendall/Hunt Pub. Co., Dubuque, Iowa, pp. 148.
Riihimaki, C.A., Anderson, R.S., Safran, E.B., Dethier, D.P., Finkel, R.C., Bierman, P.R., 2006. Longevity and progressive abandonment of the Rocky Flats surface, Front Range, Colorado. Cosmogenic Isotopes in Geomorphology 78, 265–278.
Riihimaki, C.A., Libarkin, J.C., 2007. Terrestrial cosmogenic nuclides as paleoaltimetric proxies. Reviews in Mineralogy and Geochemistry 66, 269–278.
Rind, D., Chandler, M., 1991. Increased ocean heat transports and warmer climate. Journal of Geophysical Research 96, 7437–7461.
Riquelme, R., Martinod, J., Herail, G., Darrozes, J., Charrier, R., 2003. A geomorphological approach to determining the Neogene to Recent tectonic deformation in the Coastal Cordillera of northern Chile (Atacama). Tectonophysics 361, 255–275.
Ritsema, J., Heijst, H.J.V, Woodhouse, J.H., 1999. Complex shear wave velocity structure imaged beneath Africa and Iceland. Science 286, 1925–1928.
Ritsema, J., Nyblade, A.A., Owens, T.J., Langston, C.A., VanDecar, J.C., 1998. Upper mantle seismic velocity structure beneath Tanzania, east Africa: implications for the stability of cratonic lithosphere. Journal of Geophysical Research 103, 21201–21213.
Ritsema, J., van Heijst, H., 2000. New seismic model of the upper mantle beneath Africa. Geology 28, 63–66.
Roberge, J., Wallace, P.J., White, R.V., Coffin, M.F., 2005. Anomalous uplift and subsidence of the Ontong Java Plateau inferred from CO_2 contents of submarine basaltic glasses. Geology 33, 501–504.
Rowley, D.B., 2007. Stable isotope-based paleoaltimetry: theory and validation. Reviews in Mineralogy and Geochemistry 66, 23–52.
Rowley, D.B., Currie, B.S., 2006. Palaeo-altimetry of the late Eocene to Miocene Lunpola basin, central Tibet. Nature 439, 677–681.
Rowley, D.B., Garzione, C.N., 2007. Stable isotope-based paleoaltimetry. Annual Review of Earth and Planetary Sciences 35, 463–508.
Rowley, D.B., Pierrehumbert, R.T., Currie, B.S., 2001. A new approach to stable isotope-based paleoaltimetry: implications for paleoaltimetry and paleohypsometry of the High Himalaya since the Late Miocene. Earth and Planetary Science Letters 188, 253–268.
Roy, M., Jordan, T.H., Pederson, J., 2009. Colorado Plateau magmatism and uplift by warming of heterogeneous lithosphere. Nature (London) 459, 978–982.
Roy, M., Kelley, S., Pazzaglia, F., Cather, S., House, M., 2004. Middle Tertiary buoyancy modification and its relationship to rock exhumation, cooling, and subsequent extension at the eastern margin of the Colorado Plateau. Geology 32, 925–928.
Ruddiman, W.F., 1997. Tectonic Uplift and Climate Change. Plenum Press, New York, NY.
Ruddiman, W.F., Kutzbach, J.E., 1991. Plateau uplift and climatic change. Scientific American 264(66–72), 74–75.
Ruddiman, W.F., Prell, W.L., 1997. Introduction to the Uplift-Climate Connection. Plenum Press, New York, NY.
Ruddiman, W.F., Prell, W.L., Raymo, M.E., 1989. Late Cenozoic Uplift in Southern Asia and the American West: Rationale for General Circulation Modeling Experiments. Journal of Geophysical Research 94, 18379–18391.
Sahagian, D., Proussevitch, A., 2007. Paleoelevation measurement on the basis of vesicular basalts. Reviews in Mineralogy and Geochemistry 66, 195–213.
Sahagian, D., Proussevitch, A., Carlson, W., 2002a. Timing of Colorado Plateau uplift: initial constraints from vesicular basalt-derived paleoelevations. Geology 30, 807–810.
Sahagian, D.L., Anderson, A.T., Ward, B., 1989. Bubble coalescence in basalt flows: comparison of a numerical model with natural examples. Bulletin of Volcanology 52, 49–56.
Sahagian, D.L., Maus, J.E., 1994. Basalt vesicularity as a measure of atmospheric pressure and palaeoelevation. Nature 372, 449–451.

Sahagian, D.L., Proussevitch, A.A., Carlson, W.D., 2002b. Analysis of vesicular basalts and lava emplacement processes for application as a paleobarometer/paleoaltimeter. The Journal of Geology 110, 671–685.

Schäfer, J.M., Ivy-Ochs, S., Wieler, R., Leya, I., Baur, H., Denton, G.H., Schlüchter, C., 1999. Cosmogenic noble gas studies in the oldest landscape on earth: surface exposure ages of the Dry Valleys, Antarctica. Earth and Planetary Science Letters 167, 215–226.

Schildgen, T.F., Balco, G., Shuster, D.L., 2010. Canyon incision and knickpoint propagation recorded by apatite 4He/3He thermochronometry. Earth and Planetary Science Letters 293, 377–387.

Schildgen, T.F., Hodges, K.V., Whipple, K.X., Reiners, P.W., Pringle, M.S., 2007. Uplift of the western margin of the Andean plateau revealed from canyon incision history, southern Peru. Geology 35, 523–526.

Schlunegger, F., Zeilinger, G., Kounov, A., Kober, F., Hüsser, B., 2006. Scale of relief growth in the forearc of the Andes of Northern Chile (Arica latitude, 18° S). Terra Nova 18, 217–223.

Schmitz, M., 1994. A balanced model of the southern Central Andes. Tectonics 13, 484–492.

Schoenbohm, L.M., Whipple, K.X., Burchfiel, B.C., Chen, L., 2004. Geomorphic constraints on surface uplift, exhumation, and plateau growth in the Red River region, Yunnan Province, China. Geological Society of America Bulletin 116, 895–909.

Schulte-Pelkum, V., Monsalve, G., Sheehan, A., Pandey, M.R., Sapkota, S., Bilham, R., Wu, F., 2005. Imaging the Indian subcontinent beneath the Himalaya. Nature (London) 435, 1222–1225.

Şengör, A.M.C., Ozeren, M.S., Keskin, M., Sakinc, M., Ozbakir, A.D., Kayan, I., 2008. Eastern Turkish high plateau as a small turkic-type orogen; implications for postcollisional crust-forming processes in turkic-type orogens. Earth-Science Reviews 90, 1–48.

Servant, M., Sempere, T., Argollo, J., Bernat, M., Feraud, G., Lo Bello, P., 1989. Morphogenese et soulevement de la Cordillere Orientale des Andes de Bolivie au Cenozoique. Comptes Rendus de l'Academie des Sciences, Série 2(309), 416–422.

Sheffels, B.M., 1990. Lower bound on the amount of crustal shortening, in the central Bolivian Andes. Geology 18, 812–815.

Shi, D., Zhao, W., Brown, L., et al., 2004. Detection of southward intracontinental subduction of Tibetan lithosphere along the Bangong–Nujiang suture by P-to-S converted waves. Geology 32, 209–212.

Simmons, N.A., Forte, A.M., Grand, S.P., 2007. Thermochemical structure and dynamics of the African superplume. Geophysical Research Letters 34, L02301.

Sine, C.R., Wilson, D., Gao, W., Grand, S.P., Aster, R., Ni, J., Baldridge, W.S., 2008. Mantle structure beneath the western edge of the Colorado Plateau. Geophysical Research Letters 35, L10303.

Snyder, N.P., Whipple, K.X., Tucker, G.E., Merritts, D.J., 2000. Landscape response to tectonic forcing: digital elevation model analysis of stream profiles in the Mendocino triple junction region, northern California. Geological Society of America Bulletin 112, 1250–1263.

Sobel, E.R., Hilley, G.E., Strecker, M.R., 2003. Formation of internally drained contractional basins by aridity-limited bedrock incision. Journal of Geophysical Research 108, 2344.

Sonder, L.J., England, P.C., 1989. Effects of a temperature-dependent rheology on large-scale continental extension. Journal of Geophysical Research 94, 7603–7619.

Sonder, L.J., Jones, C.H., 1999. Western United States extension: how the west was widened. Annual Review of Earth and Planetary Sciences 27, 417–462.

Spencer, J.E., 1996. Uplift of the Colorado Plateau due to lithosphere attenuation during Laramide low-angle subduction. Journal of Geophysical Research 101, 13,595–13,609.

Spicer, R.A., Harris, N.B.W., Widdowson, M., et al., 2003. Constant elevation of southern Tibet over the past 15 million years. Nature 421, 622–624.

Stanistreet, I.G., McCarthy, T.S., 1993. The Okavango fan and the classification of subaerial fan systems. Sedimentary Geology 85, 115–133.

Stark, C.P., Stewart, J., Ebinger, C.J., 2003. Wavelet transform mapping of effective elastic thickness and plate loading: Validation using synthetic data and application to the study of southern African tectonics. Journal of Geophysical Research 108, 2558.

Stock, G.M., Ehlers, T.A., Farley, K.A., 2006. Where does sediment come from? Quantifying catchment erosion with detrital apatite (U-Th)/He thermochronometry. Geology 34, 725–728.

Stockli, D.F., 2006. Thermochronometric constraints on paleoaltimetry and paleotopography – case studies from the Colorado Plateau, Tibet, and Labrador. Geochimica et Cosmochimica Acta 70, A617.

Strecker, M.R., Alonso, R.N., Bookhagen, B., Carrapa, B., Hilley, G.E., Sobel, E.R., Trauth, M.H., 2007. Tectonics and climate of the southern Central Andes. Annual Review of Earth and Planetary Sciences 35, 747–787.

Stüwe, K., White, L., Brown, R., 1994. The influence of eroding topography on steady-state isotherms. Application to fission track analysis. Earth and Planetary Science Letters 124, 63–74.

Summerfield, M.A., 1991. Global Geomorphology. Prentice Hall Longman/Wiley, London/New York.

Sutherland, R., Spasojevic, S., Gurnis, M., 2010. Mantle upwelling after Gondwana subduction death explains anomalous topography and subsidence histories of eastern New Zealand and West Antarctica. Geology 38, 155–158.

Swenson, J.L., Beck, S.L., Zandt, G., 2000. Crustal structure of the Altiplano from broadband regional waveform modeling: Implications for the composition of thick continental crust. Journal of Geophysical Research 105, 607–621.

Tabatabai Mir, S., Bergman, E., Gheitanchi, M.R., 2008. 3-Dimensional upper mantle velocity structure for Iranian Plateau revealed by Pn and Sn tomography. Journal of the Earth and Space Physics 33, 13–24.

Tapponnier, P., Zhiqin, X., Roger, F., Meyer, B., Arnaud, N., Wittlinger, G., Jingsui, Y., 2001. Oblique stepwise rise and growth of the Tibet Plateau. Science 294, 1671–1677.

Teixell, A., Ayarza, P., Zeyen, H., Fernandez, M., Arboleya, M.-L., 2005. Effects of mantle upwelling in a compressional setting: the Atlas Mountains of Morocco. Terra Nova 17, 456–461.

ten Brink, U., Stern, T., 1992. Rift flank uplifts and Hinterland Basins: comparison of the transantarctic mountains with the great escarpment of southern Africa. Journal of Geophysical Research 97, 569–585.

Thorpe, R.S., Francis, P.W., Harmon, R.S., Anonymous., 1981. Andean andesites and crustal growth. The Evolution of Passive Continental Margins in the Light of Recent Deep Drilling Results 301, 305–320.

Thouret, J.C., Wörner, G., Gunnell, Y., Singer, B., Zhang, X., Souriot, T., 2007. Geochronologic and stratigraphic constraints on canyon incision and Miocene uplift of the Central Andes in Peru. Earth and Planetary Science Letters 263, 151–166.

Tilmann, F., Ni, J., Team, I.I.S., 2003. Seismic imaging of the downwelling Indian lithosphere beneath Central Tibet. Science 300, 1424–1427.

Turkelli, N., Sandvol, E., Zor, E., et al., 2003. Seismogenic zones in Eastern Turkey. Geophysical Research Letters 30, 8039.

Turner, S., Hawkesworth, C., Liu, J., Rogers, N., Kelley, S., van Calsteren, P., 1993. Timing of Tibetan uplift constrained by analysis of volcanic rocks. Nature (London) 364, 50–54.

Valla, P.G., Herman, F., van der Beek, P.A., Braun, J., 2010. Inversion of thermochronological age-elevation profiles to extract independent estimates of denudation and relief history – I: Theory and conceptual model. Earth and Planetary Science Letters 295, 511–522.

Van der Wateren, F.M., Dunai, T.J., 2001. Late Neogene passive margin denudation history – cosmogenic isotope measurements from the central Namib desert. Global and Planetary Change 30, 271–307.

Vandervoort, D.S., Jordan, T.E., Zeitler, P.K., Alonso, R.N., 1995. Chronology of internal drainage development and uplift, southern Puna plateau, Argentine central Andes. Geology 23, 145–148.

Vassallo, R., Ritz, J.F., Braucher, R., et al., 2007. Transpressional tectonics and stream terraces of the Gobi-Altay, Mongolia. Tectonics 26, TC5013.

Wang, X., Ni, J.F., Aster, R., et al., 2008. Shear-wave splitting and mantle flow beneath the Colorado Plateau and Its boundary with the Great Basin. Bulletin of the Seismological Society of America 98, 2526–2532.

Wang, Z., Schauble, E.A., Eiler, J.M., 2004. Equilibrium thermodynamics of multiply substituted isotopologues of molecular gases. Geochimica et Cosmochimica Acta 68, 4779–4797.

Wdowinski, S., Bock, Y., 1994. The evolution of deformation and topography of high elevated plateaus 2. Application to the central Andes. Journal of Geophysical Research 99, 7121–7130.

Weeraratne, D.S., Forsyth, D.W., Fischer, K.M., Nyblade, A.A., 2003. Evidence for an upper mantle plume beneath the Tanzanian craton from Rayleigh wave tomography. Journal of Geophysical Research 108, 2427.

Wernicke, B.P., Christiansen, R.L., England, P.C., Sonder, L.J., 1987. Tectonomagmatic evolution of Cenozoic extension in the North American Cordillera. Coastal tectonics 28, 203–221.

West, M., Ni, J., Baldridge, W.S., Wilson, D., Aster, R., Gao, W., Grand, S., 2004. Crust and upper mantle shear wave structure of the southwest United States:

Implications for rifting and support for high elevation. Journal of Geophysical Research 109, B03309.
Whipple, K.X., 2001. Fluvial landscape response time: how plausible is steady-state denudation? American Journal of Science 301, 313–325.
Whipple, K.X., 2004. Bedrock rivers and the geomorphology of active orogens. Annual Review of Earth and Planetary Sciences 32, 151–185.
Whipple, K.X., 2009. The influence of climate on the tectonic evolution of mountain belts. Nature Geosci 2, 97–104.
Whipple, K.X., Tucker, G.E., 1999. Dynamics of the stream-power river incision model: implications for height limits of mountain ranges, landscape response timescales, and research needs. Journal of Geophysical Research 104, 17,661–17,674.
Whitman, D., Isacks, B.L., Chatelain, J.-L., Chiu, J.-M., Perez, A., 1992. Attenuation of high-frequency seismic waves beneath the Central Andean Plateau. Journal of Geophysical Research 97, 19929–19947.
Whitman, D., Isacks, B.L., Kay, S.M., 1996. Lithospheric structure and along-strike segmentation of the Central Andean Plateau; seismic Q, magmatism, flexure, topography and tectonics. Tectonophysics 259, 29–40.
Whittaker, A.C., Cowie, P.A., Attal, M., Tucker, G.E., Roberts, G.P., 2007. Bedrock channel adjustment to tectonic forcing: implications for predicting river incision rates. Geology 35, 103–106.
Widdowson, M., 1997. The geomorphological and geological importance of palaeosurfaces. Coastal Tectonics 120, 1–12.
Wigger, P., Baldzuhn, S., Giese, P., et al., 1994. Variations of the Crustal structure of the southern Central Andes deduced from seismic refraction investigations. In: Reuter, H.J., Scheuber, E., Wigger, P.J. (Eds.), Tectonics of the Southern Central Andes: Structure and Evolution of an Active Continental Margin. Springer, Berlin, pp. 23–48.
Wilson, D., Aster, R., Ni, J., et al., 2005. Imaging the seismic structure of the crust and upper mantle beneath the Great Plains, Rio Grande Rift, and Colorado Plateau using receiver functions. Journal of Geophysical Research 110, B05306.
Wittlinger, G., Masson, F., Poupinet, G., et al., 1996. Seismic tomography of northern Tibet and Kunlun; evidence for crustal blocks and mantle velocity contrasts. Earth and Planetary Science Letters 139, 263–279.
Wittlinger, G., Vergne, J., Tapponnier, P., et al., 2004. Teleseismic imaging of subducting lithosphere and Moho offsets beneath western Tibet. Earth and Planetary Science Letters 221, 117–130.
Wobus, C., Whipple, K.X., Kirby, E., et al. , 2006.Tectonics from topography; procedures, promise, and pitfalls. Special Paper – Geological Society of America 398, pp. 55–74.
Wobus, C.W., Hodges, K.V., Whipple, K.X., 2003. Has focused denudation sustained active thrusting at the Himalayan topographic front? Geology 31, 861–864.
Wolfe, J.A., 1992a. An analysis of present-day terrestrial lapse rates in the western conterminous United States and their significance to paleoaltitudinal estimates. U. S. Geological Survey Bulletin B 1964, 35.
Wolfe, J.A., 1992b. Climatic, floristic, and vegetational changes near the Eocene/Oligocene boundary. In: Prothero, D.R., Berggren, W.A. (Eds.), Eocene-Oligocene Climatic and Biotic Evolution. Princeton University Press, Princeton, pp. 421–436.
Wolfe, J.A., 1993. A method of obtaining climatic parameters from fossil leaf assemblages. U. S. Geological Survey Bulletin 2040, 1–71.
Wolfe, J.A., 1994. Tertiary climatic changes at middle latitudes of western North America. Palaeogeography, Palaeoclimatology, Palaeoecology 108, 195–205.
Wolfe, J.A., 1995. Paleoclimatic estimates from tertiary leaf assemblages. Annual Review of Earth and Planetary Sciences 23, 119–142.
Wolfe, J.A., Forest, C.E., Molnar, P., 1998. Paleobotanical evidence of Eocene and Oligocene paleoaltitudes in midlatitude western North America. Geological Society of America Bulletin 110, 664–678. http://dx.doi.org/10.1130/0016–7606.
Wolfe, J.A., Schorn, H.E., Forest, C.E., Molnar, P., 1997. Paleobotanical evidence for high altitudes in Nevada during the Miocene. Science 276, 1672–1675.
Wolfe, J.A., Spicer, R.A., 1999. Fossil leaf character states; multivariate analyses. In: Jones, T.P., Rowe, N.P. (Eds.), Fossil Plants and Spores; Modern Techniques. Geological Society, London, UK, pp. 233–239.
Xu, L., Rondenay, S., van der Hilst, R.D., 2007. Structure of the crust beneath the southeastern Tibetan Plateau from teleseismic receiver functions. Physics of the Earth and Planetary Interiors 165, 176–193.
Yao, H., Beghein, C., van der Hilst, R.D., 2008. Surface wave array tomography in SE Tibet from ambient seismic noise and two-station analysis – II. Crustal and upper-mantle structure. Geophysical Journal International 173, 205–219.
Yilmaz, Y., Güner, Y., Saroglu, F., 1998. Geology of the quaternary volcanic centers of the east Anatolia. Journal of Volcanology and Geothermal Research 85, 173–210.
Yuan, X., Sobolev, S.V., Kind, R., 2002. Moho topography in the central Andes and its geodynamic implications. Earth and Planetary Science Letters 199, 389–402.
Yuan, X., Sobolev, S.V., Kind, R., et al., 2000. Subduction and collision processes in the Central Andes constrained by converted seismic phases. Nature 408, 958–961.
Zandt, G., Myers, S.C., Wallace, T.C., 1995. Crust and mantle structure across the Basin and Range-Colorado Plateau boundary at 37° N latitude and implications for Cenozoic extensional mechanism. Journal of Geophysical Research 100, 10529–10548.
Zhao, W.-L., Morgan, W.J., 1987. Injection of Indian crust into Tibetan lower crust: a two-dimensional finite element model study. Tectonics 6, 489–504.
Zheng, H., Powell, C.M., Zhou, Z., Dong, G., J., 2000. Pliocene uplift of the northern Tibetan Plateau. Geology 28, 715–718.
Zhu, L., Owens, T.J., Randall, G.E., 1995. Lateral variation in crustal structure of the northern Tibetan Plateau inferred from teleseismic receiver functions. Bulletin of the Seismological Society of America 85, 1531–1540.
Zor, E., 2008. Tomographic evidence of slab detachment beneath eastern Turkey and the Caucasus. Geophysical Journal International 175, 1273–1282.
Zor, E., Sandvol, E., Gürbüz, C., Türkelli, N., Seber, D., Barazangi, M., 2003. The crustal structure of the East Anatolian plateau (Turkey) from receiver functions. Geophysical Research Letters 30, 8044.

Biographical Sketch

Julien Babault is a lecturer in Earth Surface Processes in the Department of Geology, Universitat Autònoma de Barcelona, Spain. He holds an MSc degree in Geology, and a PhD in Geology from the Department of Géosciences Rennes, Université de Rennes 1. His research interest include mountain belts dynamics of erosion at continental scale and dynamics of river network using field examples (Pyrenees, High Atlas of Morocco, Eastern Cordillera of Colombia in the Andes), quantification of erosion rates and rock/surface uplift rates, and experimental modeling.

Jean Van Den Driessche is a professor of Geology at the University of Rennes1. He has a PhD from the University of Montpellier and completed a State thesis in tectonics at the University Denis Diderot of Paris and the Institute of Earth Physics of Paris. His teaching and research concern tectonics, lithosphere mechanics and dynamics of continental erosion.